Mathematical Modelling and Optimisation of the Formulation and Manufacture of Aggregate Food Products

---

A thesis presented to the National University of Ireland, Cork, by

Nurşin Baş (MSc. Eng.)

in fulfilment of the requirements for the degree of PhD in Engineering under the supervision of

Dr. Edmond P. Byrne

Dr. John J. Fitzpatrick

July 2010

Department of Process and Chemical Engineering

University College Cork

Ireland

Table of Contents

Abstract

In this PhD study, mathematical modelling and optimisation of granola production has been carried out. Granola is an aggregated food product used in breakfast cereals and cereal bars. It is a baked crispy food product typically incorporating oats, other cereals and nuts bound together with a binder, such as honey, water and oil, to form a structured unit aggregate.

In this work, the design and operation of two parallel processes to produce aggregate granola products were incorporated:

i) a high shear mixing granulation stage (in a designated granulator) followed by drying/toasting in an oven.

ii) a continuous fluidised bed followed by drying/toasting in an oven.

In addition, the particle breakage of granola during pneumatic conveying produced by both a high shear granulator (HSG) and fluidised bed granulator (FBG) process were examined. Products were pneumatically conveyed in a purpose built conveying rig designed to mimic product conveying and packaging. Three different conveying rig configurations were employed; a straight pipe, a rig consisting two 45^o bends and one with 90^o bend. It was observed that the least amount of breakage occurred in the straight pipe while the most breakage occurred at 90^o bend pipe. Moreover, lower levels of breakage were observed in two 45^o bend pipe than the 90^o bend

pipe configuration. In general, increasing the impact angle increases the degree of breakage. Additionally for the granules produced in the HSG, those produced at 300 rpm have the lowest breakage rates while the granules produced at 150 rpm have the highest breakage rates. This effect clearly the importance of shear history (during granule production) on breakage rates during subsequent processing. In terms of the FBG there was no single operating parameter that was deemed to have a significant effect on breakage during subsequent conveying.

A population balance model was developed to analyse the particle breakage occurring during pneumatic conveying. The population balance equations that govern this breakage process are solved using discretization. The Markov chain method was used for the solution of PBEs for this process. This study found that increasing the air velocity (by increasing the air pressure to the rig), results in increased breakage among granola aggregates. Furthermore, the analysis carried out in this work provides that a greater degree of breakage of granola aggregates occur in line with an increase in bend angle.

Acknowledgements

Firstly, I would like to express my sincere thanks to my PhD supervisors Dr. Edmond P. Byrne and Dr. John J. Fitzpatrick. Their leadership, friendly manner and encouragement have always been very precious during my PhD study.

Special thanks to Dr. Kevin Cronin for the help and guidance he provided over the course of my PhD.

Thanks to National Development Plan, through the Food Institutional Research Measure (FIRM), administered by the Department of Agriculture, Fisheries and Food, Ireland for providing funding for this work.

I would like to acknowledge all staff in the Department of Process and Chemical Engineering for their help and support during the experimental and practical aspects of this PhD work, thanks to all of you: Mr. Paul Conway, Mr. Tim Twomey, Mr. John Barrett and Mr. Denis Ring. Special thanks to Ms. Anne Marie McSweeney and Ms. Julie Holand for their executive assistance.

I would like to thank all Postgraduate Students of the Department of Process and Chemical Engineering for making this a very pleasant and enjoyable time. I would like to thank the special friendship of the following people: Carina, Pankaj, Isabel, Natalie, Rocio, Luis and Yan.

I wish to express my gratitude to my family, especially my mommy and daddy, for the support they provided me through my entire life; my sister, my brothers and my sweetest nieces, Yaren and Ceren, for cheering me up and standing by me trough good times and bad.

And the most special thanks to my beloved husband, Muammer, whose endless support, understanding and company have been profound throughout the difficult times of this PhD work and at all times. Your love, encouragement and help have been invaluable along the way to success and without you I would not have been able to achieve so much. My daughter, my angel, Nazlı Deniz, for brightening my life and motivating me for the future.

List of Publications

Publications in Refereed Journals

Bas, N., Catak, M., Zumaeta, N., Fitzpatrick, J.J., Cronin, K., Byrne, E.P., (2009) Population balance modelling of protein precipitates exhibiting turbulent flow through a circular pipe, Chemical Engineering Science, 64, 4051-4059.

Bas, N., Pathare, P.B., Catak, M., Fitzpatrick, J.J., Cronin, K., Byrne, E.P. , (*in press*), Mathematical modelling of granola breakage during pipe pneumatic conveying. Powder Technology. doi:10.1016/j.powtec.2010.06.015

Catak, M., **Bas, N.**, Cronin, K., Medina, D., Byrne, E.P., Fitzpatrick, J.J., (*in press*), Markov chain modelling of fluidised bed granulation. Chemical Engineering Journal. doi:10.1016/j.cej.2010.02.022

Catak, M., **Bas, N.**, Cronin, K., O'Brien S., Byrne, E.P., (*in press*), Mathematical modelling of a solid particle motion in a gas stream. The Canadian Journal of Chemical Engineering.

Catak, M., **Bas, N.**, Cronin, K., Fitzpatrick, J.J., Byrne, E.P. , (*in press*), Discrete solution of breakage equation using Markov chains. Industrial Engineering Chemistry and Research.

Papers Presented in Conferences & Workshops

Bas, N., Pathare, P.B., Cronin, K., Fitzpatrick, J.J. and Byrne, E.P., (2010) A physical based growth model for aggregated food products produced in a high shear mixer. the World Congress on Particle Technology 6, 26-29 April, Nuremberg, Germany

Pathare, P.B., **Bas, N.**, Fitzpatrick, J.J., Cronin, K. and Byrne, E.P. (2010). Attrition during pneumatic conveying of a granola breakfast cereal produced by fluidised bed granulation, the World Congress on Particle Technology 6, 26-29 April, Nuremberg, Germany

Catak, M., **Bas, N.**, Medina, D., Pathare, P.B., Byrne, E.P.,Fitzpatrick, J.J., Cronin, K., (2009) Monte Carlo simulation of fluidised bed granulation. 8th World conference of Chemical Engineering 23-27 August, Montreal, Quebec, Canada

Bas, N., Pathare, P.B., Fitzpatrick, J.J., Cronin, K., and Byrne, E.P., (2009), Mathematical modelling of granola breakage during cylindrical pneumatic conveying systems, 9th International Symposium on Agglomeration and 4th International Granulation Workshop, 22-26 June, Sheffield, UK.

Catak, M., **Bas, N.**, Medina, D., Byrne, E.P.,Fitzpatrick, J.J., Cronin, K., (2009), Markov chain modelling for fluidised bed granulation. 9th International Symposium on Agglomeration and 4th International Granulation Workshop 22 - 26 June, Sheffield, UK

Pathare, P. B., **Bas, N.**, Fitzpatrick, J.J., Cronin K., and Byrne, E. P., (2008), Effect of high shear granulation parameters on the production of a granola cereal aggregate, 9th International Symposium on Agglomeration and 4th International Granulation Workshop 22 - 26 June, Sheffield, UK.

Bas, N., Pathare, P.B., Byrne, E.P., (2008), Population balance modelling of granola breakage during pneumatic conveying systems, 38th Annual Research Conference–Food, Nutrition & Consumer Sciences, September, University College Cork, Ireland

Cronin, K., **Bas, N.** and Byrne, E.P., (2007), Development of a computer-based teaching tool in probabilistic modeling, International Symposium for Engineering Education, 17-19 September, Dublin City University, Ireland.

List of Figures

List of Tables

Chapter 1

Introduction & Objectives

This chapter will start an introduction to the granola production process which is the basis of this work. Thereafter, the objectives of the work and a thesis overview will be provided.

1.1 Granola Production Process

Granola is an aggregated food product (Fig 1.1, Fig 1.2) used in breakfast cereals and cereal bars. It is a baked crispy food product typically incorporating oats, other cereals and nuts bound together with a binder, such as honey, water and oil, to form a structured unit aggregate. The aggregates have dimensions ranging from the size of the primary ingredient particles up to about 10 mm and are roughly spherical in shape. They typically exhibit a high degree of friability.

Aggregate food products can be produced via a number of ways. This work incorporates the design and operation of two parallel processes to produce aggregate granola products:

Figure 1.1: Granola product (High shear mixer)

Figure 1.2: Granola product (Fluidised bed granulator)

i) a high shear mixing granulation stage (in a designated granulator) followed by drying/toasting in an oven.

ii) a continuous fluidised bed followed by drying/toasting in an oven.

Granola ingredients were carefully selected for their high nutritional value. Table 1.1 displays percentage amount of the ingredients used for the high shear mixer and fluidised bed respectively. Batch size was taken as 100g in each case. The reason for slight differences in the ingredients percentages is due to different operating conditions that prevail in the fluidised bed; for example inulin becomes very hard due to its hygroscopic nature and lower liquid binder concentrations are required to enable fluidisation to occur (otherwise the wet aggregates would be to heavy to allow

fluidisation).

Table 1.1: The ingredients used for granola preparation for the high shear mixer and the fluidised bed.

Ingredients	High shear (% w:w)	Fluidised bed (% w:w)
Oat flakes	30.7	25.38
Corn flakes	3.97	5.2
Rice	3.97	5.2
Malted buckwheat (milled)	3.06	4
Malted barley (milled)	3.06	4
Brown sugar	6.73	8.8
Oil	6.42	0
Honey	24.70	15.6
Water	1.30	2.8
Oat beta glucan	13.30	17.4
Wheat germ	2.75	3.6
Inulin	5.35	0

For the purpose of drying/toasting, aggregated granola were taken from the granulator, spread on a tray and the wet cereal granules were then dried in an oven at 160^oC for 10 min. The dried granules were then placed in a desiccator for a cooling period of half an hour.

Particle breakage of the aggregated granola can occur during conveying as product is transferred as part of the production process on its way to packaging. Such breakage occurs as a result of both particle-particle and particle-wall collisions. Product from both processes will be subsequently pneumatically conveyed in a purpose built conveying rig designed to mimic product conveying and packaging. This will reveal the strength of the aggregate through the level of breakage experienced. Particle size and particle size distribution (PSD) of the primary food particles are measured prior to processing and size/PSD of the aggregates is measured both after the granulation/drying stages and after conveying. A Camsizer digital image analyzer (Retsch, Germany) was used for measuring particle size distributions of the resultant granola before and after passage through a conveying rig where aggregates are transferred by compressed air at a number of different flow rates. Figure 1.3 is a block flow diagram

showing the stages of granola production.

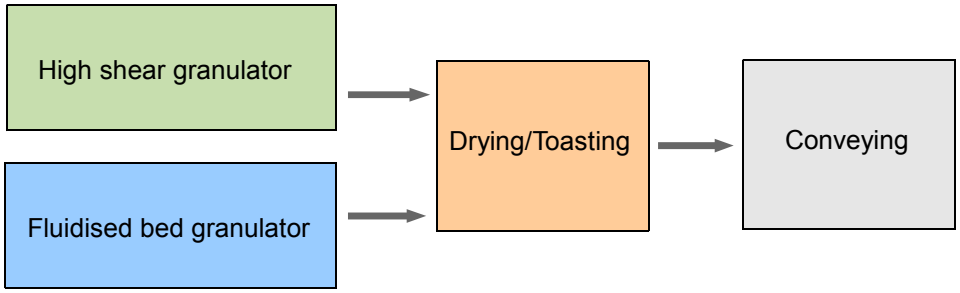

Figure 1.3: Granola production stages

The key quality parameters of size, PSD and aggregate strength are measured against a number of process inputs and parameters to ascertain optimum processing conditions. The inputs considered could include:

- process design
- composition and ratio of ingredients
- high shear mixer granulator and fluidized bed operating parameters (e.g. agitator speed, air flowrate)
- flowrate of aggregates through conveying pipe
- design of conveying pipe including pipe bends and contractions

Fundamental physical models to predict product quality in terms of aggregate size distribution and strength were developed in this work. These models will describe the various phenomena of interest such as the change in particle size distribution through the production process from prior to aggregation to storage for a given granola composition.

Population balance modeling (PBM) is a useful predictive tool which can be used to describe particle size distribution over time for processes in the food, chemical

and pharmaceutical industries. Population balance equations (PBEs) are used to define phenomena such as nucleation, growth, aggregation and breakup of particles. Modelling of the breakage process is achieved by constructing PBEs in the form of a mass balance on the granola aggregates. The solutions to the PBEs were obtained by means of discretization through the application of the Markov chains method. Using both experimental results and model predictions, the process was then optimised and process recommendations provided.

1.2 Objectives of the Thesis

1.2.1 General

The main objective of this thesis is to develop and apply both physical models and population balance models to breakage processes encounted by granola products produced in a high shear granulator and a fluidised bed granulator respectively in order to better characterize the granola production process.

1.2.2 Specifics

Objective I To develop a physical based growth model for a high shear granulation.

Objective II To describe the motion of a single particle in a high shear granulator and to investigate the application of this model as part of the Stokes number modelling approach for predicting the granulation of aggregate food products.

Objective III To experimentally investigate how process variables in both high shear and fluid bed granulators influence the strength of aggregate food particles and how this influences their breakage in pneumatic conveying lines.

Objective IV To develop a mathematical model to describe the velocity of a single particle in a pneumatic conveying rig and to investigate the application of this model with a breakage model for assessing the breakage of aggregate food products.

Objective V To develop a population balance model to investigate evolution of overall particle size distribution of a breakage process during pneumatic conveying.

1.3 Thesis Overview

In the first Chapter, the background of this PhD study is given. Firstly, an introduction to the granola production process which is the basis of this work is presented, then the objectives of the thesis are discussed.

Chapter 2 focuses on the aggregation process during granulation. A brief literature review is given with a discussion of micro-scale modelling. Then, growth and breakage mechanisms are presented as proposed in the literature.

Chapter 3 presents the literature review for particle breakage occurring during pneumatic conveying. Respective investigations on breakage mechanisms and impact breakage of particles are undertaken.

Chapter 4 describes population balance modelling. First of all an introduction to population balances is given, then population balance equations for breakage and aggregation processes incorporating a brief literature review are introduced. Finally, a synopsis of solution methods for these equations is presented.

Chapter 5 concerns granola production through aggregation in a high shear mixer and a corresponding growth model. The model describes change in particle size of

granola during high shear mixing.

Chapter 6 focuses on the particle breakage of granola which occurs during pneumatic conveying. A breakage model describing the change in particle size incorporating physical phenomena based on particle motion within a conveying rig is developed. Then, results obtained from both model and experimentation are compared and discussed.

Chapter 7 is dedicated to the particle breakage of granola which was produced in a fluidised bed granulator during pneumatic conveying. Firstly, an introduction to fluidised bed granulation is provided. Then, a breakage model describing the change in particle size incorporating physical phenomena based on the particle motion during conveying rig is proposed.

In Chapter 8, the modelling of particle breakage of granola occurring during pneumatic conveying using a population balance equation is developed. The Markov chains method, which is developed by our research team, is used as a discrete solution method of the population balance equation in this section.

Chapter 9 provides a general discussion and conclusions on the work done during the course of the PhD study.

Chapter 2

Aggregation Processes; Granulation

This chapter will focus on the aggregation process during granulation. First of all a brief literature review will be given with a discussion of micro-scale modelling. Then, growth and breakage mechanisms will be presented as proposed in the literature.

2.1 Introduction

Granulation involves the formation of large particles from smaller primary particles and is used in a wide range of industry sectors including pharmaceutical, fertilizer, food and chemical. There are two generic granulation process types; dry granulation and wet granulation.

Dry granulation is a process whereby no liquid is added to a bed of small particles and granules are produced by exposing the primary particles to high pressure.

Wet granulation involves using liquid as a binding agent which is added to primary particles to produce granules by forming liquid bridges between particles. The binder

must be viscous enough to ensure particle adhesion when the granule is subsequently dried.

Wet granulation is the most widely used process in industry. There are a number of wet granulation methods including for example, fluidized bed granulation, high shear mixer granulation, spray granulation and co–melt fluidized bed granulation.

The granulation process is quite complicated and depends on many different parameters. Two principal approaches have emerged over time in the literature; the traditional description (Sastry and Fuerstenau, 1973) and the modern approach (Snow et al., 1997a). The classifications of subgroups are given as follows;

1. **Traditional description**

   Nucleation Formation of granules starts with the initial contact between particles and binder.

   Coating/Layering/Snow-Balling/Onion-Skinning Formation of larger granules by a layer of fine particles over the surface of granules.

   Coalescence Formation of the larger granules by adhesion of two or more granules.

   Abrasion Transfer When the surfaces of two granules contact, the abraded part of one granule is transferred to the surface of the other one.

   Crushing and Layering Granules break into fine particles which form a layer over existing granules.

2. **Modern approach**

   Wetting and Nucleation Wetting and nucleation mostly occur at the beginning of granulation. Dry powder in the bed becomes wet and sticky after the beginning of binder addition. Wet and sticky powders form the basis of granule formation and are called nuclei.

Consolidation and Growth (Coalescence) Some of collisions between particles and granules (particle-particle, particle-granule, or granule-granule collisions) lead to new granules and a particle size enlargement process occurs. Granule collisions with other granules and the walls of the equipment lead to granule consolidation. As a result, aggregate sizes reduce and they become less porous. Entrapped air squeezes out and even binder may squeeze out to the surface. Final granule strength is controlled by porosity. Consolidation and growth rates are the main factors affecting particle size enlargement in a granulation process.

Attrition and Breakage Dry or wet granules break as a result of collisions with other granules or with physical parts of the granulator. If the granule is very compact (and strong) attrition is the dominant breakage mechanism. Attrition is a process in which at least one of the fragments after breakage is substantially larger than the other fine particles. If the granule is soft (and weak) it is more likely to break into roughly equal sized fragments and therefore fragmentation is the breakage mechanism.

A schematic representation of these two approaches shown in the Figure 2.1.

2.2 Literature review

Among the earliest studies on granulation were those by Newitt and Conway-Jones (1958), Kapur and Fuerstenau (1964) and Capes and Danckwerts (1965). These groups mostly worked on drum granulation of pellets. Newitt and Conway-Jones (1958) focused on the effects of internal structure of granules on granule growth, porosity and strength. Kapur and Fuerstenau (1964) defined three regions in the granulation process: nuclei growth region, transition region and the ball growth re-

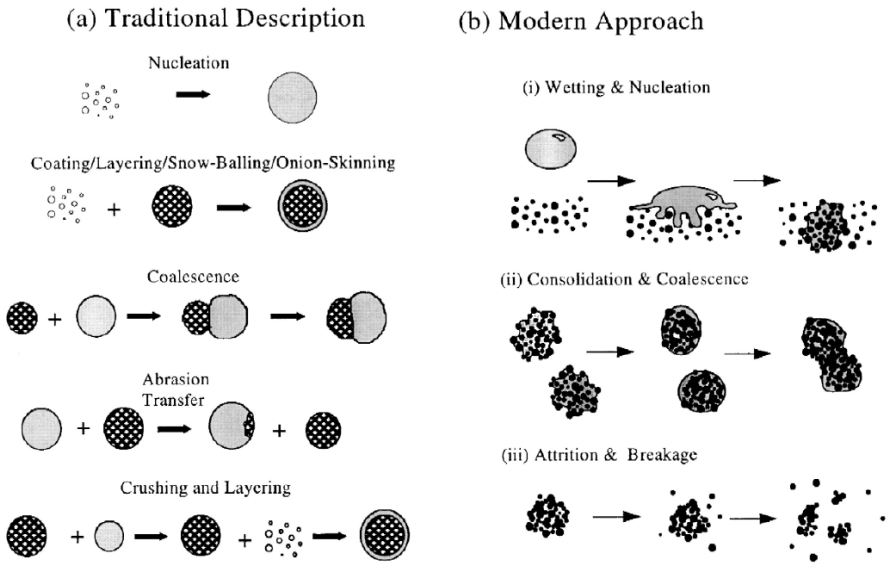

Figure 2.1: Schematic of granulation processes a) traditional and b) modern approach (Iveson et al., 2001)

gion. Capes and Danckwerts (1965) studied the mechanism of granule growth. Later studies on granulation include those by Kapur and Fuerstenau (1969); Capes (1980); Sherrington and Oliver (1981); Snow et al. (1997a); Parikh (2000); Iveson and Litster (1998); Iveson et al. (2001); Lui and Litster (2002); Gantt and Gatzke (2005); Salman et al. (2007b).

The granular structure proposed by Newitt and Conway-Jones (1958) includes three states of binder liquid content; the pendular state, the capillary state and the funicular state. In the pendular state, not much binder liquid is present and liquid bridges bind particles together. In the funicular state, more binder liquid exists and a continuous network of binder bonds particles in the granule. In the capillary state, much more binder liquid exists and all pores of the granule are filled with binder. In addition to these three states, York and Rowe (1994) defined two more binder liquid states for the granular structure; the droplet state and the pseudo-droplet state. In the droplet state, particles are bound within or at the surface of a liquid drop. In pseudo-droplet, however, unfilled voids exist within the liquid drop together with particles. The different states of binder liquid content of granules are shown in Figure 2.2.

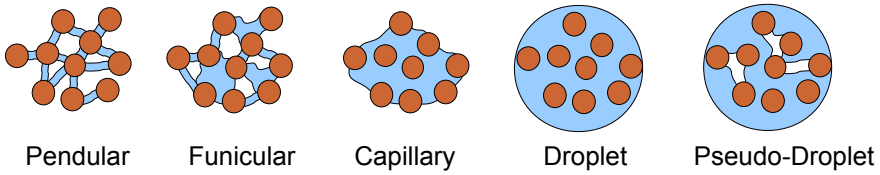

Figure 2.2: The different states of binder liquid content of granules; pendular, funicular, capillary (Newitt and Conway-Jones, 1958) and droplet and pseudo-droplet (York and Rowe, 1994).

In 1975, a model to predict the probability of permanent granule coalescence was developed by Ouchiyama and Tanaka (1975). In their model, granules coalescence successfully occurred when the binder bond between granules was strong enough to resist being broken by the forces in the granulator. The strength of this bond was assumed to be proportional to the contact area of granules. Based on the work of Ouchiyama and Tanaka (1975), Kristensen et al. (1985) found a critical size of granules above which collisions resulted in no further coalescence.

In another approach, Ennis et al. (1991) assumed that the coalescence between granules occurs if the surfaces of granules are surrounded by a liquid to bind them. They found that successful coalescence occurs when the collision kinetic energy was completely dissipated by viscous dissipation in the binder and elastic losses in the solid. On this basis, they derived a viscous Stokes number (St_{vis}) and a critical viscous Stokes number (St^*_{vis});

$$St_{vis} = \frac{8\rho r u}{9\mu} \tag{2.1}$$

$$St^*_{vis} = \left(1 + \frac{1}{e}\right) ln\left(\frac{h}{h_a}\right) \tag{2.2}$$

where ρ is the granule density, e is the coefficient of restitution, h is the thickness of the surrounding liquid layer, h_a is the typical height of surface asperities, μ is viscosity of the liquid binder, u is the relative collision velocity of the granules and r is the harmonic mean granule radius, i.e., if two particles of radiuses r_1 and r_2 collide then

$r = \frac{r_1 \times r_2}{r_1 + r_2}$.

According to this model, no coalescence will occur if the viscous Stokes number is bigger than the critical viscous Stokes number and the coalescence will occur if the viscous Stokes number is less than the critical viscous Stokes number, that is;

If $St_{vis} > St^*_{vis}$, then inertial effects dominate and all collisions are unsuccessful.

If $St_{vis} < St^*_{vis}$, then viscous effects dominate and all collisions are successful.

Moreover, Ennis et al. (1991) characterized three regimes of granulation by examining the limits of the ratio $\overline{St}_{vis}/St^*_{vis}$ where $\overline{St}_{vis}$ is the spatial average of St_{vis}. As a result of this, a *noninertial* regime was defined when $St_{vis} \ll St^*_{vis}$ and all collisions are successful provided binder is present. The growth rate is independent of granule kinetic energy and binder viscosity. In this regime binder distribution is the parameter that controls growth. An *inertial* regime occurs when granules grow lager and the maximum Stokes number becomes equal to the critical Stokes number, $St_{vis(max)} \sim St^*_{vis}$. In contrast to the nonintertial regime, granule kinetic energy and binder viscosity determine the growth. Increasing the binder viscosity or decreasing the agitation intensity will increase granule growth. Further growth in granule size finally will balance the average Stokes number and the critical average Stokes number, $\overline{St}_{vis} \sim St^*_{vis}$ which was defined as a *coating* regime. In this regime, all collisions are unsuccessful but growth continues by coating of granules by binder. Three regimes of granulation is represented in Figure 2.3.

It is also reported that the transition between these regimes depend on the hydrodynamic conditions of the bed. Consequently these three regimes can be summarized in terms of the magnitude of St_{vis} and St^*_{vis} as;

$St_{vis} \ll St^*_{vis}$ non-inertial regime (all collisions successful)

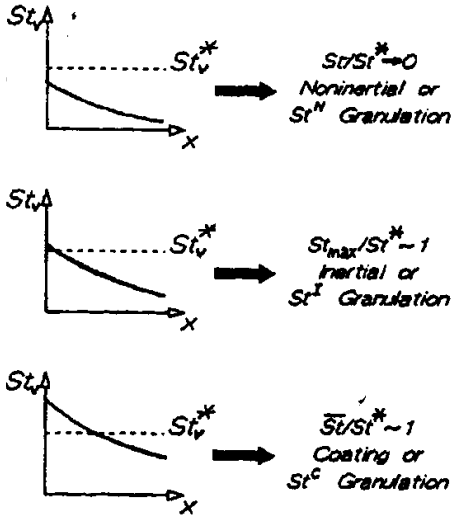

Figure 2.3: Three regimes of granulation (Ennis et al., 1991)

$St_{vis} \approx St^*_{vis}$ inertial regime (some collisions successful)

$St_{vis} \gg St^*_{vis}$ coating regime (no collisions successful)

Iveson and Litster (1998) defined two important types of growth behavior namely *steady growth* and *induction*. Where *steady growth* prevails the average granule size increases linearly in time. This occurs in systems in which the granules are weak and easily deform. Increasing the binder content increases the rate of growth, but produces weaker granules in nature. In general, *steady growth* occurs where particles are relatively coarse and narrowly sized and when the viscosity of binder is low. Where *induction growth* occurs, the period of growth is relatively long but stronger which are less easily deformable granules result. Increasing the binder content generally decreases the induction time. *Induction growth* occurs in systems where particles are fine with wide particle size distribution and the binder is generally viscous. Figure 2.4 illustrates both *steady growth* and *induction* behavior as a function of granulation time.

Iveson and Litster (1998) also modeled granule growth behavior as a function of pore liquid saturation and granule impact deformation. Granule pore liquid saturation

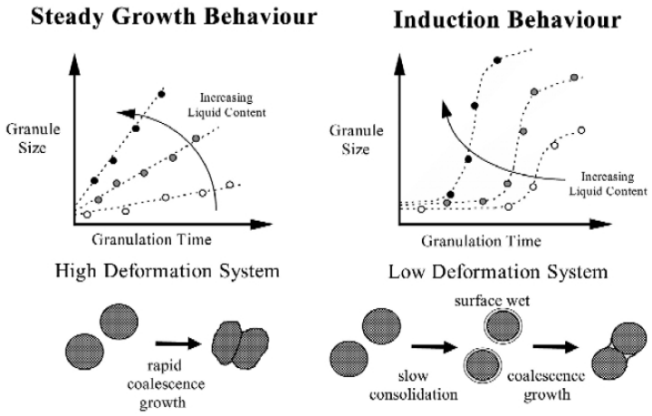

Figure 2.4: Steady-growth and induction behavior of granules (Iveson and Litster, 1998)

varies in time due to binder evaporation, granule consolidation and the dissolution of soluble components. Hence, the maximum granule pore saturation s_{max} is defined as;

$$s_{max} = \frac{w\rho_s(1-\varepsilon_{min})}{\rho_1\varepsilon_{min}} \tag{2.3}$$

where w is the mass ratio of liquid to solid, ρ_s is the density of the solid particles, ρ_1 is the liquid density and ε_{min} is the minimum porosity.

On the other hand, the granule impact deformation was defined as a function of granule rheology and agitation intensity. The amount of impact deformation was characterized by the Stokes deformation number;

$$St_{def} = \frac{\rho_g U_c^2}{2Y_g} \tag{2.4}$$

where U_c is the collision velocity in the granulator and represents the process intensity, ρ_g is the granule density and Y_g is the dynamic yield stress. The deformation number is a measure of the ratio of impact kinetic energy to the plastic energy absorbed per unit strain. The proposed granule growth behavior as a function of pore saturation and deformation number on a regime map is shown in Figure 2.5. Particles either remain as a dry free-flowing powder or form nuclei at very low s_{max}. A few larger

granules which are too weak to form permanent granules will form a crumb material at medium s_{max}. A slurry or over-wet mass will form when very high liquid content is present.

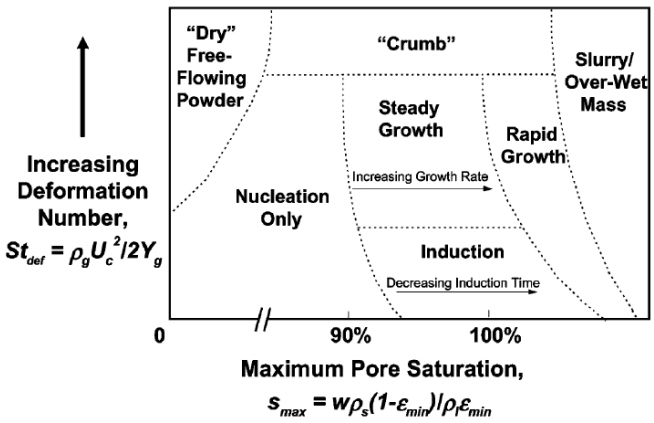

Figure 2.5: Granule growth regime map as a function of pore saturation and deformation number. (Iveson and Litster, 1998)

Lui et al. (2000) extended the model of Ennis et al. (1991) to include granule deformation behavior during collisions assuming the mechanical properties of granules to be strain-rate independent and not a function of stress–strain history. They defined the granule mechanical behavior by elastic modulus, E, and dynamic yield stress, Y_d. Two types of coalescence model were considered, namely Type I and Type II. In Type I, granules coalesce by viscous dissipation in the surface of binder layer before their surfaces come into contact. In Type II coalescence, granules are slowed to a halt during rebound after initial contact of their surfaces. The conditions for Type I and Type II coalescence were given as follows;

Type I:

$$St_{vis} < ln\left(\frac{h_0}{h_a}\right) \tag{2.5}$$

Type II:

$$\begin{aligned}\Big(\frac{Y_d}{E^*}\Big)(St_{def})^{-9/8} &< \frac{0.172}{St_{vis}}\Big(\frac{\tilde{D}}{h_0}\Big)\Big[1-\frac{1}{St_{vis}}ln\Big(\frac{h_0}{h_a}\Big)\Big]^{5/4}\\ &\times\Big[\Big(\frac{h_0^2}{h_a^2}-1\Big)+\frac{2h_0}{\delta''}\Big(\frac{h_0^2}{h_a^2}-1\Big)+\frac{2h_0^2}{(\delta'')^2}ln\Big(\frac{h_0}{h_a}\Big)\Big]\\ &\times\Big[1-7.86\Big(\frac{Y_d}{E^*}-1\Big)(St_{def})^{1/4}\times\Big(1-\frac{1}{St_{vis}}ln\Big(\frac{h_0}{h_a}\Big)\Big)^{-1/2}\Big]^2\end{aligned} \tag{2.6}$$

and

$$St_{vis} < 2\ ln\Big(\frac{h_0}{h_a}\Big)\quad for\quad \delta''\approx 0. \tag{2.7}$$

where h_0 is the binder layer thickness, h_a is granule surface asperity, E^* is Young's modulus of the granules and δ'' is the extent of permanent plastic deformation number given as;

$$\begin{aligned}\delta'' = &\Big(\frac{8}{3\pi}\Big)^{1/2}(St_{def})^{1/2}\tilde{D}\Big[1-\frac{1}{St_{vis}}ln\Big(\frac{h_0}{h_a}\Big)\Big]\\ &\times\Big[1-7.86\Big(\frac{Y_d}{E^*}-1\Big)(St_{def})^{1/4}\times\Big(1-\frac{1}{St_{vis}}ln\Big(\frac{h_0}{h_a}\Big)\Big)^{-1/2}\Big]\end{aligned} \tag{2.8}$$

St_{def} and St_{vis} are the Stokes deformation number and viscous Stokes number respectively defined as;

$$St_{def} = \frac{\tilde{m}u^2}{2\tilde{D}^3Y_d} \tag{2.9}$$

$$St_{vis} = \frac{8\tilde{m}u^2}{3\pi\mu\tilde{D}^2} \tag{2.10}$$

where u is the collision velocity, μ is the binder viscosity, $\tilde{D}$ and $\tilde{m}$ are the harmonic mean granule diameter and mass respectively. The harmonic mean granule sizes of $\tilde{D}$ and $\tilde{m}$ are described for the two colliding masses m_1, m_2 and for the two colliding

granules of diameters L, λ as;

$$\tilde{m} = \frac{m_1 m_2}{m_1 + m_2} \tag{2.11}$$

$$\tilde{D} = \frac{L\lambda}{L + \lambda} \tag{2.12}$$

St_{def} number shows the amount of plastic deformation except if there exists no binder layer on the surface of granules. The model predicts that the likelihood of coalescence depends on the critical Stokes number at low St_{def}.

Moreover, Vonk et al. (1997) added a colored liquid at the start of the granulation process and observed the dispersion of the dye through a process of **destructive nucleation** where loosely bonded nuclei are broken down into smaller fragments via attrition or fragmentation as shown in Figure 2.6. The initial weak nuclei were quite large in these experiments, 5 mm diameter. This process can be viewed as simply a subset of breakage processes in the granulator.

All the theoretical models presented above involve different assumptions about the mechanical properties of the particles, characteristics of the binder and the granule collision velocity. The model developed by Ouchiyama and Tanaka (1975) was then simplified by Kristensen et al. (1985). However, this model is still restricted to deformable granules without any binder layer on the surface of the granule. The uncertainty of the bond strength term makes application of the model difficult. The model derived by Ennis et al. (1991) is the first model to include the dynamic affects such as viscous dissipation yet it can only be applied to non-deformable wet surface granules. Lui et al. (2000) extended the model of Ennis et al. (1991) to consider deformable granules. Although they improved the previous model, the assumptions in the model are restricted to small amounts of deformation while capillary forces were neglected. The granule growth behavior postulated by Iveson and Litster (1998)

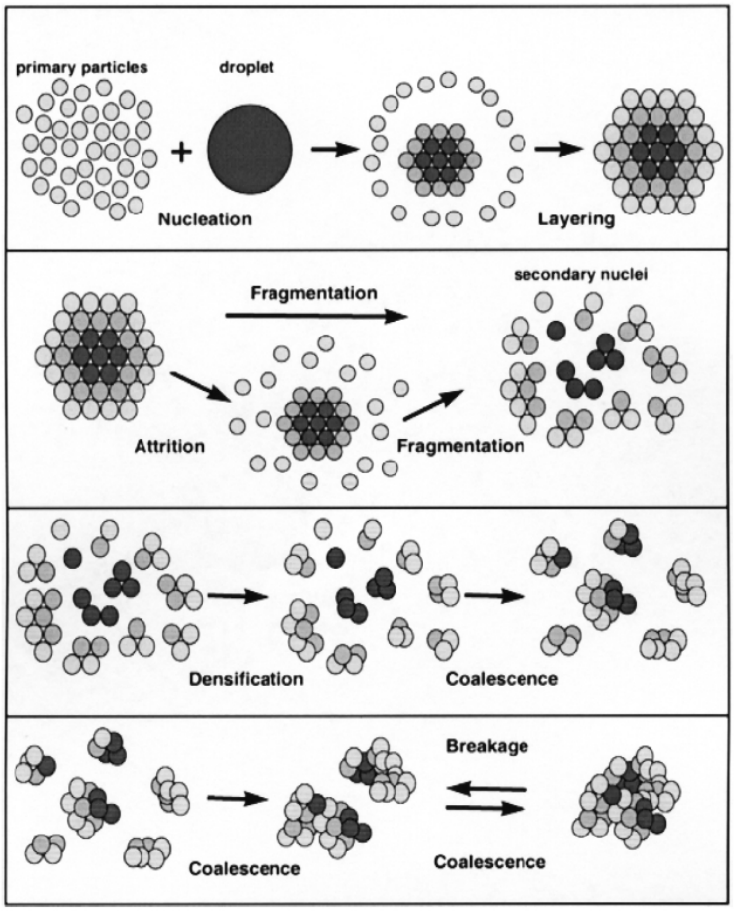

Figure 2.6: The destructive nucleation mechanism (Vonk et al., 1997)

is successful at qualitatively explaining the observed effects of different parameters. However, it is assumed that the granules are rigid-plastic materials and the model is only a descriptive tool and not a predictive one.

2.3 Growth Mechanism

Broadly, it can be stated that the granule growth is controlled by the balance between the granule strength and the shearing forces in the granulator. If the granule strength is high enough to resist the shearing forces then the growth mechanism will be controlled by coalescence. If the granule strength is too low then the growth mechanism will be determined by simultaneous coalescence and breakage of the aggregates.

Stokes coalescence

The condition for coalescence of two particles covered by the binder is determined by the ratio of the initial kinetic energy of the system to the energy dissipated in the liquid bridge collision (Ennis et al., 1991);

$$St_{vis} = \frac{\text{initial kinetic energy}}{\text{dissipated enegry in the bridge}}$$

which is,

$$St_{vis} = \frac{2m_p u^2}{2F_{vis}h} = \frac{8\rho_p r u}{9\mu} \tag{2.13}$$

with

$$F_{vis} = \frac{3\pi\mu u r^2}{4h} \tag{2.14}$$

$$St^*_{vis} = \left(1 + \frac{1}{e}\right) \ln\left(\frac{h}{h_a}\right) \tag{2.15}$$

where ρ_p is the particle density, r is the harmonic mean particle radius, that is if two particles of radiuses r_1 and $r_2$collide then $\frac{r}{2} = \frac{r_1 \times r_2}{r_1 + r_2}$.

e is the coefficient of restitution, h_a is the typical height of surface asperities, h is the thickness of the surrounding binder layer, μ is viscosity of the binder, u is the relative collision velocity.

If $St_{vis} > St^*_{vis}$, then inertial effects dominate and all collisions are unsuccessful.

If $St_{vis}<St^*_{vis}$, then viscous effects dominate and all collisions are successful.

Using the above equations the critical granule size can be calculated for transition between different regimes as $St_{vis}=St^*_{vis}$ with a critical granule size r^{coal}_{cr} (Tardos et al., 1997);

$$r^{coal}_{cr} = \left(\frac{9\mu St^*_{vis}}{8\rho_p\, w}\right)^{1/2} \tag{2.16}$$

Growth will be rapid until the system reaches the critical size and above the critical size it will be comparatively slow. This is because the coalescence of smaller particles will continue to form granules but in a layering type whereas the coalescence of the bigger particles will stop at the critical size.

Accordingly, growth can be characterized as being proportional to the difference between St^*_{vis} andSt_{vis}. The determination of the St^*_{vis} is not a easy task to achieve for this work as we have an inhomogeneous set of primary particles/ ingredients which will have different coefficient of restitution and the thickness of the surrounding binder layer is too difficult to measure. However, by using the critical size for coalescence it will be possible to get a value for St^*_{vis}. This critical size can be obtained from experimental measurements (Tardos et al., 1997).

2.4 Breakage Mechanism

The breakage term can be defined as the inverse mechanism of coalescence where agglomerate fractures into two or more similar sized segments. Breakage occurs when an external shear force is applied to particles. It may result from inter-particle collisions and collisions between the particles and walls of the granulator.

A simple model for breakage of particles in wet granulation is defined by Tardos et al. (1997). They consider an agglomerate of mass m, traveling at a speed u_0 where shear force of magnitude τ is applied. The Stokes deformation number (Stokes deformation number, St_{def}, is equivalent to deformation number, De, divided by two) for breakage and is defined as;

$$St_{def} = \frac{\frac{1}{2}mu_0^2}{V_\tau} \tag{2.17}$$

where V is the volume of the agglomerate.

It is assumed that that there is a critical Stokes number St^*_{def} where breakage occurs for;

$$St_{def} > St^*_{def}$$

There are several experimental observations in granulation processes.Some preferential growth mechanisms in tumbling granulation may involve attrition or breakage of weak granules. However, breakage is much more likely in higher-shear mixer granulators.

Stokes deformation (Breakage or Unsuccessful aggregation)

The deformation of wet granules is described by the following relationship (Tardos et al., 1997);

$$St_{def} = \frac{\text{externally applied kinetic energy}}{\text{enegry required for deformation}} \tag{2.18}$$

There two equations defined for Stokes deformation in the literature:

$St_{def} = \frac{m_g U^2}{2V_g \tau_y} \equiv \frac{\rho_g U^2}{2\tau_y}$ (Tardos et al., 1997)

$St_{def} = \frac{m_g U^2}{2V_g Y_g} \equiv \frac{\rho_g U^2}{2Y_g}$ (Iveson and Litster, 1998)

where V_g is the granule volume, m_g is the granule mass, τ_y which is the characteristic

stress in the granule is the flow stress of a non-Newtonian liquid, Y_g the dynamic granule yield strength and U is the collision velocity of the granules ($U = aw$ where w is impeller angular speed (or shear rate) and a is the granule radius) and ρ_g is the granule density.

The only difference is that Tardos et al. (1997) defined the Stokes deformation number in terms of the flow stress of a non-Newtonian liquid whereas Iveson and Litster (1998) used the dynamic yield strength of a solid.

Similar to the critical size for the coalescence, a critical size at which the granules start to deform and break above the critical size developed by Tardos et al. (1997) at the critical point when St_{def}=St^*_{def} for the granule deformation;

$$r_{cr}^{def} = \frac{\left(\frac{2\tau_y St^*_{def}}{\rho_p}\right)^{1/2}}{w} \tag{2.19}$$

Chapter 3

Breakage during Pneumatic Conveying

This chapter will focus on the literature review for particle breakage occurring during pneumatic conveying. It will reflect the various investigations on breakage mechanisms and impact breakage of particles.

3.1 Introduction

Pneumatic conveying is widely used in food processing and other chemical engineering applications. Particles are usually transported along a pipe system by compressed air though compressed nitrogen may be used when there is a risk of explosion. Particle breakage can be a problem during conveying, particularly if the particles involved are granular and/or friable. In general terms two breakage mechanisms for dry granules have been proposed; firstly erosion or attrition and secondly fracture or fragmentation (Iveson et al., 2001). Where erosion is the dominant breakage mechanism, there results one large fragment of size close to the parent aggregate and a number of

smaller fine particles. Where breakage is by fracture, this results in the production of a number of smaller fragments. In addition, the fracture type of breakage is divided into two modes; cleavage in which parent particles break into a small number of fragments of similar size and shattering which results in many fragments of a wide range of sizes (Redner, 1990). Particle breakage is usually considered an undesirable process since it can result in reduction in particle size, in changes to particle size distribution, dust generation and handling and storage problems which may cause the particles to no longer satisfy the requirement specifications (Salman et al., 2003).

3.2 Literature review

There are a number of papers which are devoted to particle breakage in pneumatic conveying systems (Hilbert, 1984; Huber and Sommerfeld, 1998; Kalman, 1999; Salman et al., 2002; Rajniak et al., 2008). In these papers, particle breakage is examined for a given conveying rig, and the effects of various parameters such as air velocity, bend angle and number of bends are investigated. Particle breakage in a pneumatic conveying system is dependent on many parameters and each of the aforementioned studies investigate such parameters through each for their own rig. Therefore, it is not possible to directly apply the results of one particular system or configuration to another.

Hilbert (1984) carried out experiments using three bends; long radius bend, short radius elbow and a blinded tee. It was found that less attrition occurred in the blinded tee and more attrition occurred in the long radius bend.

Huber and Sommerfeld (1998) developed a physical based model for the numerical prediction of wall-bounded particle flows which include effects such as turbulent two-way coupling, particle transverse lift forces, particle-wall collisions and inter–particle

collisions. They used a Euler-Lagrange approach to predict gas-solid flows in pipe systems. They reported that wall roughness reduces the gravitational settling of the particles on the bottom of the pipeline and inter-particle collisions are important in determining the mass flux even for low mass loading.

The factors affecting the particle breakage in a conveying rig have been divided into three groups (Kalman, 1999). These are;

1. Particle strength
    - Particle material
    - Particle size and shape
2. Operating parameters
    - Particle velocity
    - Particle concentration– loading ratio
3. Bend structure
    - Angle of collision (Radius of curvature)
    - Construction material
    - Bend angle
    - Number of bends

Kalman (1999) examined pneumatic conveying pipe lines as devices for attrition control. He conducted three case studies; i) to prevent attrition in cases that the conveying is used only to transfer the bulk from one process to another without significantly changing its character, ii) to increase attrition in order to replace or to reduce the use of a grinder or micronizer at the pipe line end and iii) to select an appropriate of attrition that will result in round particles by breaking the sharp corners that will reduce

dustiness during further processing. He found that the median size decreases significantly (threefold) after five passes through the system at a higher velocity ($24ms^{-1}$), while at lower velocity studies ($15.6ms^{-1}$) the attrition rate is negligible (Figure 3.1) for different types of powder for example, acicular particles (AP)and epoxy-polyester (EP). It shows that the effect of the superficial air velocity on the attrition rate is significant. In addition, Kalman (1999) notes that breakage at the bends is significant since flow direction changes at the bends resulting in particle–wall collisions.

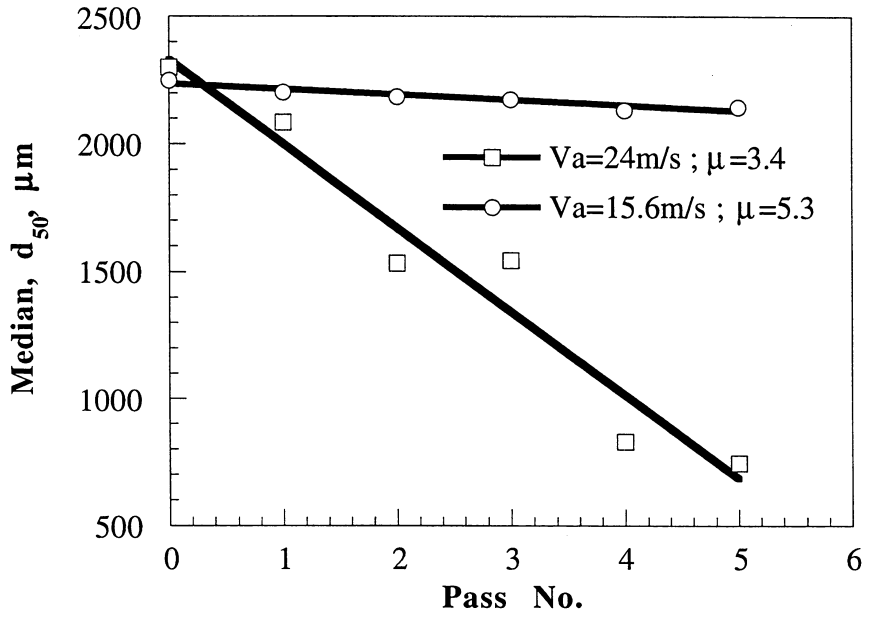

Figure 3.1: Attrition rate at two superficial air velocities, median particle size vs. number of passes through the system (Kalman, 1999).

Salman et al. (2002) reported results consistent with Kalman's study (Kalman, 1999). They found that negligible breakage occurred in a straight pipeline. Accordingly, they inferred that the inter-particle collision can be neglected in a dilute phase conveying system and the particle breakage occurs only when particles hit the walls. Salman et al. (2002) also examined the effects of impact angles on the particle breakage.

As is shown in Figure 3.2, Salman et al. (2002) reported that the degree of particle breakage is very sensitive to impact velocity and impact angle with greater angles resulting in significantly greater levels of breakage. Figure 3.3 is from Salman et al.

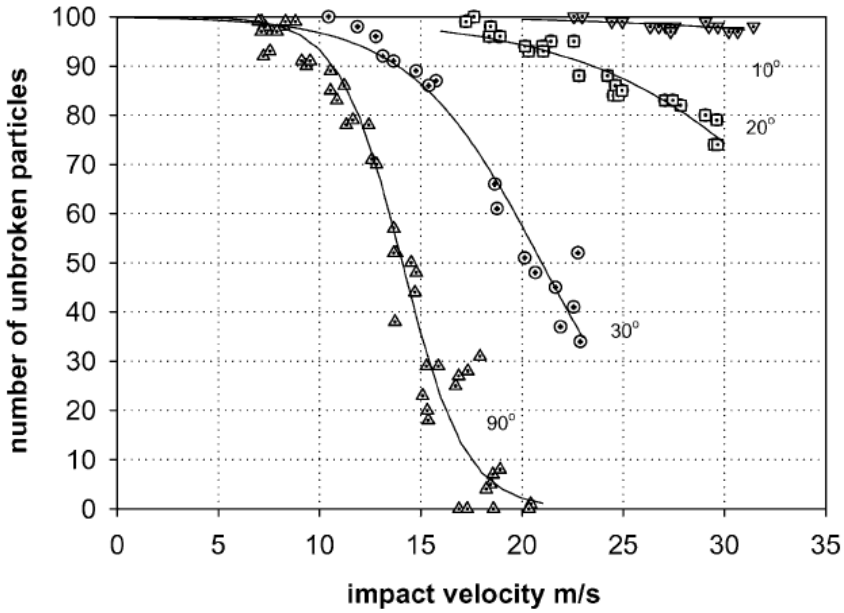

Figure 3.2: The relationship between the number of unbroken 3.2 mm fertilizer particles and impact velocity for impact angles from 90^o to 10^o (Salman et al., 2002)

(2002) and shows that larger fertilizer granules suffer a greater degree of breakage than smaller granules at a given flow velocity.

Salman et al. (2002) characterized a threshold impact velocity as the maximum velocity at which no breakage occurs and found that this decreases with increasing particle size. Different sized particles give different breakage characteristic for the same impact velocities. The number of unbroken particles is described by Salman et al. (2002) as;

$$N_0 = 100e^{-\left(\frac{\nu_i}{c}\right)^m} \tag{3.1}$$

where ν_i is the impact velocity and c and m are curve fitting parameters. The parameter m was found almost constant and the parameter c was found to vary with impact angles. Thus, equation (3.1) shows that the particle breakage increases logarithmically with increasing in the impact velocity.

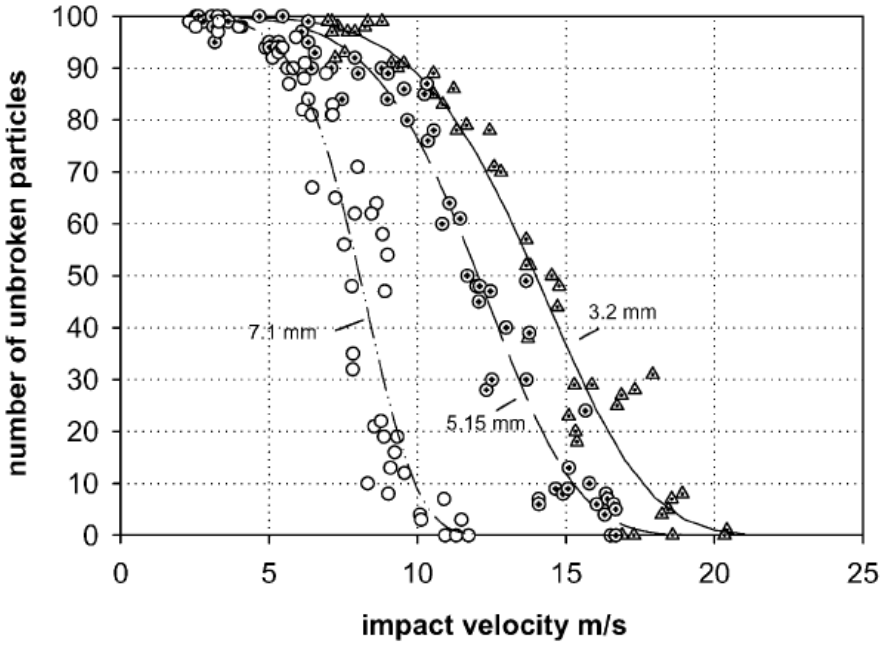

Figure 3.3: The relationship between the number of unbroken fertiliser particles and impact velocity for 3.2 mm, 5.15 mm and 7.1 mm particles at an impact angle of 90^o (Salman et al., 2002)

Salman et al. (2002) also showed that the effect of the number of impacts on particle breakage depends on the particle type. The number of impacts has no effect on the breakage for fertilizer particles, but the number of broken particles of polystyrene has a linear increase in the number of impacts.

While Salman et al. (2002) state that there is a threshold velocity under which no breakage occurs, a certain velocity is of course required for conveying. To avoid breakage therefore they suggested using long radius bends which decrease the impact angle.

Additionally, Maxim et al. (2002) studied the breakage probability of fertiliser granules. They developed a relationship, which explains the effect of impact angle θ on the parameter c as follows:

$$c = \frac{u_f}{\sin(\theta)} \tag{3.2}$$

where u_f is defined as the normal failure velocity, which is a function of the material properties and particle size.

Recently Rajniak et al. (2008) reported a study on granule attrition during pneumatic conveying. They developed three different methods to model breakage such as (i) 2D computational fluid dynamics (CFD), (ii) population balance modelling (PBM) and (iii) a combination of CFD and PBM. They reported that generally a power law equation is used to represent the breakage frequency of the particles as;

$$b(l_i) = kl_i^{\gamma} \tag{3.3}$$

where l_i is the representative particle size and k and γ are the breakage constants. The values of the breakage rate parameters k and γ can be derived by fitting the population balance models to experimental data. Alternatively, these parameters can be evaluated from independent experimental measurements in laboratory impact testers and by employing mechanistic models and computer simulations (Rajniak et al., 2008).

In the literature there are many different expressions for the fragment particle size distribution (Marchisio and Fox, 2003; Vanni, 2000; Diemer and Olson, 2002c). The optimum fragment particle size distribution function can be chosen using semi-empirical methods such as observing the particle breakage in the pipeline during conveying to obtain optimum fit to experimental results (Rajniak et al., 2008).

3.3 Impact Breakage of Particles

Pneumatic conveying is used for transporting particulate material in industry. However, a significant amount of particle breakage may occur during during this operation. This may cause changes in particle size, shape and appearance. These changes may result in a failure to meet required product qualifications and may affect the product market value. Particle breakage in pneumatic conveying is dependent on several variables such as, particle-particle collisions, particle-pipe wall collision, material of the particles and the movement of the particles in the system. Single impact studies can be used to analyse these variables in terms of particle breakage.

According to material characteristics, particle breakage can be categorized as the fracture strength and the deformation behaviour. Fracture strength can be defined in terms of the energy required to cause fracture (or critical tensile stress). Material deformation behaviour can be classified as elastic (brittle) or inelastic. Inelastic behaviour includes semi-brittle, plastic and quasi-brittle. Stress conditions can be classified by type of stresses applied (compressive or shear), number of loading points, stressing intensity and stressing rate (Tavares, 2007).

A single particle subjected to stresses contributes to an elementary breakage micro event which can provide an understanding of several variables described above. The breakage micro event can be classified among two main modes; major mode and minor mode. In the major mode, a particle is subjected to compressive stresses, resulting in disintegrative fracture. In the minor mode, called attrition or abrasion, the particle suffers gradual wearing of its surface leaving the parent particle largely intact but usually more rounded, the result of stress concentration at some surface sites on the corners or protrusions, leading to abrasion (Tavares, 2007).

There have been a number of studies on impact breakage of single particles (Yuregir

et al., 1987; Shipway and Hutchings, 1993; Salman et al., 1995; Papadopoulos and Ghadiri, 1996; Salman and Gorham, 2000; Maxim et al., 2002; Samimi et al., 2004). In these studies, experiments were mostly carried out using air/gas guns to fire individual particles against a solid target. Among these researches, Yuregir et al. (1987) and Papadopoulos and Ghadiri (1996) studied the fragmentation probability with the impact velocity. Samimi et al. (2004) investigated the effect of impact angle on the extent and regime of breakage of two types of soft agglomerates. They found that there was a threshold impact velocity, below which the effect of the impact angle was negligible.

In their paper Ghadiri and Zhang (2002) studied the mechanical breakdown of single particles resulting from impact on a rigid target in a velocity range which corresponds to that prevailing in process equipment by the application of indentation fracture mechanics. They developed a mechanistic model of impact attrition of particulate solids, having a semi-brittle failure mode. Accordingly a dimensionless attrition propensity parameter, η , was derived;

$$\eta = \frac{\rho v^2 l H}{K_c^2} \tag{3.4}$$

where ρ is the particle density, v is the impact velocity, l is a characteristic particle size, H is the hardness and K_c is the fracture toughness.

With the aim of predicting the particulate breakage in pneumatic conveying, Salman et al. (2002) used a numerical model to calculate the particle trajectory in dilute-phase pipe transport. They considered a dilute system where inter-particle collisions were neglected and fragmentation was only considered upon impact with pipe walls. The effect of several variables such as impact velocity, impact angle, particle diameter, target type and hardness on particle fragmentation were investigated. Using results from single impact studies, their paper has provided valuable information on how to minimise particle fragmentation, particularly in pneumatic conveying systems. They

concluded that particle breakage at the bend can be reduced by decreasing the impact angle. This can be achieved by using long radius bends and by reducing the conveying velocity.

Furthermore, a numerical simulation of a particle in a horizontal pipe with the variation of aerodynamic forces has been carried out by Salman et al. (2005). They found that the major forces that control particle motion are drag in the axial direction, and lift due to air velocity gradient and due to spin in the transverse direction.

Xiang and McGlinchey (2004) developed a gas-solids two-dimensional mathematical model for plug flow of cohesionless particles in a horizontal pipeline in dense phase pneumatic conveying. A combined approach of the Discrete Element Method (DEM) and Computational Fluid Dynamics (CFD) was used for the model. They integrated the Navier–Stokes equations considered for the gas phase and the Newtonian equations of motion of individual particles for the particle motion. Additionally, a nonlinear spring and dash pot model for both normal and tangential components was used for particle contact.

On the other hand, Rajniak et al. (2008) proposed a methodology combining theoretical and experimental techniques for characterizing and predicting the friability of granules in laboratory scale pneumatic conveying systems. They developed a two dimensional (2–D) computational fluid dynamics (CFD) model of the gas-solid flow within the Malvern Mastersizer laser diffraction equipment to simulate impact of different inlet jet pressures on the flow properties and to calculate average velocity and average volume fraction of particles in the equipment and a simple maximum-gradient population balance (MG-PB) mathematical model of breakage and a CFD–PB model combining CFD and the Quadrature Method of Moments (QMOM) methodologies. They compared the simulation results with attrition experimental data and found that the model was able to capture the qualitative trends and quantitatively predict the

Sauter mean diameter (d_{32}) at the outlet.

Chapter 4

Population Balance Modelling

This chapter will describe population balance modelling. First of all an introduction to population balances will be given. Then, population balance equations for breakage and aggregation processes incorporating a brief literature review will be introduced. Finally, a synopsis of solution methods for these equations will be presented.

4.1 Introduction

Population balance modelling (PBM) is a useful predictive tool which can be used to describe particle size distribution over time for processes in the food, chemical and pharmaceutical industries. Population balances trace their origins from the Boltzman equation which was developed in 1872 (Boltzmann, 1872). However, the application of population balances to process engineering systems is a relatively new development. Early examples include Hulburt and Katz (1964) who applied their model to dispersed phase systems, while Randolph and Larson (1964) primarily focused on crystallization. Since then, there have been many articles published dealing with population balances as applied to process engineering systems (Hidy and Lilly, 1965; Gelbard and Seinfeld,

1980; Batterham et al., 1981; Hounslow et al., 1988; Hill and Ng, 1995; Kumar and Ramkrishna, 1996b; Diemer and Olson, 2002a; Marchisio et al., 2003; Kostoglou and Karabelas, 2004; Immanuel and Doyle-III, 2005).

Population balance equations (PBEs) are used to define phenomena such as nucleation, growth, aggregation and breakup of particles. PBEs are underpinned by the law of conservation of mass and the equations describe the relationships that define the number balance on particles of given particulate states. Alternatively, the number balance can also be considered in terms of mass or volume in some instances. A continuous number density function in PBEs makes the model quite powerful in analyzing the dynamics of a process. However, the structure of the population balance equation entails partial integro-differential equations and hence analytical solutions may not be possible except for simple cases. Nonetheless some simplified approaches which allow for population balance equations to be solved are available in the literature (Hidy and Lilly, 1965; Gelbard and Seinfeld, 1978; Bapat et al., 1983; Hounslow et al., 1988; Hill and Ng, 1995, 1996; Kumar and Ramkrishna, 1996a; Nicmanis and Hounslow, 1998; Vanni, 1999; Kostoglou and Karabelas, 2002; Diemer and Olson, 2002b; Marchisio et al., 2003). These approaches help simplify the rigorous population balance equations and include mathematical methods such as Monte-Carlo simulation, method of moments, discrete formulations and Laplace transforms. A comprehensive discussion about various applications and detailed solution techniques of PBEs is presented in Ramkrishna (2000).

4.2 Population balances for breakage

Particle breakage can be defined as separation of fragments from a whole particle. Breakage occurs in many engineering applications, such as mixing, conveying operations, liquid-liquid dispersion, milling and grinding applications, crystallisation and

precipitation production, transport and separation.

Modeling a breakage process can be achieved by constructing a population balance equation in the form of breakage functions. This can be either in continuous or in discrete form. Moreover, two types of breakage equations are defined;

- a number density based breakage equation
- a mass density based breakage equation

It should be noted that, when particles display homogenous density then a mass density based breakage equation can be considered as equivalent to a volume density based breakage equation.

There are a number research studies dealing with breakage processes (Hounslow et al., 2001; Nere and Ramkrishna, 2005; Kostoglou, 2006; Bilgili et al., 2006; Kostoglou and Karabelas, 2007). Among them Nere and Ramkrishna (2005), Kostoglou (2006) and Kostoglou and Karabelas (2007) studied the breakage in turbulent pipe flow.

Bilgili et al. (2006) formulated a phenomenological non-linear population balance theory that can be used to explain the complex non-first-order breakage kinetics for certain grinding processes. They used a non-linear population balance framework to explain the non-first-order breakage rates that originate from multi-particle interactions.

In their paper, Hounslow et al. (2001) described tracer studies using a population balance framework. They linked a two internal coordinates population balance equation with the evolution time of granule-size and tracer-mass distributions to underlying rate processes.

Additionally, a recent book edited by Salman et al. (2007a) provides a brief overview

of particle breakage from the small scale of a single particle, to the study of whole processes for breakage; both through experimental study and mathematical modelling.

4.2.1 Breakage equation

A homogenous breakage process describing the evolution of particle size distribution in time for a batch process can be described according to the following expression (Ramkrishna, 2000);

$$\frac{\partial f(x,t)}{\partial t} = \int_x^\infty p(x,y)b(y)f(y,t)dy - b(x)f(x,t) \tag{4.1}$$

In this equation $f = f(x,t)$ is the particle size distribution defined on the domain of particles of size x at time t. $p(x,y)$, which is known as breakage kernel or daughter size distribution (fragment size distribution), is the probability distribution of particles of size x resulting from the breakup of particles of size y. $b(x)$ is the breakage frequency (the breakage rate) at which particles of size x break per unit time. Table 4.1 shows the most commonly used breakage rates and 4.2 displays several expressions for breakage rate used in the literature. A list of well–known fragment size distributions is given in Table 4.3.

Table 4.1: Breakage rate functions

Breakage rate	$b(x)$
Constant	c_1
Power law	x^{c_2}
Exponential	$\exp(c_3 x^{c_4})$

The integral part of the equation (4.1) is the birth rate of particles and it describes the

production of daughter size particles by breakage of parent size particles. The death rate of particles, which describes the average volume fraction of particles lost from the domain of particles of diameter x, is formulated as $b(x)f(x,t)$ in equation (4.1). A figure which represents the breakage birth and breakage death for particle of size x is given in Figure 4.1.

Table 4.2: Some breakage rates proposed in the literature.

System	b(x)	Source
Liquid-liquid	$k_1 x^{-2/3}\varepsilon^{1/3}\exp[-\frac{k_2\sigma}{\rho_d\varepsilon^{2/3}x^{5/3}}]$	Coulaloglou and Tavlarides (1977)
Liquid-liquid	$c_4\left(\frac{\epsilon}{x^2}\right)^{1/3}\int_{\xi_{min}}^{1}\frac{(1+\xi)^2}{\xi^{11/3}}\exp\left(-\frac{12c_f\sigma}{\beta\rho_c\epsilon^{2/3}x^{5/3}\xi^{11/3}}\right)d\xi$	Luo and Svendsen (1996)
Solid-liquid	$c_1\nu^{\alpha}\varepsilon^{\beta}x^{\gamma}$	Kramer and Clark (1999) Wojcik and Jones (1998)
Solid-liquid	Ax^b	Boadway (1978) Pandya and Spielman (1982)
Solid-liquid	$\frac{1}{\sqrt{15}}\left(\frac{\varepsilon}{\nu}\right)\exp\left(-\frac{\tau_f}{\mu(\frac{\varepsilon}{\nu})^{1/2}}\right)$	Ayazi Shamlou et al. (1994)

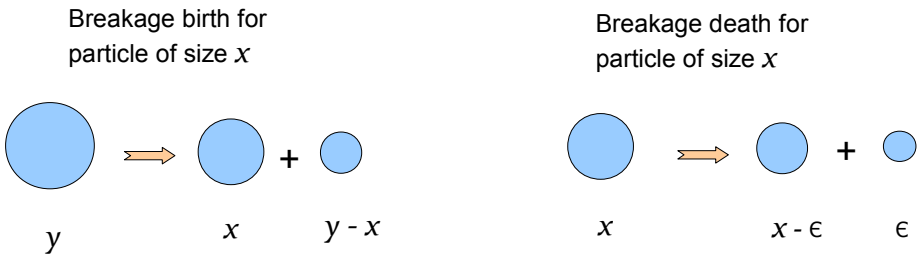

Figure 4.1: Breakage birth and death for particle of size x.

Table 4.3: Fragment size distributions. In all cases binary breakage is considered.

Mechanisim	$p(x,y)$
Uniform	$\begin{cases} \frac{1}{y}, & \text{if } 0 < x < y; \\ 0, & \text{else.} \end{cases}$
Erosion	$\begin{cases} 1, & \text{if } x = x_0; \\ 1, & \text{if } x = x - x_0; \\ 0, & \text{else.} \end{cases}$ x_0 is the primary particle size.
Equisized	$\begin{cases} 2, & \text{if } x = \frac{y}{2}; \\ 0, & \text{else.} \end{cases}$

Note that the function $p(x,y)$ should satisfy the mass conservation requirement such that all of the volume fractions formed sum to unity. It can be expressed as the following equation (McGrady and Ziff, 1986);

$$\int_0^y p(x,y)dx = 1 \tag{4.2}$$

In addition, it is convenient to use the cumulative fragment size distribution, $P(x,y)$, to correlate experimental data on breakage. $P(x,y)$ describes the volume fraction of particles that are smaller than or equal to particles of diameter x which are broken from particles of diameter y. Accordingly, $P(x,y)$ can be formulated as;

$$P(x,y) = \int_0^x p(x',y)dx' \tag{4.3}$$

where x' is a dummy diameter.

4.2.2 Discretized population balance for breakage equation

The analytical solution of population balance equations of integro-differential form is not a trivial matter except for some simple examples. To overcome this difficulty, discrete methods can be employed to solve integro-differential type PBEs. There are a number of numerical techniques presented in the literature (Hill and Ng, 1995; Kumar and Ramkrishna, 1996a,b; Vanni, 1999; Diemer and Olson, 2002b; Marchisio and Fox, 2003).

Hill and Ng (1995) applied a discretization procedure to the breakage equation. A fixed pivot technique (Kumar and Ramkrishna, 1996a) and a moving pivot technique (Kumar and Ramkrishna, 1996b) have also been used for the discretization of continuous population balance equations. Vanni (1999) proposed a discretization method by a modification of the method developed by Hill and Ng (1995) and considered size range as divided into m arbitrary sections. Diemer and Olson (2002b) presented a moment methodology for solving simultaneous population balances for coagulation and breakage. They developed a technique with a view towards coupling population balances with computational fluid dynamic (CFD) simulations. Marchisio and Fox (2003) simulated the simultaneous aggregation and breakage of particles in a Taylor-Couette reactor by implementing the quadrature method of moments in a commercial CFD code.

Discretizing the size domain

Classification of a continuous size range into discrete intervals is the first step in constructing a discretized population balance equation. Two main approaches can be used to select the classification of the states.

- Uniform Discretization: According to this approach, the interval of each state

is constant, i.e., $\check{r} = x_i - x_{i-1}$.

- Geometric Discretization: In this approach, the interval of the next state is directly proportional to its previous state, i.e., $\check{r} = \frac{x_i}{x_{i-1}}$

where x_{i-1} and x_i are lower and upper limits of the interval i, respectively. Figure 4.2 represents the discretized size range of particles with respect to uniform discretization. The discretized size range of particles with respect to geometric discretization is displayed in Figure 4.3.

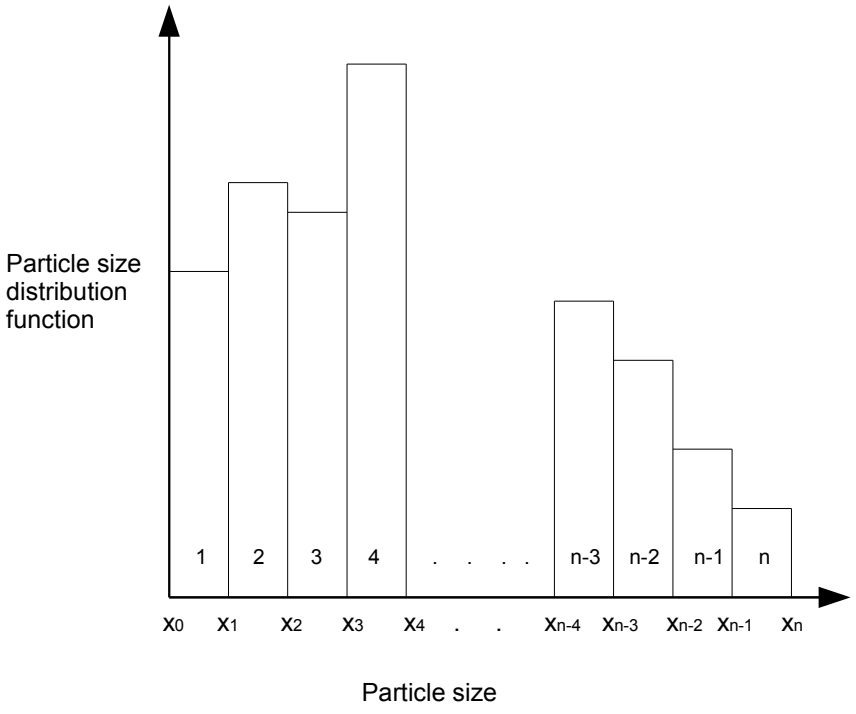

Figure 4.2: The particle size distribution function in discrete size intervals with respect to uniform discretization.

Although uniform discretization is numerically more stable it may lead a very large number of intervals. On the other hand, the number of intervals that result with geometric discretization can be much more reasonably dealt with and stable results may be obtained provided that the value of $\check{r}$ is well chosen.

The underlying basis of these numerical techniques is to turn the main population

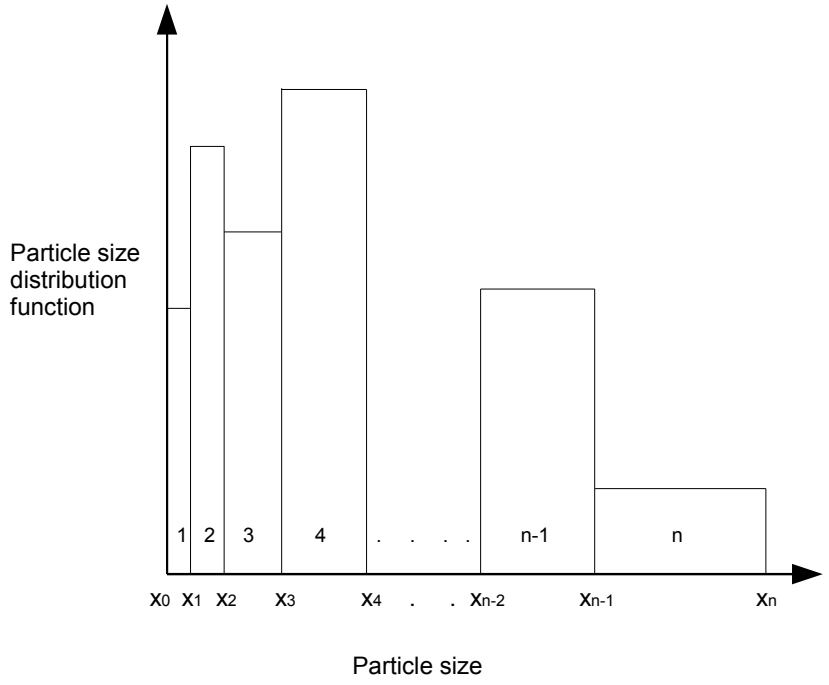

Figure 4.3: The particle size distribution function in discrete size intervals with respect to geometric discretization.

balance of integro-partial differential equations into an ordinary differential equation by applying discretization as in the following type of equation;

$$\frac{dN_i}{dt} = \sum_{j=i+1}^{\infty} p_{ji} b_j N_j - b_i N_i \tag{4.4}$$

where, N_i is the discretized distribution of particles in interval i containing particles larger than x_{i-1} and smaller than or equal to x_i at time t. b_i is the discrete breakage frequency of particles in the i_{th} interval. The discretized breakage function p_{ji} is the fragment size distribution of particles broken from interval j that go to interval i. Any broken particle in interval j cannot go into interval j i.e.

$$\sum_{i=1}^{j-1} p_{ji} = 1 \tag{4.5}$$

The restriction in equation (4.5) is frequently used for the discretized breakage equation in the literature. Consequently, the discretized fragment size distribution can be written by the following equation;

$$p_{ji} = \int_{x_{i-1}}^{x_i} p(x, x_{j-1})dx \tag{4.6}$$

Note that, the cumulative fragment size distribution for the discrete case has the form;

$$p_{ji} = P(x_i) - P(x_{i-1}) \tag{4.7}$$

4.3 Population balances for aggregation

Aggregation is a term used for size enlargement processes whereby small particles are gathered into larger, relatively permanent masses in which the original particles can still be distinguished (Snow et al., 1997b). It is prevalent across many diverse sectors of industry including pharmaceuticals, fertilizers and chemicals. Aggregation occurs between at least two particles. There are a number of processes that aggregation covers; *coalescence* is the formation of the larger granules by adhesion of two or more particles, *coagulation* is a floc of particles held by surface forces without having physical contact. Studies dealing with aggregation processes using population balance equations include those by Hidy and Lilly (1965); Gelbard and Seinfeld (1978); Bapat et al. (1983); Hounslow et al. (1988); Kumar and Ramkrishna (1996a); Diemer and Olson (2002a); Marchisio and Fox (2003); Immanuel and Doyle-III (2005) and Poon et al. (2008).

Moreover, the aggregation kernel is the most important function of the population balance equation of an aggregation process and it represents the fraction of two

aggregating particles per unit time. Determining the aggregation kernel has been a core element of many studies (Adetayo and Ennis, 1997, 2000; Lui and Litster, 2002; Tan et al., 2004a).

Adetayo and Ennis (1997) presented a physical based kernel for population balance modelling of granule growth by coalescence. They used a size-independent kernel in which all collisions with an effective average granule size less than a critical value are successful. Furthermore, in their paper Adetayo and Ennis (2000) considered a new generation coalescence kernel that is capable of modeling various seemingly contradictory experimental observations. They proposed a growth model using a constant kernel with a cut-off size.

On the other hand, Lui and Litster (2002) developed a more generalized coalescence kernel from the physical properties of the granules and binder liquid. It was found that the effect of granule size on coalescence is not monotonic and is dependent on the granule and binder properties.

4.3.1 Aggregation equation

Aggregation processes take place in many engineering processes and throughout nature. Some examples of aggregation processes are; coalescence between droplets or bubbles in a wide variety of dispersed phase systems in industrial processes, coalescence of water vapour droplets in the atmosphere, which result in the formation of rain from clouds, aggregation between cells in biological processes and aggregation of particles in the manufacture of foods and pharmaceuticals.

A general form of the continuous aggregation equation for a batch system can be

given as;

$$\frac{\partial f(x,t)}{\partial t} = \frac{1}{2}\int_0^x a(x-\epsilon,\epsilon,t)f(x-\epsilon,t)f(\epsilon,t)d\epsilon - f(x,t)\int_0^\infty a(x,\epsilon,t)f(\epsilon,t)d\epsilon \tag{4.8}$$

where $f(x,t)$ is the size distribution of particles at time t, $a(x,\epsilon)$ is the aggregation kernel of aggregating particles of size x and ϵ.

Equation (4.8) states that the change in the number of particles of size x over an incremental time step at time t depends on the number of new particles of size x produced by aggregation of particles smaller than x, and depends on the average number of particles lost by aggregation of particles of size x.

The first integral part of the right hand side of equation (4.8) represents *aggregation birth* for particle of size x. That is, particles of size $x-\epsilon$ and ϵ aggregate to form a new particle of size x. The second integral part of the right hand side of equation (4.8) represents *aggregation death* for particle of size x. In other words, particles of size x and ϵ aggregate to produce a new particle of size $x+\epsilon$. Figure 4.4 shows the aggregation birth and breakage death for particle of size x.

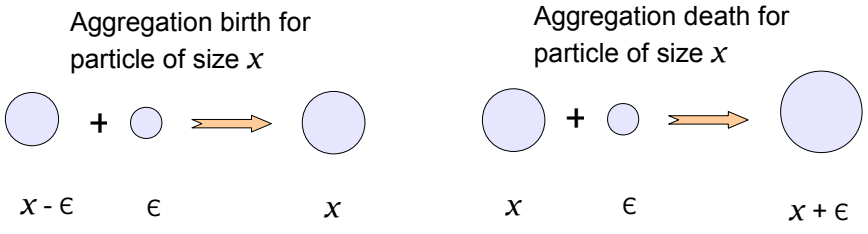

Figure 4.4: Aggregation birth and death for a particle of size x.

In their work Sastry and Fuerstenau (1975) subdivided the aggregation kernel $a(x,\epsilon)$ into two parts to create a consruct which has been widely used in the literature;

$$a(x,\epsilon) = a_0 a^*(x,\epsilon) \tag{4.9}$$

where a_0, which is the rate constant and the size independent part, and a^* is the size dependent part. A list of aggregation kernels proposed in the literature is given in Table 4.4.

Table 4.4: Aggregation kernels proposed in the literature.

$a(x,\epsilon)$	Source
a_0	Kapur and Fuerstenau (1969)
$a_0 \frac{(x+\epsilon)^\alpha}{(x\epsilon)^\beta}$	Kapur (1972)
$a_0 \frac{(x^{2/3}+\epsilon^{2/3}}{\frac{1}{x}+\frac{1}{\epsilon}}$	Sastry and Fuerstenau (1975)
$a_0(\frac{1}{x}+\frac{1}{\epsilon})^{1/2}(x^{1/3}+\epsilon^{1/3})^2$	Friedlander (2000)
$\begin{cases} a_0, & \frac{(x\epsilon)^\alpha}{(x+\epsilon)^\beta} \leq w^*; \\ 0, & \frac{(x\epsilon)^\alpha}{(x+\epsilon)^\beta} > w^*. \end{cases}$ w^* is the critical granule size.	Adetayo and Ennis (1997)
$a_0(x+y)^2\sqrt{\frac{1}{x^3}+\frac{1}{y^3}}$	Hounslow (1998)

Additionally, three basic aggregation kernels can be stated as follows;

i) Constant kernel: Aggregation rate of all particles equals a constant.

$$a(x,\epsilon) = a_0$$

ii) Linear kernel: Aggregation rate of particles is directly proportional to their total volume.

$$a(x,\epsilon) = a_0(x+\epsilon)$$

iii) Product kernel: Aggregation rate of particles is directly proportional to the product of their volumes.

$$a(x, \epsilon) = a_0 x \epsilon$$

4.3.2 Discretized population balance for aggregation equation

The structure of population balance equations incorporate partial integral differential equations. The framework of these equations is complex and analytical solutions may be impossible. However, some simplified approaches which make the solution of population balance equations possible, have been developed in the literature (Hidy and Lilly, 1965; Gelbard and Seinfeld, 1980; Batterham et al., 1981; Hill and Ng, 1996; Hounslow et al., 1988; Vanni, 2000).

The underlying basis of discretization is to turn the main population balance of integro-differential equations into ordinary differential equations. To achieve this, the integral signs of the continuous equation (4.8) are turned to summation signs, and continuous functions are replaced by corresponding discrete functions;

$$\frac{dN_i}{dt} = \frac{1}{2} \sum_{j=1}^{i-1} a_{j,i-j} N_j N_{i-j} - N_i \sum_{j=1}^{\infty} a_{i,j} N_j \tag{4.10}$$

where N_i is the number of particles in the interval i and $a_{i,j}$ is the discrete aggregation kernel of the particles in the intervals i and j.

There should be a finite state space to model the system, that is j cannot be increased to infinity in the second part of right hand side of equation (4.10). On this basis, two realistic approaches can be described as follows;

i) A maximum particle size x_{max} that can be realised in the process is assigned; that is, any two particles cannot aggregate if their total size is greater then x_{max}. This kind of limitation is encountered for example, where if aggregation occurs in a pipe or similar geometry where physical parameters mostly determine the maximum particle size. If the maximum state is represented by n^{th} state, then equation (4.10) can be rewritten as;

$$\frac{dN_i}{dt} = \frac{1}{2}\sum_{j=1}^{i-1} a_{j,i-j} N_j N_{i-j} - N_i \sum_{j=1}^{n-i} a_{i,j} N_j \tag{4.11}$$

Equation (4.11) produces some restrictions on particle aggregation. If the maximum state number n=40 and i=5, a particle in the interval 5 cannot aggregate with another particle in the interval j when $i + j > 40$, such as 36, 37, 38, 39, 40.

ii) A maximum particle size x_{max} that is represented by n^{th} interval can join to aggregation process is defined; that is, the maximum aggregated particle size can be $2x_{max}$. If the intervals are created by using a uniform method, then the total number of intervals will be $2n$. Thus, equation (4.10) can be defined as;

$$\frac{dN_i}{dt} = \frac{1}{2}\sum_{j=1}^{i-1} a_{j,i-j} N_j N_{i-j} - N_i \sum_{j=1}^{n} a_{i,j} N_j \tag{4.12}$$

Hidy and Lilly (1965) contributed numerical solutions of population balance equations while Gelbard and Seinfeld (1980) developed a discrete method to predict a single property of the particle such as total number or volume. Hill and Ng (1996) presented a new discretization procedure for an aggregation equation where they mitigated the intrinsic problems encountered through discretization by using proper probability density functions. Moreover, Hounslow et al. (1988) published a discrete solution of nucleation, growth and aggregation equations for a crystallization process. On the other hand, Vanni (2000) discussed the characteristics of approximate methods for

modelling aggregation by considering their accuracy, ability to produce error estimates, ease of implementation and speed.

The quadrature method of moments was tested for size-dependent growth and aggregation by Marchisio et al. (2003). They have been validated this method by comparison with both Monte Carlo simulations and analytical solutions using several functional forms for the aggregation kernel.

Darelius et al. (2005) used a population balance approach based on splitting the coalescence kernel into two factors, the first describing the collision frequency of particles and the second describing the collision efficiency. They applied this coalescence kernel to modelling wet granulation in a high shear mixer.

In their work, Tan et al. (2004a) have demonstrated how a growth kernel can be derived based on the principle of kinetic theory of granular flow. They used the equipartition of kinetic energy (EKE) kernel to describe the evolution of granule size distributions in fluidized bed granulation

Immanuel and Doyle-III (2005) presented an effective and robust technique for the numerical solution of three-dimensional population balance models describing granulation processes. Simpler forms of the aggregation kernels were employed in their study.

A three-dimensional population balance model was discussed for wet granulation by Poon et al. (2008) who tried to capture particle level phenomena and their influence on the population-level behaviour. The particle size, binder content, and porosity of the granules were used as the three dimensions of population distribution. These three particle dimensions are represented in terms of three equivalent traits, namely, the solid volume, liquid volume and gas volume of the granules in formulation of the population balance.

4.4 Solution methods for population balance equations

Analytical solutions of population balance equations are available only for limited simple examples. However, a number of numerical techniques have been developed to make the solution of population balance equations possible. Moments of the particle size distribution function are frequently used in engineering calculations and it may be possible to obtain moment equations from the PBEs. Monte Carlo simulation is quite a powerful technique for the solution of PBEs in spite of its computation requirements. Discretized population balance equations can be a more effective solution technique in rapid solutions for specific applications. More detailed reviews and solution techniques of PBEs are available in Ramkrishna (2000). A list of methods for the solution of population balance equations is given as follows;

The Method of Laplace Transformations The population balance equation in particle mass, having a convolution integral in the death function, can be solved by Laplace transforms in integration systems. It is suitable to use Laplace transforms in order to obtain the analytical solutions for such population balance equations.

Monte-Carlo Simulation Monte-Carlo simulation is based on solving certain population balance equations by using random numbers. The appearance of new particles and disappearance of existing particles in the population domain in a process are generally random with specified probability. A sample path of the process can be created by artificially generating random variables that satisfy the specified probability laws of change. The mean behavior of the system can be calculated by averaging all of the sample paths.

Discrete Formulations Derivatives and integrals can be represented by finite dif-

ference methods in order to provide a discretization of particle state space for a direct solution of the population balance equation. Discretization of particle size is written by numerical consideration in approximating the integral or the derivative.

The Method of Successive Approximations The method of successive approximations (or Picard iteration) provides a method that can, in principle be used to solve any initial value problem. In this method, the value of an unknown quantity can be estimated by repeated comparison to a sequence of known quantities.

The Method of Moments and Weighted Residuals Calculating the moments of the number density function may be practical in some population balance equations. The calculation of moments can be done by taking the moments of such population balance equations which produce a set of moment equations.

Chapter 5

High Shear Granulation

This chapter concerns granola production through aggregation in a high shear mixer and involves developing a corresponding growth model. Firstly, an introduction to high shear granulation will be provided. Secondly, materials and methods will be introduced. Thereafter, a model describing change in particle size of granola during high shear mixing will be proposed. Finally, results and discussion will be presented and conclusions will be drawn.

5.1 Introduction

High shear mixer granulators are used in a broad range of industries including chemicals, detergents, food, pharmaceutical and ceramics. Mixer granulators include an agitator in order to mix particles and a chopper which helps to break down larger granules. A liquid binder is added to bind the particles.

Impellers typically rotate at tip speeds of approximately $5-15\ ms^{-1}$ which correspond to around $100-1500\ \mathrm{rpm}$. Choppers rotate at similar tip speeds but because of their smaller diameter the rate of revolutions is between 1500-4000rpm. The process stages

in a typical high shear mixer are as follows:

- mixing of dry materials with high speed impeller and chopper for 2–3 minutes.
- addition of a liquid binder either by pouring, pumping or spraying onto the materials with a constant impeller and chopper speed for 1-2 minutes.
- wet massing with high impeller and chopper speed for 5-15 minutes
- discharge of wet granules
- drying the granules

The above steps are typical though production parameters and may vary from product to product in terms of binder addition rate, times for each of the stages and impeller and chopper speeds.

5.2 Materials and Methods

Granola is a baked crispy food product where oats, other cereals and nuts are bound together with a binder, in this case honey, water and oil, to form a structured unit aggregate. The granola ingredients in this study were carefully selected for their high nutritional value. These include oat flakes, corn flakes, puffed rice, malted buckwheat, malted barley, brown sugar, oat beta glucan, wheat germ and inulin. A mixture of honey, water and oil was used as a binding agent. Detailed ingredient proportions are displayed in Table 1.1 of Chapter 1.

Aggregation of the granola ingredients takes place in a high shear mixer (Procept, 4M8, Belgium). Figure 5.1 shows the high shear mixer used. The mixing chamber is a glass bowl. The bolt are provided at the top of the bowl permits the loading as well

as emptying of the mixer. The impeller and chopper are both positioned vertically (Figure 5.2). The impeller is 17 cm in depth and the blade of impeller is 8 cm in length having a 45^o inclination. Geometric details of the high shear mixer are provided in Table 5.1.

Figure 5.1: Laboratory scale of the high shear mixer.

The dry ingredients (Table 1.1) were added to the high shear granulator, and pre mixed over a 2 minute period at impeller rotation speeds of either 150 rpm, 200 rpm and 300 rpm and at chopper speed 500 rpm. These impeller rotation speeds were chosen because preliminary granulation trials showed that at an impeller speed of 100 rpm and a wet massing period of 3 minutes, granules were not formed. Batch size was 100g in each case. This was followed by the binder addition step (at the same impeller and chopper speeds), whereby the binder was poured onto the rotating ingredient bed at rates of either 0.22 gs^{-1}, 0.33 gs^{-1} and 0.65 gs^{-1}. A honey-water mixture (95:5) was used as the binder. Total binder addition was 32 g for all runs,

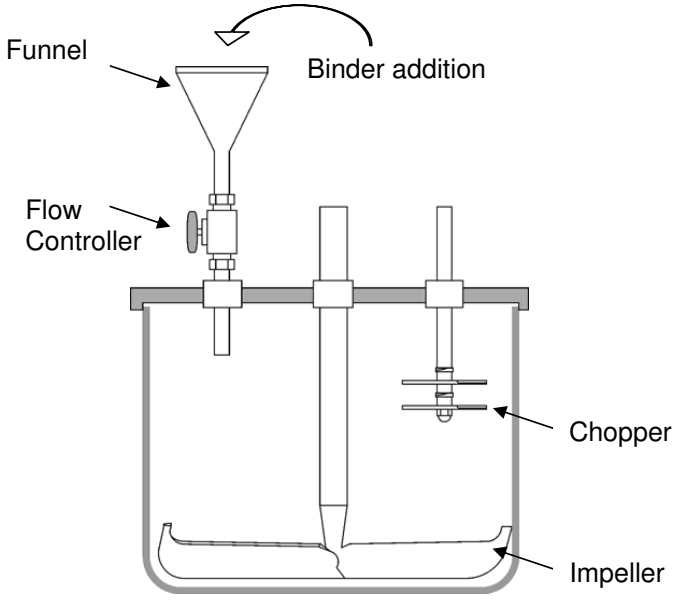

Figure 5.2: A schematic diagram of the high shear mixer.

though addition time varied with addition rates. For all the granulation experiments the same composition of the binder solution was used. After adding the binder, the mixture was wet massed for a period of 6, 9 and 12 minutes at the respective impeller speeds. The purpose of wet massing phase is to distribute the liquid / binder system evenly throughout the system. The resultant wet granules were taken from the mixer and spread on a tray and dried in an oven at 160^oC for 10 min followed by a period of cooling in a desiccator over 30 minutes.

Table 5.1: Geometry of the high shear mixer.

Component	size
Impeller depth	$17\ cm$
Impeller blade width	$2.5\ cm$
Impeller blade inclination	45^o
Impeller blade length	$8\ cm$
Bowl diameter	$17\ cm$
Bowl depth	$18\ cm$
Chopper depth	$14.5\ cm$

5.2.1 Particle size measurements

A Camsizer (Retsch, Germany) digital image analyzer was used for measuring particle size distributions and aggregate relative density. D_{10}, D_{50} and D_{90} sizes were recorded. This unit can also produce particle images. It is possible to measure the particle sizes in the range $30\mu m$ to $30mm$ with a high degree of accuracy using the Camsizer.

The Camsizer operates by means of two CCD (Charge-Coupled Device) cameras, a basic camera (CCD-B) which records large particles and a zoom camera (CCD-Z) which records the small ones (Figure 5.3). There are three possible options for measurement: measurements using CCD-B, measurements using CCD-Z and measurements using both cameras. The measuring range of CCD-B is approximately $400\mu m$ to $30mm$. The measuring range of CCD-Z ranges from $30\mu m$ up to approximately $3mm$.

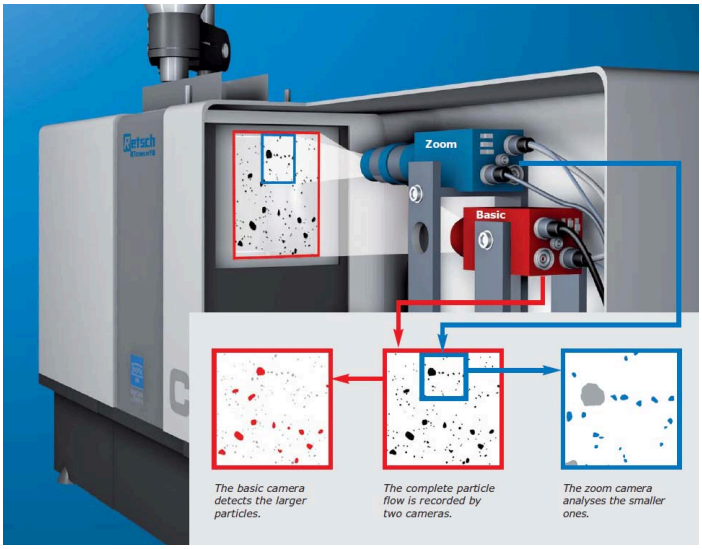

Figure 5.3: Positions of two cameras in the Camsizer.

The sample is fed in from the feed channel so that all particles fall through the measurement field by a vibrating feeder (Figure 5.4). The contact-free optical measurement is carried out in real time and simultaneously obtains all the required information

about particle size and particle shape. After the digital images have been processed electronically, the analytical results are saved in more than 1,000 size classes according to the density of information. The feed hopper has a capacity of 3.5 liters. The 75 mm feed chute helps to measure very big particles.

Figure 5.4: The Camsizer unit.

5.2.2 Textural properties

Textural properties of samples were measured using a TA-XT2i texture analyzer (Stable Microsystems Ltd, Godalming, UK) equipped with an SMS P/75 compression platen (d = 75 mm) and 50 kg load cell. A flat-ended cylindrical stainless steel plate having 75 mm diameter was used for compression. The sample is placed on the lower plate of the instrument and the flat-ended cylindrical plate moves downwards until it reaches a distance of 15 mm at a constant speed of 1.0 mms^{-1}. Each sample was measured in 5 replicates. During the test run, the resistance of the sample was recorded and plotted on a force (N) versus distance (mm) plot. The hardness and crispness of granola were measured. The hardness is defined as the maximum applied force, beyond which the granola starts to permanently deform during the compression.

Crispness is related to the brittleness of the granulation. In technical terms the slope of the force curve over distance determines the level of crispness.

5.3 Growth Model

Broadly, it can be stated that granule growth is controlled by the balance between the granule strength and the shearing forces in high shear mixers. If the granule strength is high enough to resist the shearing forces of the impeller then the growth mechanism will be controlled by coalescence. If the granule strength is too low then the growth mechanism will be determined by simultaneous coalescence and breakage of the aggregates. In addition, if the binder has sufficiently high viscosity (approximately larger than 100 mPa.s) then the breakage of agglomerates becomes insignificant (Schafer, 2001).

5.3.1 Particle Velocity

A high speed camera (AOS, X-Motion, Switzerland) (500 frames per second) was used to determine particle velocity inside the high shear mixer. Figure 5.5 shows side view of the particle motion in the mixer. When the particle meets with the blade, it is carried up to the tip of the blade and then released with a vertical (axial) velocity u_v and a horizontal (tangential) velocity u_h. Figure 5.5 (B) displays the path of the particle with respect to the blade. When the particle reaches its maximum height, it has a vertical velocity u_v and gravity force (F_g) acting on it.

The impeller tip speed for corresponding impeller revolution, which is given in Table 5.2, is calculated as;

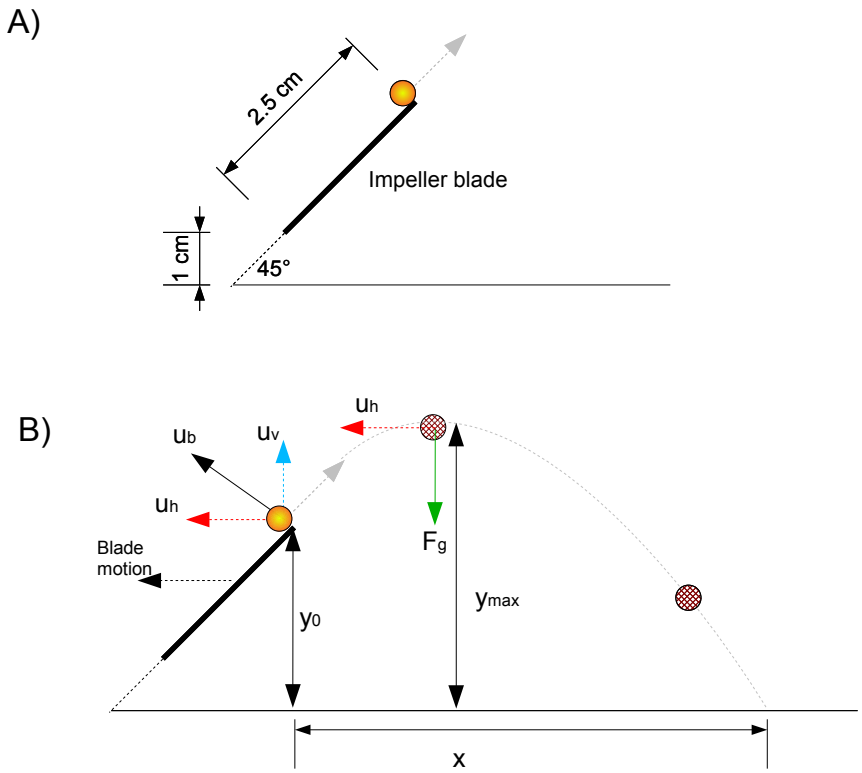

Figure 5.5: A schematic diagram of the particle velocity and forces acting on the particle in the high-shear granulator. A) The dimensions and the position of the blade. B) The path of the particle motion in the granulator with respect to the blade.

$$u = \frac{\pi D_b N}{60} \tag{5.1}$$

where u is tip speed, D_b is blade diameter and N is number of revolution per minute.

Table 5.2: Impeller rotations, corresponding impeller tip speeds and periods.

Impeller Rotation	Impeller Tip Speed	Impeller Period
150 rpm	$1.25\ ms^{-1}$	$T_1 = 0.4s$
200 rpm	$1.7\ ms^{-1}$	$T_2 = 0.3s$
300 rpm	$2.5\ ms^{-1}$	$T_3 = 0.2s$

The horizontal velocity of the particle changes because of air drag force; F_d. Otherwise the motion of the particle would be identical to the motion of the blade. Air drag force starts to apply on the particle when the particle leaves the blade. Accordingly, the tangential motion of the particle can be defined by the following equations;

$$F_d = F_{net} \tag{5.2}$$

$$F_d = -c_T(u_p - u_a)|u_p - u_a| \tag{5.3}$$

where c_T is the turbulent drag coefficient, u_p is the particle velocity and u_a is air velocity. Air velocity can be considered negligible with respect to the particle velocity and hence the equation (5.3) becomes;

$$F_d = -c_T u_p^2 \tag{5.4}$$

which is,

$$m\frac{du_p}{dt} = -c_T u_p^2 \tag{5.5}$$

where m is the particle mass and t is time.

The solution of differential equation (5.5) is calculated as;

$$u_p = \frac{m}{c_T t + mk} \qquad , \quad k = constant \tag{5.6}$$

Using the initial condition for the particle horizontal velocity;

$$u_p|_{t=0} = u_h \tag{5.7}$$

Equation (5.6) can be written as;

$$u_p = \frac{mu_h}{u_h c_T t + m} \tag{5.8}$$

Single Particle Reynolds number

Single particle Reynolds number can be calculated according to the following equation (Turton and Levenspiel, 1986);

$$Re_p = \frac{dU\rho_a}{\mu} \tag{5.9}$$

where d is diameter of the particle, U is the relative velocity, ρ_a is the air density and

μ_a is the dynamic viscosity of air.

The value of c_T can be found as follows;

$$c_T = 0.5 C_d \rho_a A_p \tag{5.10}$$

where C_d is drag coefficient ρ_a is air density and A_p is cross-section area of the particle.

If $Re_p > 500$ then the particle is in Newton's law region and $C_d = 0.44$ (Turton and Levenspiel, 1986). The average particle area calculated for diameter of size 0.5 cm as, $A_p = 0.25\pi cm^2$. Accordingly, c_T can be written as;

$$c_T = 6.6\pi \times 10^{-6}\ (\mathrm{kg\ m^{-1}}) = 20.74 \times 10^{-6} \tag{5.11}$$

An average mass of a particle of diameter $0.5cm$ is $0.07g = 7 \times 10^{-5} kg$.

Using equation (5.8) the particle velocity is calculated in terms of the impeller speed of u_h as;

$$u_p = \frac{7 \times 10^{-5} \times u_h}{u_h \times 20.74 \times 10^{-6} t + 7 \times 10^{-5}} \tag{5.12}$$

or by simplification;

$$u_p = \frac{u_h}{0.3 u_h t + 1} \tag{5.13}$$

The velocity of the particle is changed when it is hit by a blade. There are three blades

in the system and when the particle hit by one blade there will be a time difference τ until being hit by the next blade. The angular displacement between one blade and the following blade equals to

$$S = r\theta \tag{5.14}$$

where θ is the distance between two consecutive blades and r is the radius of the blade;

$$\theta = \frac{2\pi}{3} \qquad \text{and} \qquad r = 0.08m$$

which yields,

$$S = \frac{16 \times 10^{-2}\pi}{3} \tag{5.15}$$

Thus, the time difference τ can be calculated using the following relationship;

$$(u_b - u_p)\tau = \frac{16 \times 10^{-2}\pi}{3} \tag{5.16}$$

$$\left(u_b - \frac{u_h}{0.3u_h\tau + 1}\right)\tau = \frac{16 \times 10^{-2}\pi}{3} \tag{5.17}$$

Note that $u_h = u_b/\sqrt{2}$ because of an angle of 45^o of the blade. Thus,

$$\left(u_b - \frac{u_b}{0.3u_b\tau + \sqrt{2}}\right)\tau = \frac{16 \times 10^{-2}\pi}{3} \tag{5.18}$$

Equation (5.18) can be solved for τ by using three different impeller tip speeds. For the first case the impeller tip speed is $1.25\ ms^{-1}$;

$$\left(1.25 - \frac{1.25}{0.3 \times 1.25\tau_1 + \sqrt{2}}\right)\tau_1 = \frac{16 \times 10^{-2}\pi}{3} \tag{5.19}$$

which results in $\tau_1 = 0.37s$

For the second case the impeller tip speed is $1.7\ ms^{-1}$;

$$\left(1.7 - \frac{1.7}{0.3 \times 1.7\tau_2 + \sqrt{2}}\right)\tau_2 = \frac{16 \times 10^{-2}\pi}{3} \tag{5.20}$$

which results in $\tau_2 = 0.27s$

For the last case the impeller tip speed is $2.5\ ms^{-1}$;

$$\left(2.5 - \frac{2.5}{0.3 \times 2.5\tau_3 + \sqrt{2}}\right)\tau_3 = \frac{16 \times 10^{-2}\pi}{3} \tag{5.21}$$

which results in $\tau_3 = 0.18s$

The particle is hit by the blade each τ time. Therefore equation (5.13) can be written as;

$$u_p = \frac{u_h}{0.3u_h \mathrm{mod(t,\ } \tau) + 1} \tag{5.22}$$

5.3.2 Binder layer thickness

The binder layer thickness is calculated by the following equation (Lui et al., 2000);

$$h = \begin{cases} \dfrac{D(\upsilon - \varepsilon s^*)}{6} & \text{if } \upsilon > \varepsilon s^* \\ 0 & \text{if } \upsilon < \varepsilon s^* \end{cases} \tag{5.23}$$

where D is the diameter of the granule, ε is the granule porosity, s^* is the granule saturation at which a surface binder layer first appears and it should theoretically be unity and υ is the volume fraction of binder in the granule (i.e. $\upsilon{=}\varepsilon s$ where s is the granule saturation which is the ratio of binder to pore volume).

In the case of this work, the volume fraction of binder in the granule, υ, can be written as a function of volumetric binder addition rate. The volumetric binder addition rate, V_{br}, can be found from the binder mass flow rate, b_r. The binder thickness layer will increase during the binder addition time. Thus, the volume fraction of binder in the granule,υ, will be of following form;

$$\upsilon = \frac{\varepsilon(V_{br}t^*)}{\varepsilon_v} \tag{5.24}$$

where ε_v is the pore volume and t^* is the binder addition time increment until the binder addition ceases. Note that the wet massing time starts after the binder addition and no significant granule growth was observed until all binder has been added.

Table 5.3: Parameters used in evaluation of binder thickness.

Binder viscosity	$\mu_b = 1.47\ Pa.s$
Binder density	$\rho_b = 1230\ kgm^{-3}$
Pore volume	$\varepsilon_v = 20 \times 10^{-6}\ m^3$
Dry ingredients volume	$V_i = 160 \times 10^{-6}\ m^3$
Porosity	$\varepsilon = \frac{20\times10^{-6}}{160\times10^{-6}} = 0.125$

Parameters used in evaluation of binder thickness are displayed in Table 5.3. The binder mass flow rates and the corresponding volumetric binder addition rates are given in Table 5.4;

Table 5.4: Binder mass flow rates and corresponding volumetric binder addition rates used in experimentations.

Binder mass flow rates	Volumetric binder addition rates
$0.22gs^{-1} = 22 \times 10^{-4}\ kgs^{-1}$	$V_{br} = 0.18 \times 10^{-6}\ m^3s^{-1}$
$0.33gs^{-1} = 33 \times 10^{-4}\ kgs^{-1}$	$V_{br} = 0.27 \times 10^{-6}\ m^3s^{-1}$
$0.65gs^{-1} = 65 \times 10^{-4}\ kgs^{-1}$	$V_{br} = 0.53 \times 10^{-6}\ m^3s^{-1}$

5.3.3 Coefficient of restitution

The coefficient of restitution, e, of the granules is the ratio of the separation velocities after collision to the approaching velocities of two colliding granules. It can also be found by the square root ratio of the bounce height to the drop height of the granule. Using a high speed camera the coefficient of restitutions of an average granule size is found as;

$e = 0.32$ (bounce height $\sim$ 2cm and drop height=20cm) for granule-stainless steel

impact.

$e = 0.30$ (bounce height $\sim$ 1.8cm and drop height=20cm) for granule-glass impact.

$e = 0.17$ (bounce height $\sim$ 0.6cm and drop height=20cm) for granule-granule impact.

An average coefficient of restitution was found in order to use in model. Various sizes of granules were used with 5 repetitions. The effect of rotation or spinning was ignored.

5.3.4 Granule Surface roughness

1) Particle image analysis: Particle image was analyzed using high speed camera (AOS, X–Motion, Switzerland) by drawing a perfect circle around the particle as shown in Figure 5.6.

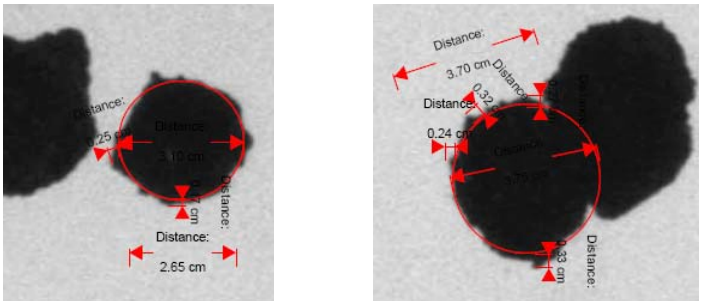

Figure 5.6: Surface asperity measurement by image analysis.

According to the calculations, an approximate surface asperity was found as;

$$h_a \approx 0.01 \times D$$

2) Surface roughness device: The surface roughness device was used for a flattish surface of the granules. The results were found as 9 micron, 12 micron, 18 micron, 23 micron and 25 micron for different particle sizes. This makes the surface asperity

to be,

$$h_a \approx 0.009D$$

As a result, the surface asperity was taken as;

$$h_a = 0.01 \times D \tag{5.25}$$

Equation (5.25)is based on experimental measurements.

5.3.5 The Coalescence model

Particle size growth of granola in high shear mixer was modeled using viscous Stokes number (St) and the corresponding critical Stokes number (St^*). Calculations were carried out using D_{50} values as a representative particle size of the granola since D_{10} and D_{90} values broadly track D_{50} values for the system under investigation. The amount of change in median granule size (D_{50}) was considered to be a function of Stokes and critical Stokes number (Ennis et al., 1991) which include certain physical parameters of the system such as impeller speeds, binder addition rate and time. Accordingly, the model has the following structure;

$$\frac{dD(t)}{dt} = K(u)\left(\frac{St_v^* - St_v}{St_v^*}\right) \tag{5.26}$$

or in discrete case;

$$\Delta D = D(t + \Delta t) - D(t) = K(u)\left(\frac{St_v^* - St_v}{St_v^*}\right)\Delta t \tag{5.27}$$

where $K(u)$ is a function of granule velocity. St_v and St_v^* have the following form respectively (Ennis et al., 1991);

$$St_v = \frac{4\rho_g u D}{9\mu_b} \tag{5.28}$$

$$St_v^* = \left(1 + \frac{1}{e}\right) ln\left(\frac{h}{h_a}\right) \tag{5.29}$$

where ρ_g is the granule density, u is the granule velocity, D is the granule diameter (D_{50}), μ_b is the binder viscosity, e is the coefficient of restitution for dry granules, h is the binder thickness and h_a is the granule surface asperity.

The function $K(u)$ in equation (5.27) was found as;

$$K(u) = 8.5 \times 10^{-5} u \tag{5.30}$$

Equation (5.30) was used for data fitting of the model to the experimental results.

The open form of the equation (5.27) might be written as;

$$\Delta D = 8.5 \times 10^{-5} u \times \frac{\left(1 + \frac{1}{e}\right) ln\left(\frac{h}{h_a}\right) - \frac{4\rho_g u D}{9\mu_b}}{\left(1 + \frac{1}{e}\right) ln\left(\frac{h}{h_a}\right)} \Delta t \tag{5.31}$$

Finally, the granule diameter, D, is calculated as;

$$D = D_0 + \Delta D \tag{5.32}$$

5.4 Results and Discussion

The granola growth has been examined at three different impeller speeds; 150 rpm, 200 rpm and 300 rpm, at various binder addition rates; 0.22 g/s, 0.33 g/s and 0.65 g/s. Equation (5.27) was employed for the modelling median aggregate diameter of these nine different cases.

The solution of equation (5.27) was carried out using numerical analysis. For the necessary calculations of critical Stokes number, equations (5.23), (5.24) and (5.25) were invoked into the equation (5.29), while equation (5.28) was used to find the Stokes number. The function $K(u)$ which is a function of granule velocity (impeller speed) in equation (5.27) was employed as a model coefficient to minimize the difference between the experimental results and model estimation via a least squares error technique. $K(u)$ values for each impeller speed applied are shown in Table 5.5.

Table 5.5: $K(u)$ values at different impeller speeds.

$K_{150} = 10.63 \times 10^{-5}$
$K_{200} = 14.45 \times 10^{-5}$
$K_{300} = 21.25 \times 10^{-5}$

The results for median size (D_{50}) of granola produced at 300 rpm at different binder addition rates are displayed in Figure 5.7. Among the three binder addition rates, the model correlates best with the experimental results for the case of 0.22 g/s binder addition rate. The model estimates are over–predicted at the binder addition rate of 0.33 g/s while its estimates are less than the experimental results at the 0.65 g/s binder addition rate. As binder addition rate increases, the time required to fill in intra-granular spaces decreases. This may help explain why when a relatively high impeller speed is employed the actual rate of growth at the highest binder addition

rate is significantly higher than what the model predicts.

Comparisons of the growth model and the experimental results at 200 rpm at a binder addition rates of 0.22 g/s, 0.33 g/s and 0.65 g/s are depicted in Figure 5.8. Although, the overall agreement is reasonable, the model estimates more rapid growth than the experimental results after 9 minutes of the process,but lower growth rates earlier in the wet massing period.

The experimental and model results at 150 rpm at different binder addition rates are shown in Figure 5.9. The model predicts the experimental results with a fair degree of accuracy at the binder addition rates of 0.22 g/s and 0.33 g/s. However, the model results diverge from the experimental results in a similar fashion to those at 200 rpm, underpredicting in the early stages of wet massing and overpredicting after 9 minutes.

Aggregation of granola is a complex process due to the natural variation inherent in the ingredients. There are fine particles (e.g. inulin, oat beta glucan) as well as large and fragile particles (e.g. puffed rice and corn flakes). For that reason, it is difficult to get the same results even if applying exactly same experimental parameters. In general, the growth model reasonably tracks the experimental results at 6 and 9 minutes. However, the agreement between the model predictions and the experimental results becomes insufficient at 12 minutes. Granules become more compact over time and reduced levels of growth occurs. Whereas, in practice this steady state position appears to be achieved much earlier from about 6 minutes. Moreover, the model reaches its steady state position after approximately 15 minutes of wet massing time. The consolidation mechanism, which occurs during the granulation process, isn't considered in this model and this may be a reason for the difference between the model and the experimental results.

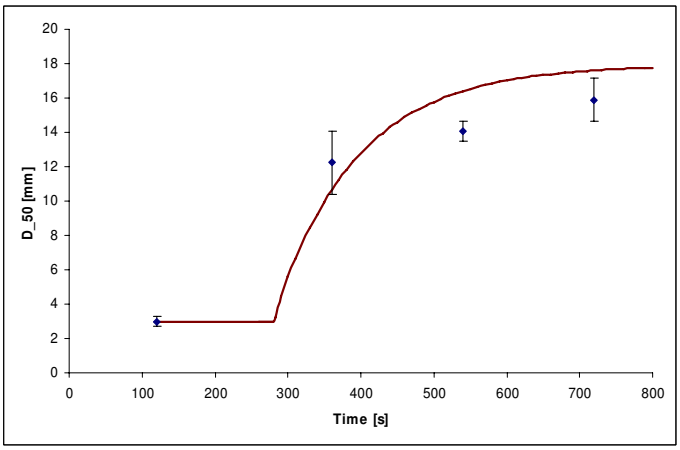

(a) 0.22 g/s

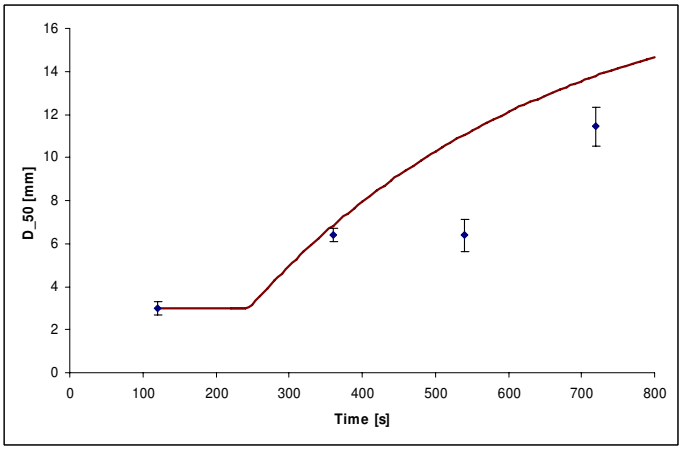

(b) 0.33 g/s

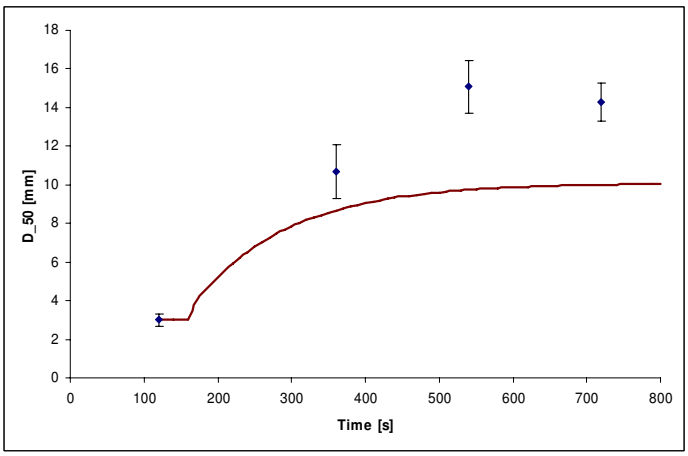

(c) 0.65 g/s

Figure 5.7: Growth model vs experimental results at 300 rpm at 0.22 g/s, 0.33 g/s and 0.65 g/s binder addition rate. (Continuous line displays model results, points are experimental data). Error bars represent standard deviations.

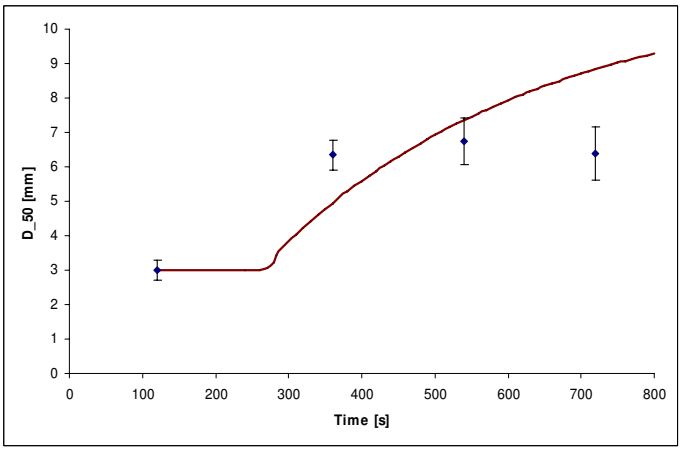

(a) 0.22 g/s

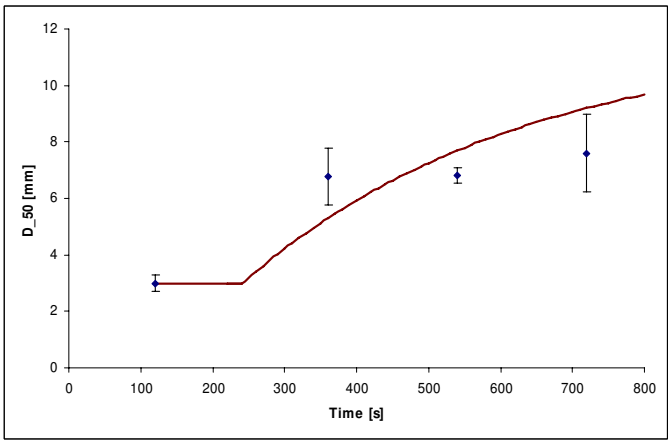

(b) 0.33 g/s

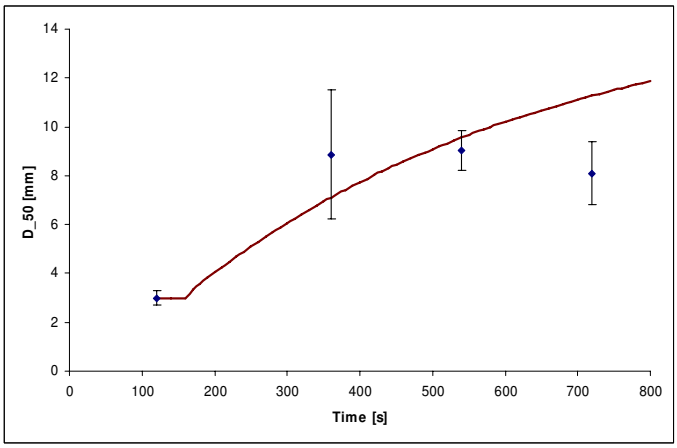

(c) 0.65 g/s

Figure 5.8: Growth model vs experimental results at 200 rpm at 0.22 g/s, 0.33 g/s and 0.65 g/s binder addition rate. (Continuous line displays model results, points are experimental data.)

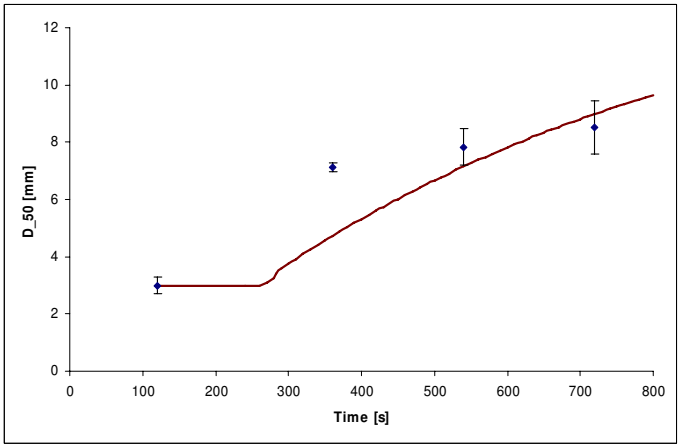

(a) 0.22 g/s

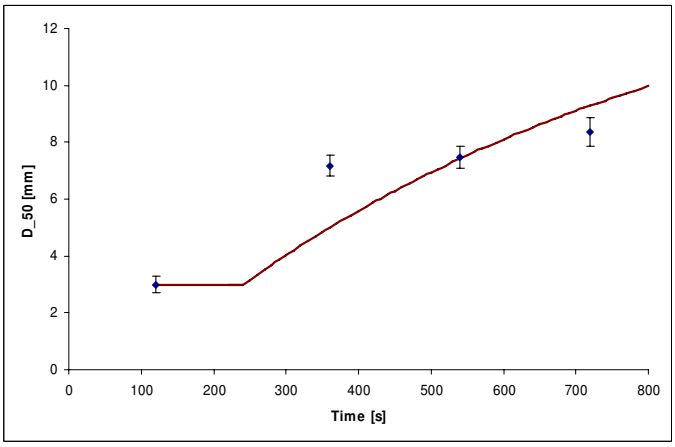

(b) 0.33 g/s

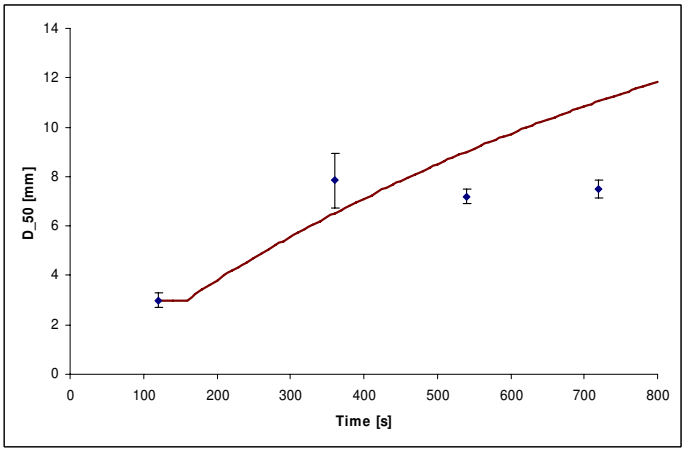

(c) 0.65 g/s

Figure 5.9: Growth model vs experimental results at 150 rpm at 0.22 g/s, 0.33 g/s and 0.65 g/s binder addition rate. (Continuous line displays model results, points are experimental data.)

5.5 Conclusion

In this chapter, a growth model based on physical properties for granola production in a high shear mixer at different impeller speeds and at different binder addition rates was developed. One key indicative particle property, namely the median particle size, was chosen as the indicative output parameter for the model. The well-known Stokes number criteria were used to predict particle coalescence in the mixer. The model includes basic physical phenomena of the system such as impeller speed, binder addition rate and coefficient of restitution. Despite it is not valid for all the cases, the granule growth was modelled to be directly proportional to the impeller speed and the binder addition rate. On the contrary, the model is inversely proportional to the binder viscosity and granule density.

Iveson and Litster (1998) defined two important types of growth behavior namely *steady growth* and *induction*. Where *steady growth* prevails the average granule size increases linearly in time. This occurs in systems in which the granules are weak and easily deform. Increasing the binder content increases the rate of growth, but produces weaker granules in nature. In general, *steady growth* occurs where particles are relatively coarse and narrowly sized and when the viscosity of binder is low. Where *induction growth* occurs, the period of growth is relatively long but stronger which are less easily deformable result. Increasing the binder content generally decreases the induction time. *Induction growth* occurs in systems where particles are fine with wide particle size distribution and the binder is generally viscous. Figure 2.4 in Chapter 2 illustrates both *steady growth* and *induction* behavior as a function of granulation time. In this work binder viscosity is high and the volume fraction of fine particles is dominant. Therefore, the model results are consistent with the induction type growth proposed by Iveson and Litster (1998).

Chapter 6

Breakage during Pneumatic Conveying; Products from High Shear Granulation

This chapter will focus on the particle breakage of granola which occurs during pneumatic conveying. After a brief introduction, materials and methods will be introduced. Thereafter, a breakage model describing the change in particle size incorporating physical phenomena based on particle motion within a conveying rig will be developed. Then, results obtained from both model and experimentation will be compared and discussed in the results and discussion section. Finally, conclusions of the work undertaken in this chapter will be provided.

6.1 Introduction

Pneumatic conveying is widely used in food processing and other process and chemical engineering applications. Particles are usually transported along a pipe system by compressed air though compressed nitrogen may be used when there is a risk of explosion. Particle breakage can be a problem during conveying, particularly if the particles involved are granular and/or friable. In general terms two breakage mechanisms for dry granules have been proposed; firstly erosion or attrition and secondly fracture or fragmentation (Iveson et al., 2001). Where erosion is the dominant breakage mechanism there results one large fragment of size close to the parent aggregate and a number of smaller fine particles. Where breakage is by fracture, this results in the production of a number of smaller fragments. In addition, the fracture type of breakage is divided into two modes; cleavage, in which parent particles break into a small number of fragments of similar size and shattering which results in many fragments over a wide range of sizes (Redner, 1990). Particle breakage is usually considered an undesirable process since it can result in reduction in particle size, in changes to the particle size distribution, dust generation and handling and storage problems which may cause the particles to not satisfy the requirement specifications any longer (Salman et al., 2003).

6.2 Materials and Methods

The aggregation of the granola ingredients (Chapter 1, Table 1.1) took place in the high shear mixer subject to impeller agitation at 150 rpm, 200 rpm and 300 rpm for 6, 9 and 12 minutes with binder flow rates of 0.22 g/sec, 0.33 g/sec and 0.65 g/sec. The aggregates were then baked in an oven for 10 minutes at 160^o.

The pneumatic conveying rig comprised a horizontal pipe of internal diameter 25 mm with different bend configurations (straight pipe, two 45^o bend and 90^o bend)(Fig. 6.1). The outer diameter of the large Perspex pipeline is 33.5 mm, giving a wall thickness of 4.25 mm. All sections of pipeline are made of transparent PMMA (Perspex), so that granola breakage and flow behaviour can be observed. The particle size distribution of the granola was measured after passage through the each rig configuration at each air pressure for various numbers of cycles.

A straight pipe was used as the first conveying rig. The straight pipeline has 1.3 m length horizontal axis and 25 mm internal diameter (Figure 6.2). Air is supplied by a compressor and regulated to deliver pressures of 200 kPa, 300 kPa and 400 kPa. The granola is fed into the apparatus by hand at the location indicated on the diagram. A soft, fine-mesh piece of cloth is used to capture the granola at the end of the rig for measurement of its particle size distribution.

A rig comprising two 45^o bends, comprised of an initial section 0.7 m long and two short sections of 0.30 m length with the same internal diameter of 25 mm was also employed (Figure 6.3). The granola is fed into the apparatus by hand at the location indicated on the diagram. A soft, fine-mesh piece of fabric is used to capture the granola at the end of the rig for measurement of its particle size distribution.

Finally, a 90^o bend conveying rig was used for propelling the granola. The initial section of the pipeline is 1 m long and a short 0.30 m length of pipeline with the same diameter as the initial section was attached to the 90^o bend (Figure 6.4).For each of the configuration average air flow velocities of $23\ ms^{-1}$, $34\ ms^{-1}$ and $42\ ms^{-1}$ were used. These correspond to applied compressed air pressures of 200 kPa, 300 kPa and 400 kPa respectively. Velocities didn't vary greatly between configurations due to the relatively large pipe diameter used. The granola is fed into the apparatus by hand at the location indicated on the diagram. A soft, fine-mesh piece of fabric is

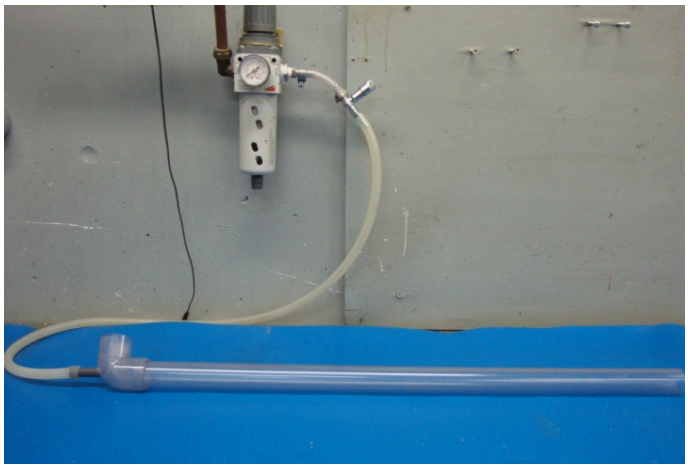

(a) A straight pipe rig

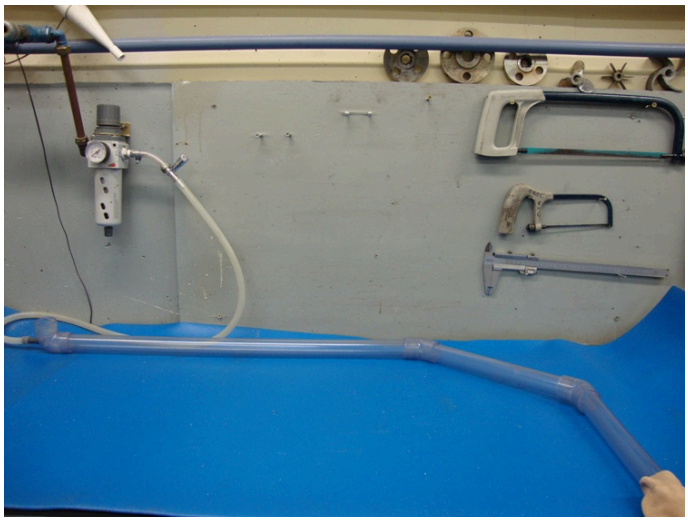

(b) A rig comprising two 45^o bends

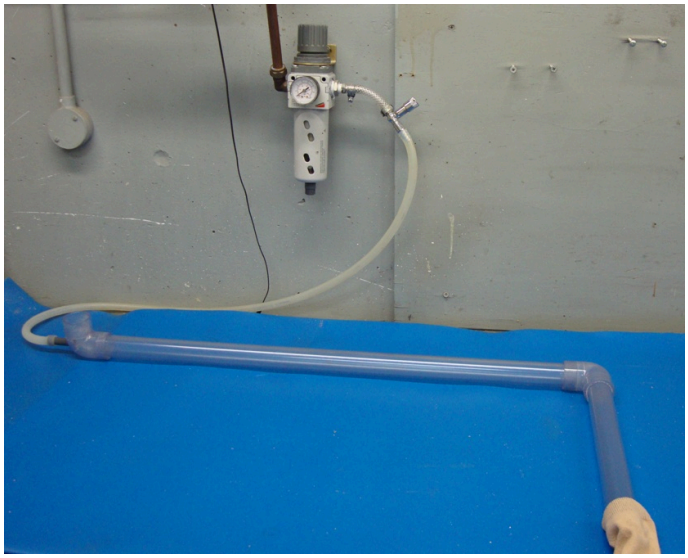

(c) A rig comprising one 90^o bend

Figure 6.1: Photograph of the pneumatic conveying rigs used in this work.

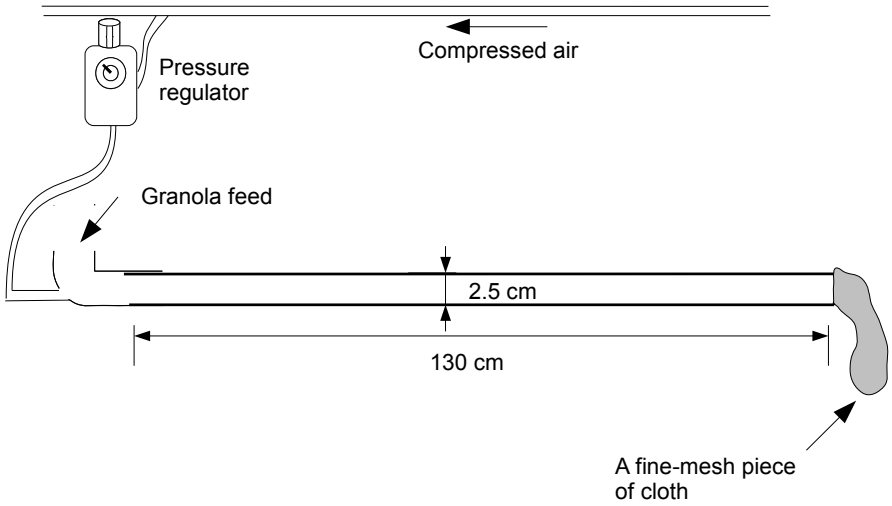

Figure 6.2: A schematic diagram of the straight pipeline used for pneumatic conveying of granola.

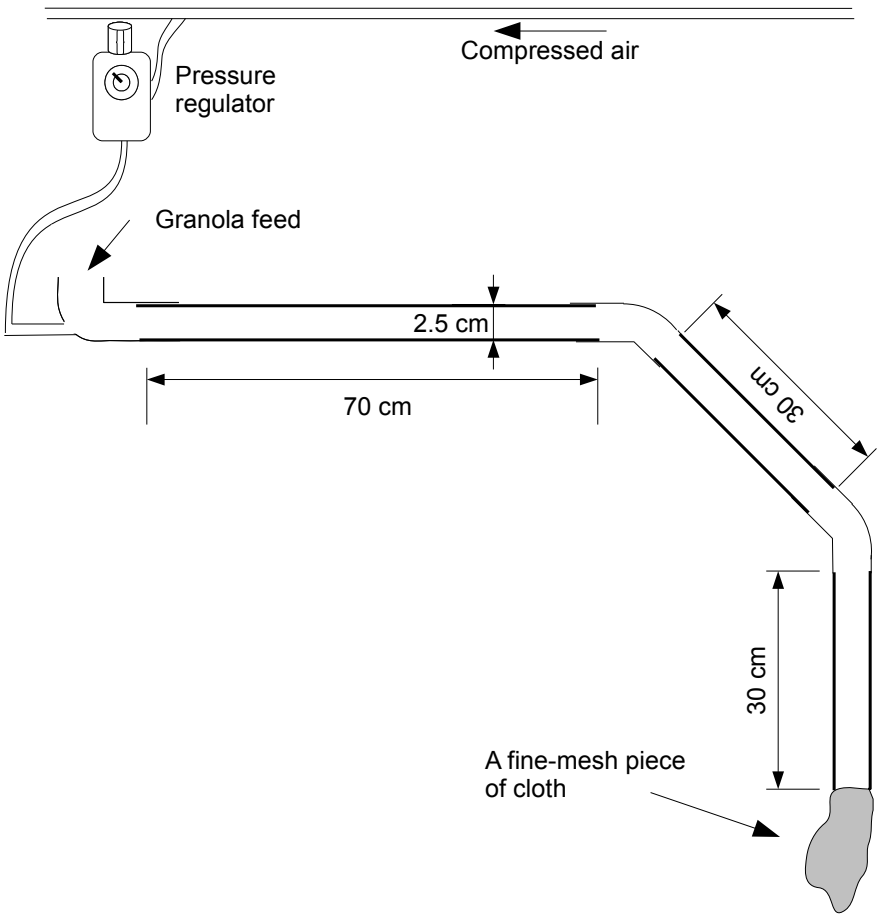

Figure 6.3: A schematic diagram of the two 45^o bend pipeline used for pneumatic conveying of granola.

used to capture the granola at the end of the rig for measurement of its particle size distribution.

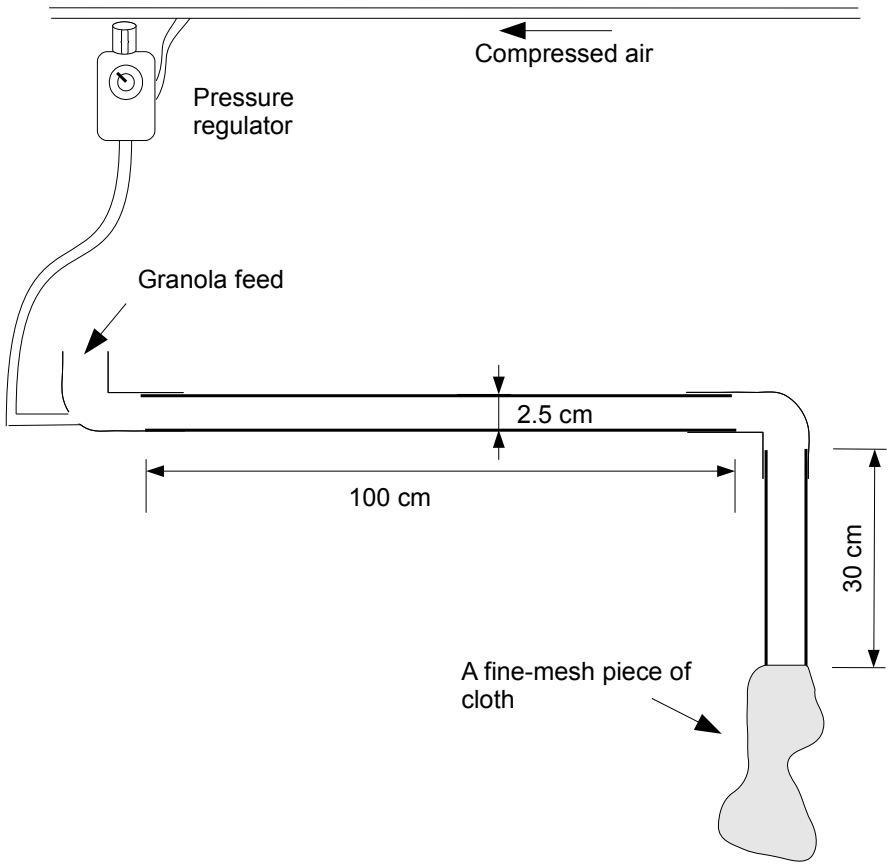

Figure 6.4: A schematic diagram of the 90^o bend pipeline used for pneumatic conveying of granola.

Moreover, the transparent PMMA (Perspex) pipeline enabled observation of the breakage behaviour of particles. Particle conveying through the pipeline was observed using a high speed camera (AOS, X-Motion, Switzerland) and visual inspection of particle flows appeared to suggest the type of breakage mechanism present.

A Camsizer (Retsch, Haan, Germany) digital image analyzer was used for measuring particle size distributions of the resultant granola before and after passage through a conveying rig where aggregates are transferred by compressed air at a number of different flow rates and for a number of passes. Since the granules produced in this work were very dense, possible breakage occurring during vibratory conveying on the

Camsizer tray was ignored.

6.3 Breakage Model

The pneumatic conveying rig comprised a horizontal pipe of internal diameter $25\ mm$ with various bend configurations (straight pipe, two 45^o bends and a 90^o bend). As already mentioned, runs were carried out by applying compressed air pressures of 200 kPa, 300 kPa and 400 kPa which resulted in air flow velocities of $23\ ms^{-1}$, $34\ ms^{-1}$ and $42\ ms^{-1}$ respectively. The particle size distribution of the granola was measured after passage through the each rig configuration at each air pressure for various numbers of cycles.

As a means of designing the breakage model, particle motion during pneumatic conveying rig was observed initially and then breakage rate of particles was defined as a function of different pipe configurations and various applied air velocities.

6.3.1 Single particle motion in pneumatic conveying

Single particle motion was examined to determine the particle impact velocity during pneumatic conveying. Figure 6.5 represents a free body diagram of a particle in the rig. The main force acting on the particle in the horizontal direction in the pneumatic conveying rig is drag force (F_d) as the air surrounding the solid particle produces a drag force of the moving particle. The horizontal velocity of the particle thus changes due to the air drag force; F_d. The net force acting on the particle equals the air drag force;

$$F_d = F_{net} \tag{6.1}$$

The magnitude and the direction of the drag force are dependent on the relative velocity of the particle with respect to the ambient fluid. The drag force is described as;

$$F_d = -c_T(u_p - u_a)|u_p - u_a| \tag{6.2}$$

where c_T is the turbulent drag factor, u_p is the particle velocity and u_a is air velocity. The absolute sign is necessary to ensure the correct direction of the drag force. The terminal velocity of the particle cannot be bigger than the air velocity and hence the maximum velocity that the particle attains equals the air velocity;

$$u_T = u_a \tag{6.3}$$

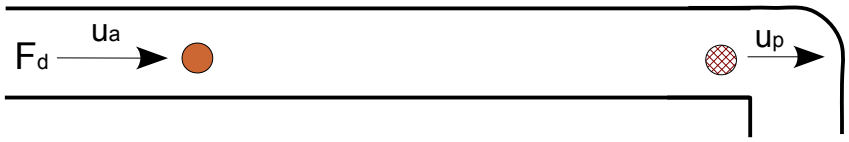

Figure 6.5: A free body diagram showing particle motion in the pneumatic conveying rig.

Since particle velocity is less than or equal to air velocity, equation (6.2) can be re-written;

$$F_d = c_T(u_a - u_p)^2 \tag{6.4}$$

The value of c_T can be found according to the following expression (Rhodes, 2008);

$$c_T = 0.5 C_d \rho_a A_p \tag{6.5}$$

where C_d is drag coefficient ρ_a is air density and A_p is cross-sectional area of the particle.

The drag coefficient is solely defined by the Reynolds number. In the literature there are several formulae used to estimate drag coefficient. A commonly used relation which is valid for Reynolds number less than 2×10^5 is given as (Turton and Levenspiel, 1986);

$$C_d = \frac{24}{Re}\left(1 + 0.173 Re^{0.657}\right) + \frac{0.413}{1 + 16300 Re^{-1.09}} \tag{6.6}$$

Reynolds number can be calculated according to the following equation;

$$Re_p = \frac{dU\rho_a}{\mu_a} \tag{6.7}$$

where

d is diameter of the particle, U is relative velocity, is fluid density, and is dynamic viscosity of air. Parameters used in evaluation of Reynolds number is given in Table 6.1. The representative diameter d is chosen as the average median size (D_{50}) prior to conveying. The other parameters in Table 6.1 represent standard values for the conditions applied.

Table 6.1: Parameters used in evaluation of Reynolds number.

d	$5 \times 10^{-3} m$
U	$\lvert u_a - u_p \rvert m/s$
ρ_a	$1.2 kg m^{-3}$
μ_a	$1.85 \times 10^{-5} Pa.s$

If $2 \times 10^5 > Re_p > 500$ then the particle is in the Newton's law region and $C_d = 0.44$ (Rhodes, 2008). If for example a particle diameter of 0.5 cm is chosen (typical of particles studies in this work) then the average particle area, $A_p = D^2\pi/4$ and for this particle c_T can be written as;

$$c_T = 0.066\pi D^2 \tag{6.8}$$

On the other hand, equation (6.4) can be written as;

$$m\frac{du_p}{dt} = c_T(u_a - u_p)^2 \tag{6.9}$$

The solution of (6.9) can be displayed as follows;

$$\frac{du_p}{(u_a - u_p)^2} = \frac{c_T}{m}dt \tag{6.10}$$

Integrating equation (6.9) gives;

$$\frac{1}{u_a - u_p} = \frac{c_T}{m}t + k \tag{6.11}$$

where k is a constant. Thus;

$$u_p = u_a - \frac{m}{c_T t + km} \tag{6.12}$$

By applying the following initial condition;

$$u_p|_{t=0} = 0 \tag{6.13}$$

the constant k is found to be $k = 1/u_a$. Thus, equation (6.12) has the following form;

$$u_p = u_a - \frac{u_a m}{u_a c_T t + m} \tag{6.14}$$

Assuming that particles are spherical and of broadly homogenous density, the mass term, m, in equation (6.14) can be written in terms of particle density, ρ_p, and diameter D as follows;

$$u_p = u_a - \frac{u_a(\rho_p D^3/6)}{u_a c_T t + (\rho_p D^3/6)} \tag{6.15}$$

By invoking (6.8), equation (6.15) will have the following form;

$$u_p = u_a - \frac{u_a \rho_p D}{0.396 u_a t + \rho_p D} \tag{6.16}$$

The displacement of the particle along the long section of the pipe (up to the bend) is formulated as follows;

$$y(t) = \int u_p(t)dt \tag{6.17}$$

which yields,

$$y(t) = u_a t - 2.525\,\rho_p\,D \ln\left(0.396\,u_a t + \rho_p\,D\right) + K \tag{6.18}$$

where K is a constant. By applying the initial condition for the displacement;

$$y(t)|_{t=0} = 0 \tag{6.19}$$

the constant K is found as;

$$K = 2.525\rho_p\ D \ln(\rho_p\ D) \tag{6.20}$$

Thus, the displacement of the particle within the pipe has the following form;

$$y(t) = u_a t - 2.525\,\rho_p\,D \ln\left(0.396\,u_a t + \rho_p\,D\right) + 2.525\rho_p\ D \ln(\rho_p\ D) \tag{6.21}$$

6.3.2 Particle impact breakage

Particle size measurements of the granola were carried out using a Camsizer (Retsch, Haan, Germany) digital image analyzer before and after passage through the conveying rig. D_{10}, D_{50} and D_{90} particle sizes were obtained as well as particle size distributions. In this study, the calculations were carried out using D_{50} values as a

representative particle size of the granola since D_{10} and D_{90} values broadly track D_{50} values for the system under investigation and D_{50} is represented as D. Each of the cycles (a single passage through the conveying rig) was considered as a time step τ; particles were conveyed a number of times (cycles) through the rig. Henceforth in this discussion for the purpose of normalizing the particle size, the change in particle size after each cycle was divided by the initial particle size. Breakage rate of the particles was obtained by dividing the normalized particle size change by time step difference;

$$b = \frac{D_i - D_\tau}{D_i \Delta\tau} \tag{6.22}$$

The breakage model is considered to be a function of particle impact force and the force required to cause breakage of the particle (the threshold particle breakage force). The particle impact force, F_i is a function of impact velocity and particle mass. The threshold force required to break the particle is related to particle hardness and hence in the case of the granola aggregates produced in the high shear granulator, to agitation impeller speed. That is,

$$F_i = Cmv_i \tag{6.23}$$

and

$$F_H \propto w \tag{6.24}$$

where C is a coefficient, v_i is impact velocity and w is the impeller agitation. Please note that (6.24) is not always true. The relationship between the impeller speed and strength of the granules depends on the range of the impeller speed among other factors.

The impact velocity was calculated using equations (6.17) and (6.21) for three dif-

ferent air flow velocities of $23\ ms^{-1}$, $34\ ms^{-1}$ and $42\ ms^{-1}$. The results are given in Table 6.2.

Table 6.2: Air flow velocities and corresponding particle impact velocity.

Applied air pressure	Air flow velocity	Impact velocity
$200\ kpa$	$23\ ms^{-1}$	$7.5\ ms^{-1}$
$300\ kpa$	$34\ ms^{-1}$	$11.2\ ms^{-1}$
$400\ kpa$	$42\ ms^{-1}$	$13.7\ ms^{-1}$

An analysis of these results reveals that the particle impact velocity is roughly one third of the applied air velocity. i.e.,

$$v_i \approx \frac{u_a}{3} \tag{6.25}$$

On the other hand, the relationship between the hardness of the granola produced at different impeller agitation is displayed in Figure 6.6. According to this figure, the hardness of granola increases with an increase in impeller agitation speed.

Accordingly, granola hardness may be considered to be an exponential function of impeller agitation speed. Thus, the threshold particle breakage force is defined as;

$$F_H = c_1 \exp(c_2 w) \tag{6.26}$$

where c_1 and c_2 are constants.

Moreover, the magnitude of impact force is related to the impact angle in the conveying rig. Salman et al. (2002) defined a relationship between impact velocity and

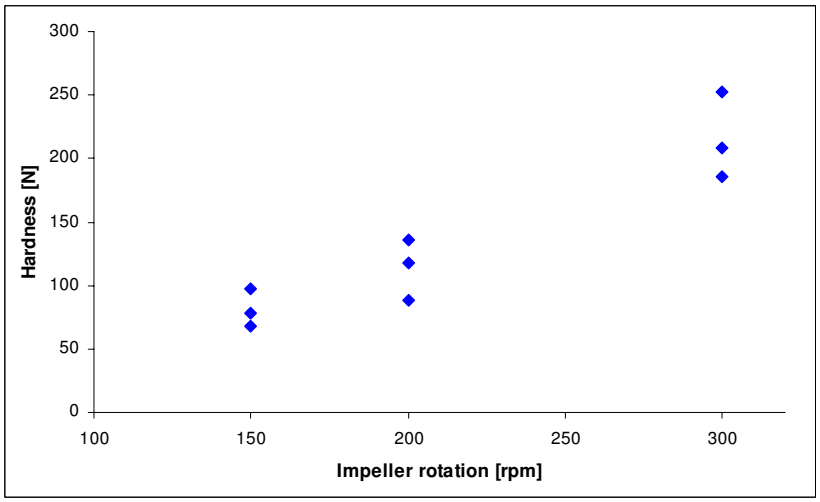

Figure 6.6: Relationship between granola hardness and impeller rotation.

unbroken particles as a function of two parameter cumulative Weilbull distribution.

$$N_0 = 100e^{-\left(\frac{\nu_i}{c}\right)^m} \tag{6.27}$$

where ν_i is the impact velocity and c and m are curve fitting parameters. The parameter m is found almost constant and the parameter c is found to vary with impact angles. From this point of view, in order to avoid an insignificant effect by the straight pipe configuration (0^o bend) on particle breakage, the impact angle was defined in the form of a Cauchy distribution. This will allow that an increase in impact angle will result in an increase in breakage force. It describes the distribution of random angle between the vertical axis and a tilted line segment. The cumulative distribution function of Cauchy distribution has the following form;

$$\frac{1}{\pi}\arctan\left(\frac{\theta-\theta_0}{\gamma}\right)+\frac{1}{2} \tag{6.28}$$

where θ is the impact angle, $\theta_0 > 0$ is the location parameter and $\gamma > 0$ is the scale parameter of the distribution. The larger the angle that particle hits the wall the

more force transferred. That is,

$$F_i \times \left[\frac{1}{\pi}\arctan\left(\frac{\theta-\theta_0}{\gamma}\right)+\frac{1}{2}\right] \tag{6.29}$$

As a result, a proposed breakage model which defines the breakage rate of granola during pneumatic conveying as a function of its shear history during formation (in the high shear granulator) has the following form;

$$b = \frac{K_1 F_i \times \left[\frac{1}{\pi}\arctan\left(\frac{\theta-\theta_0}{\gamma}\right)+\frac{1}{2}\right] - F_H}{(F_H)^n} \tag{6.30}$$

where K_1 and n are proportionality coefficients.

Equation (7.6) was used for the experimental calculations. On the other hand, equation (6.30) was the main equation of the breakage model developed in this Chapter.

6.4 Results and Discussion

Breakage of granola has been studied at three different geometries namely, a straight pipeline (0^o), a pipeline with two 45^o bends and a pipeline with one 90^o bend. Three different air pressures were applied to each configuration; $23\ ms^{-1}$, $34\ ms^{-1}$ and $42\ ms^{-1}$. The aggregated granola was produced subject to impeller agitation at 150 rpm, 200 rpm and 300 rpm for 6, 9 and 12 minutes with binder mass flow rates of 0.22 g/sec, 0.33 g/sec and 0.65 g/sec. The effects of flow geometry, applied air pressures and agitation history on breakage rate will be examined in turn. Equation (6.30) was employed for the modelling of granola breakage during pneumatic conveying.

6.4.1 Effect of applied air pressure

The effect of applied air pressures on breakage rate of the granola is displayed in Figure 6.7. Breakage rate is expressed in terms of the ratio difference between the median size at cycle τ ($D_{50}(\tau)$) and the initial median size ($D_{50}(0)$) to the initial median size per unit cycle as per equation (6.31). $b(\tau)$ is therefore dimensionless. The breakage rates shown are for granules produced at 0.33 g/s binder addition rate for 9 minutes subject to impeller agitation at 300 rpm. In general, overall the breakage rates are low; a maximum value was obtained of about 0.05 after the first cycle. The breakage rates decrease sharply after the first five cycles. After 10th cycle, the breakage rate appears to approach a limiting rate about 0.01. This suggests that weak particles are broken during initial cycles leaving a stronger core which remains intact over the course of the 20 cycle regime.

$$b(\tau) = \frac{D_{50}(0) - D_{50}(\tau)}{D_{50}(0)\tau} \tag{6.31}$$

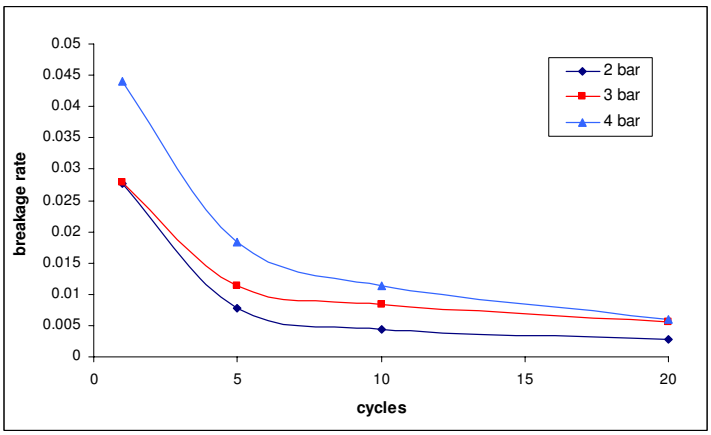

(a) A straight pipe

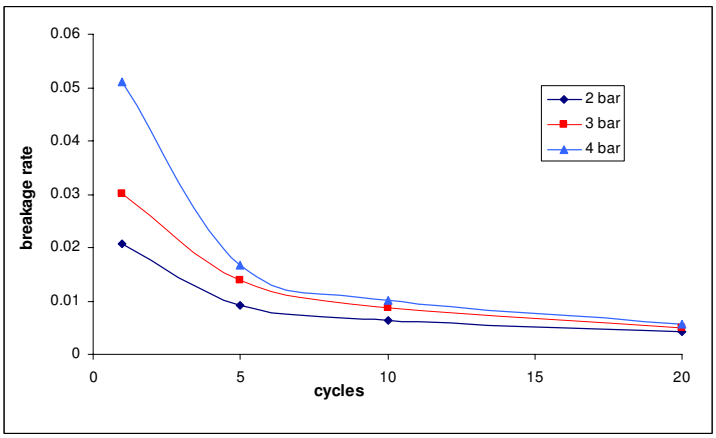

(b) A two 45^o bend pipe

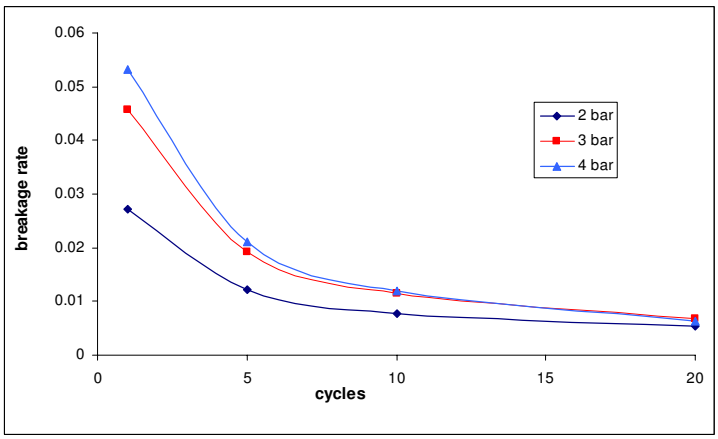

(c) A 90^o bend pipe

Figure 6.7: Breakage rates for different applied air pressures at three flow geometries. Granules produced at a 0.33 g/s binder addition rate for 9 minutes subject to impeller agitation at 300 rpm.

6.4.2 Effect of flow geometry

The effect of flow geometry on breakage rate is displayed in Figure 6.8. The breakage rates of granules produced at 0.33 g/s binder addition rate for 9 minutes subject to impeller agitation at 300 rpm are shown. In Figure 6.8, it is seen that more breakage occurred in the 90^o bend configuration than that which obtained in the 45^o bend pipe and the straight pipe for all applied air pressures. As might be expected the overall breakage rate obtained in the straight pipe was the smallest. This implies that the breakage rate has positive dependency on the impact angle. That is, the breakage rate increases with increasing bend angle. This is consistent with the results presented by previous researchers (Kalman, 1999; Salman et al., 2002). In addition to this, less breakage occurs at the 45^o bend configuration than the 90^o bend. This might indicate that a minimum threshold force is required for breakage as the particle impacts with the pipe wall.

When the applied pressure was increased, the difference between the breakage rates at various impact angles was reduced. This result shows that if the applied pressure is high enough, this could become the dominant factor affecting the breakage rate during the pneumatic conveying.

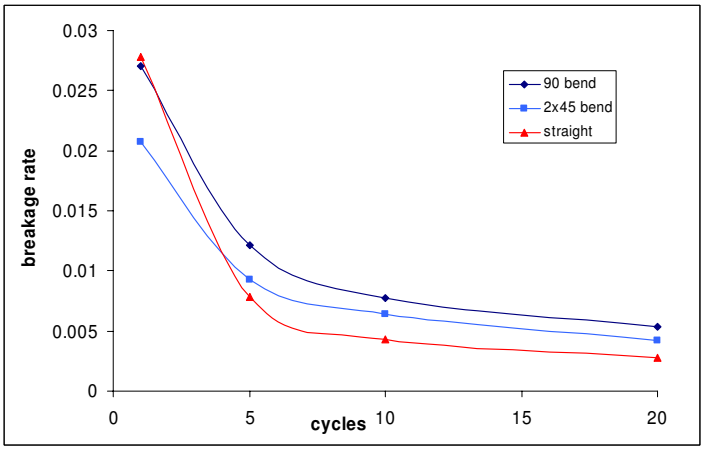

(a) Applied air pressure of 2 bar

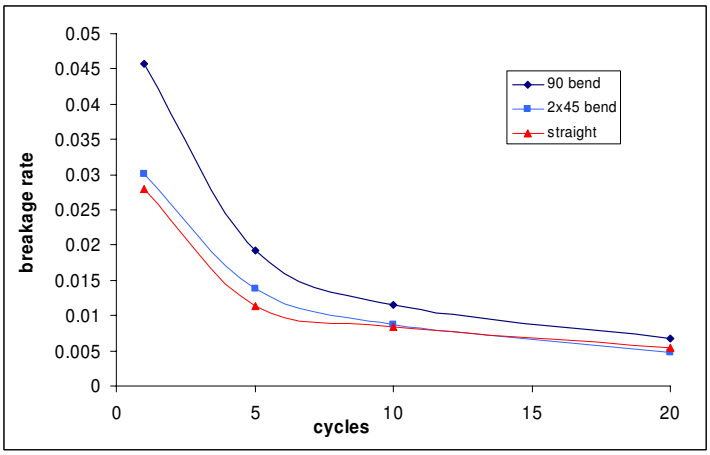

(b) Applied air pressure of 3 bar

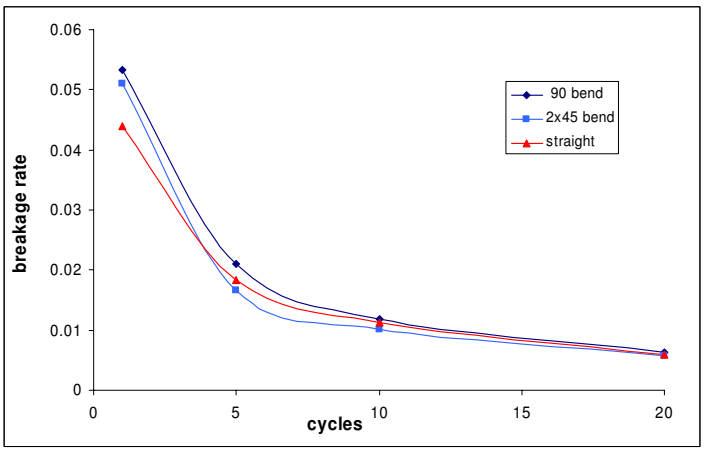

(c) Applied air pressure of 4 bar

Figure 6.8: Breakage rates for different flow geometries at air pressures of 2 bar, 3 bar and 4 bar. Granules produced at 0.33 g/s binder addition rate for 9 minutes subject to impeller agitation at 300 rpm.

6.4.3 Effect of agitation intensity

The effect of agitation intensity on breakage rate is shown in Figure 6.9. In this case, breakage rates were obtained from granules produced at 0.33 g/s binder addition rate for 12 minutes. Granules produced at 300 rpm have the lowest breakage rates while granules produced at 150 rpm have the highest breakage rates. This effect clearly demonstrates the importance of shear history (during granule production) on breakage rates during subsequent processing. This is because of the fact that granules become denser and stronger with increased applied shear force. Additionally, the breakage rates were almost constant for the granola produced at 300 rpm at the straight and 45^o bend pipe lines. This may suggest the existence of a threshold applied shear rate during production for given subsequent processing configuration and applied pressures, which result in strong particles with constantly low levels of breakage.

6.4.4 Effect of particle size profile

The relationship between the breakage rate and the particle size in the 90^o bend for 2, 3 and $4\ bar$ air pressures are depicted in Figure 6.10. D_{90} represents the top ten percentile of aggregate sizes while D_{50} represents the median sizes and D_{10} represents the smallest ten percentile. Figure 6.10 shows that the breakage rates increases consistently across the particle sizes with increasing air pressures. However, an increased level of breakage was observed for small particles (fines) as demonstrated by the D_{10} at the highest applied pressure. Indeed, the magnitudes of the experimentally obtained breakage are very close to each other for all size classes at applied air pressure of $4\ bar$ (Figure 6.10c). The effect of increased air pressure (see Figure 6.7) is more dominant than the effect of any other parameter examined such as rig configurations. It also suggests that there may be a limiting applied velocity which might be applied in order to prevent the emergence of a large number of unwanted fines.

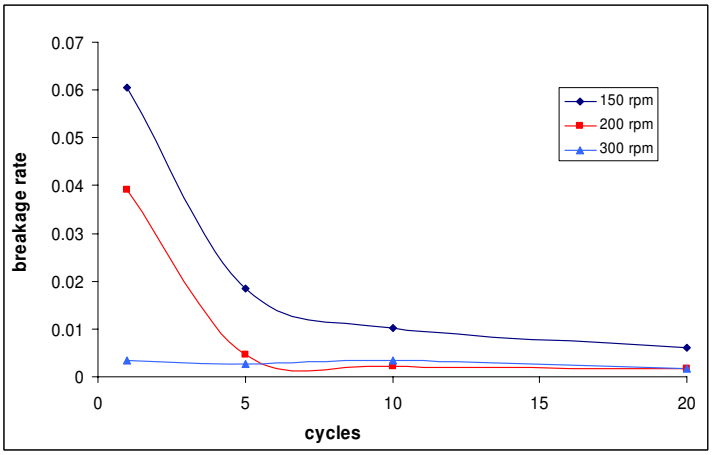

(a) A straight pipe

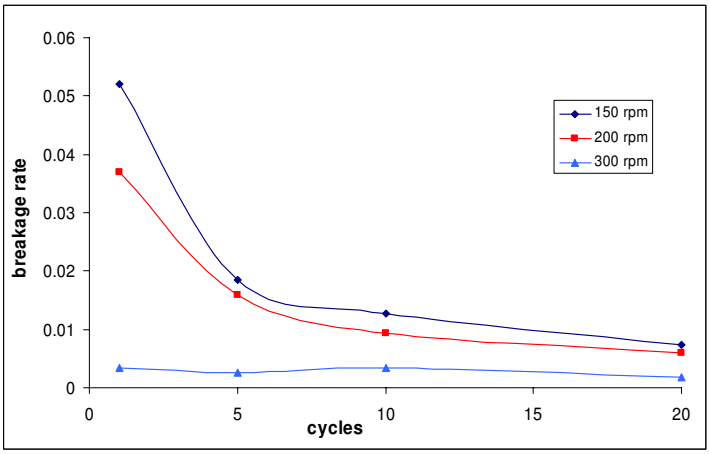

(b) A two 45^o bend pipe

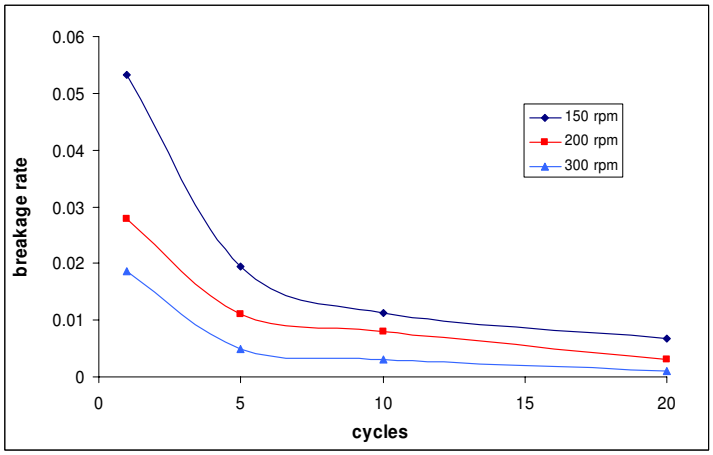

(c) A 90^o bend pipe

Figure 6.9: Breakage rates for granules produced at different impeller speeds at various flow geometries. Granules produced at 0.33 g/s binder addition rate for 12 minutes.

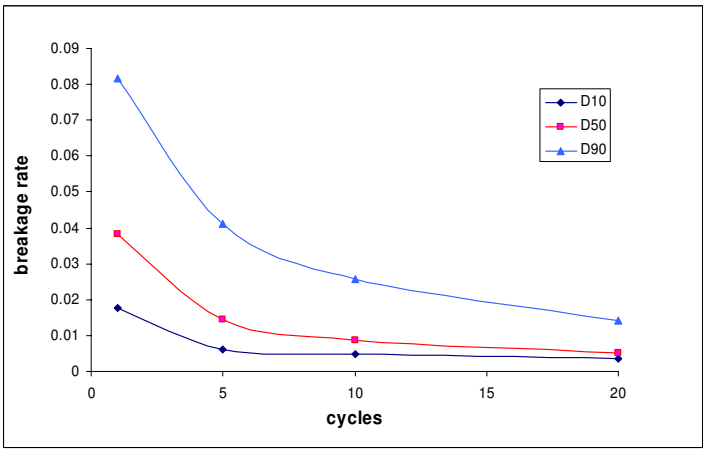

(a) At applied air pressure of 2 bar

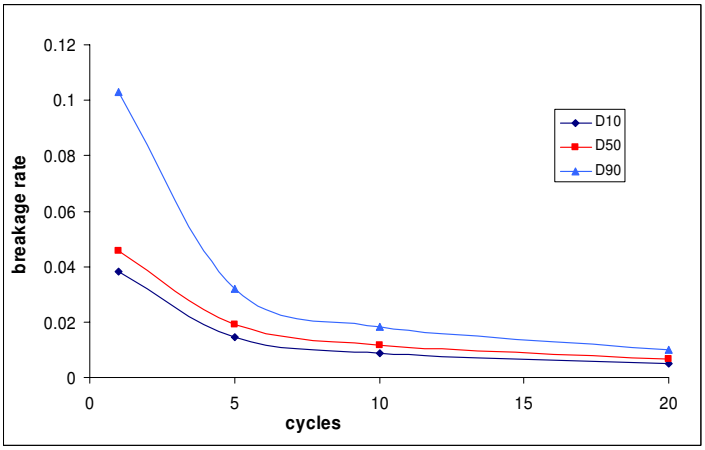

(b) At applied air pressure of 3 bar

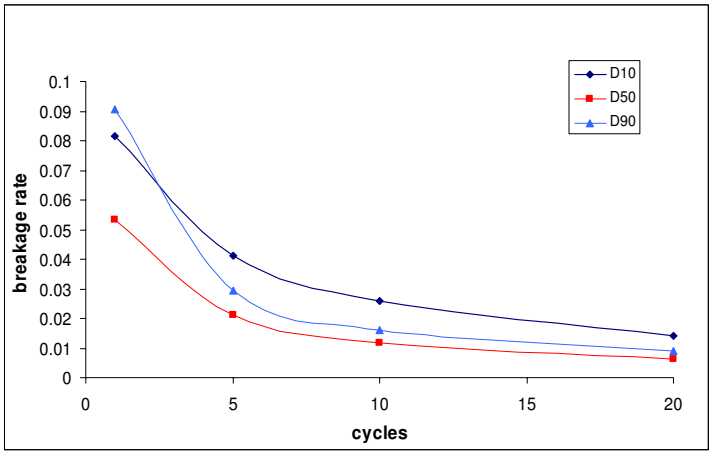

(c) At applied air pressure of 4 bar

Figure 6.10: Breakage rates for different particle sizes at various applied air pressures in 90^0 pipeline.

6.4.5 Model results

Equation (6.30) was used to model the breakage rate in the pneumatic conveying rig. The proportionality coefficients were estimated by minimizing the error between predicted and experimental breakage rate applying to the full data set of high shear granulations The constant coefficients were found to be $c_1 = 25$, $c_2 = 0.007$, $C = 7 \times 10^9$, $K_1 = 5 \times 10^{-5}$ and $n = 0.5$. The particle velocity was obtained using equations (6.17) and (6.21) for a number of air velocity and various rig configurations. Figure 6.11 displays particle velocity during the 90^o bend pipeline for different air flow velocities. The impact velocity at 90^o bend is below $10\ ms^{-1}$ at $23\ ms^{-1}$ air flow velocity while its value approaches to $15\ ms^{-1}$ at $42\ ms^{-1}$ air flow velocity. The particle leaves the pipeline with a velocity of $4.7\ ms^{-1}$ at the lowest air flow velocity, and $8\ ms^{-1}$ at the highest air velocity.

Figure 6.12 exhibits particle velocity in the two 45^o bend pipeline for different air flow velocities. In this configuration, particles hit the first bend at a velocity of $7\ ms^{-1}$, then they hit the second bend at a velocity of $5\ ms^{-1}$, and leave from the pipe at a velocity of $4.7\ ms^{-1}$ at the lowest applied air velocity. Particles reach a velocity of $12\ ms^{-1}$ at the first bend, $6\ ms^{-1}$ at the second bend, and leave from the pipe at a velocity of $5.7\ ms^{-1}$ at the highest applied air velocity.

Figure 6.13 shows particle velocity during the straight pipeline for different air flow velocities. In this case, particles leave from the pipeline at a velocity of $9\ ms^{-1}$ at $23\ ms^{-1}$ air flow velocity, at a velocity of $13\ ms^{-1}$ at $34\ ms^{-1}$ air flow velocity, and at a velocity of $15\ ms^{-1}$ at $42\ ms^{-1}$ air flow velocity.

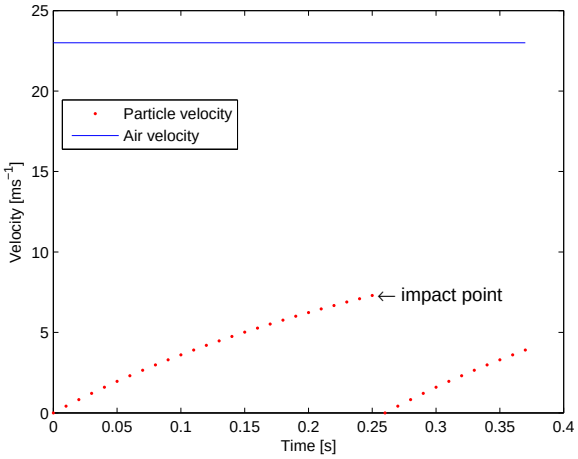

(a) At 2 bar air pressure

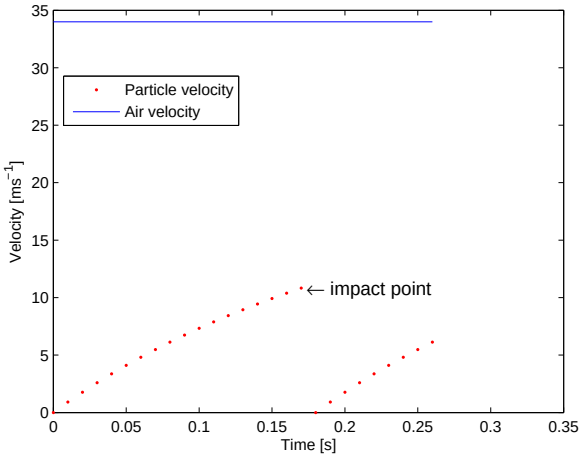

(b) At 3 bar air pressure

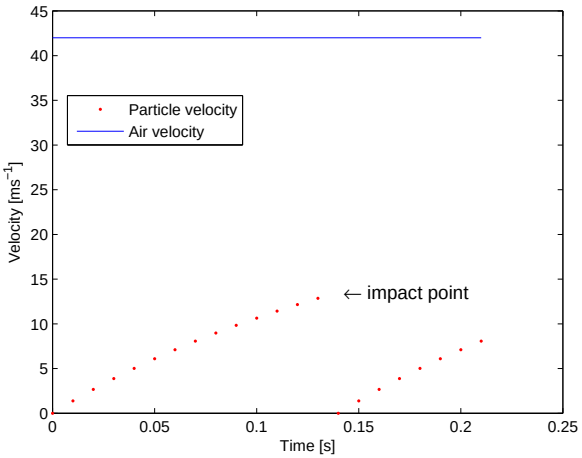

(c) At 4 bar air pressure

Figure 6.11: Particle velocity at various applied air pressures in a 90^0 bend pipeline.

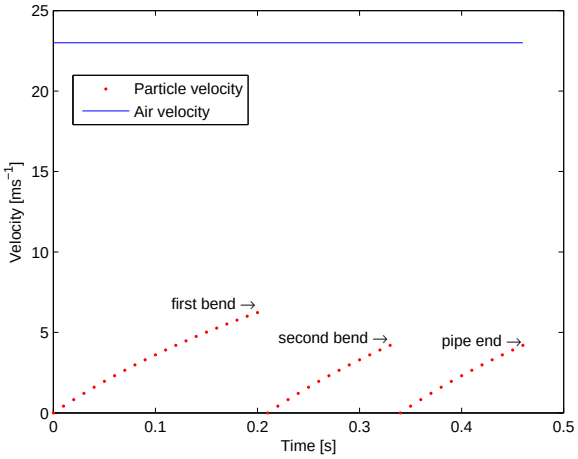

(a) At 2 bar air pressure

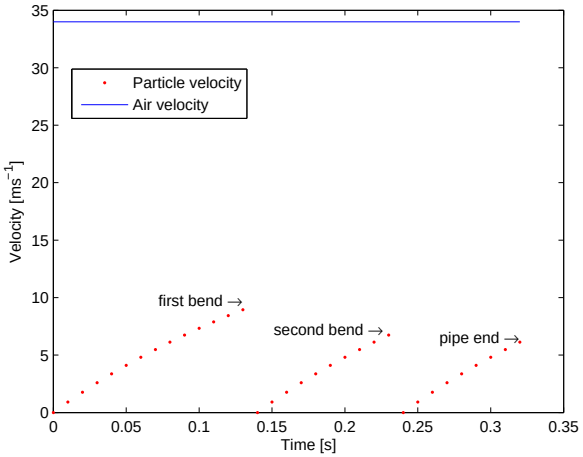

(b) At 3 bar air pressure

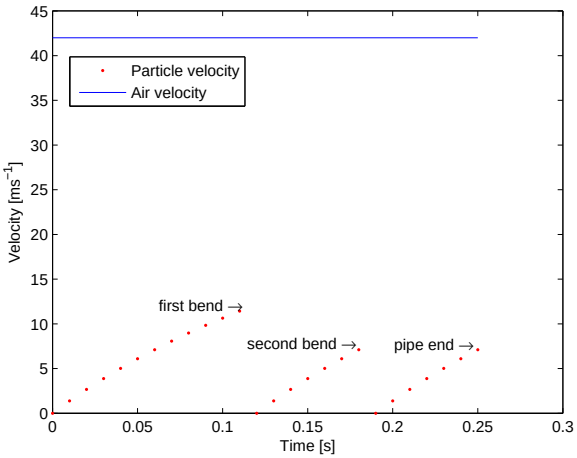

(c) At 4 bar air pressure

Figure 6.12: Particle velocity at various applied air pressures in the two 45^0 bend pipeline.

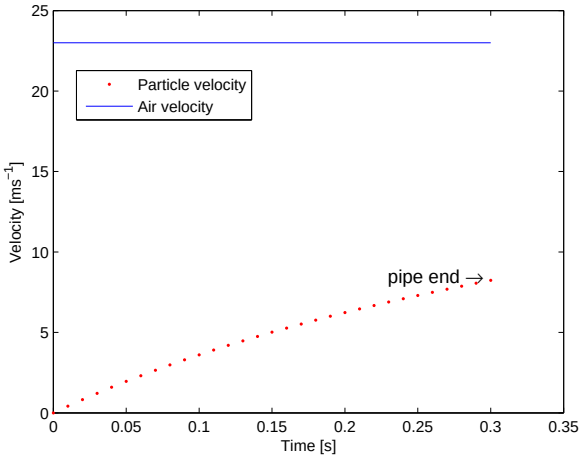

(a) At 2 bar air pressure

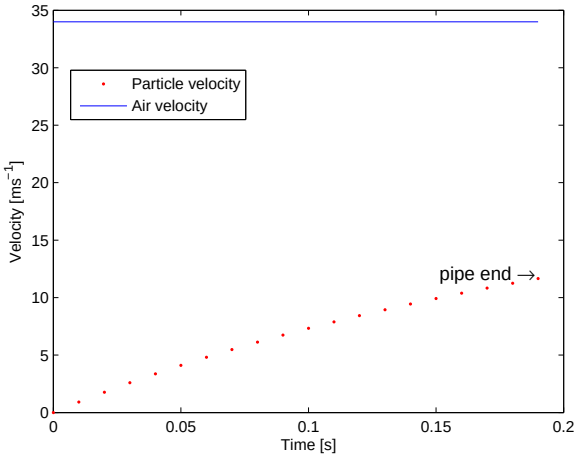

(b) At 3 bar air pressure

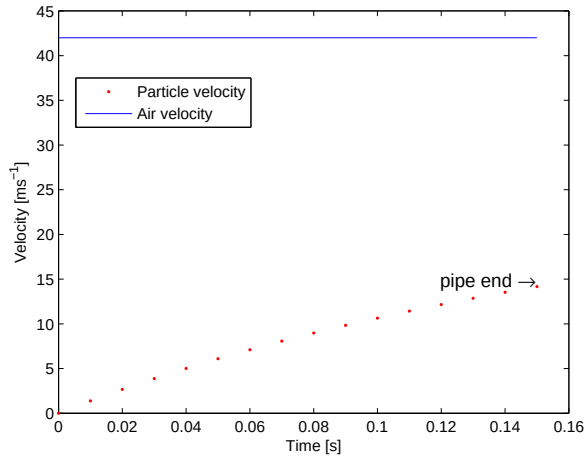

(c) At 4 bar air pressure

Figure 6.13: Particle velocity at various applied air pressures in the straight pipeline.

The model results obtained from equation (6.30) were compared with the experimental results. Figures 6.14, 6.15 and 6.16 show the comparison of the model with the experimental results for three different air flow velocities at 90^o bend pipeline, two 45^o bend pipeline and straight pipeline respectively. Figures 6.14 and 6.15 exhibit good overall agreement between the model and the experimental results. Although the model overpredicts the experimental results for the configurations with bends (Figures 6.14 and 6.15), it tends to underpredict the breakage rate in the straight pipe (Figure 6.16). However, after about 10 cycles in the straight pipe there tends to better agreement.

The model in this work was also employed to particles with different shear histories (during granule production). It was tested on granules produced at different agitation intensity; 150 rpm, 200 rpm and 300 rpm. Results obtained from the model and experimentation are compared in Figure 6.17. The model overpredicts breakage rates at 150 rpm (Figure 6.17a) and 200 rpm (Figure 6.17b) and underpredicts initial breakage rates at 300 rpm (Figure 6.17c).

In general, the model estimates a greater rate of breakage than experimental results. A possible reason for this is that the breakage model may not be able to either measure or predict the impact of various parameters such as hardness and impact forces due to large and natural variations in the complex system that is the granola manufacturing process. Moreover, the granule produced in the high shear mixer is dense and the breakage mostly occurs via attrition which results in the formation of very small particles and fines. During pneumatic conveying, these smaller dusty particles are lost in the collecting cloth at the end of the rig. Granola samples were weighed before and after each conveying cycle, and according to obtained data the average loss of fines is 1% (w:w). Therefore, this loss decreases the experimentally measured breakage rate and it becomes lower than its exact value.

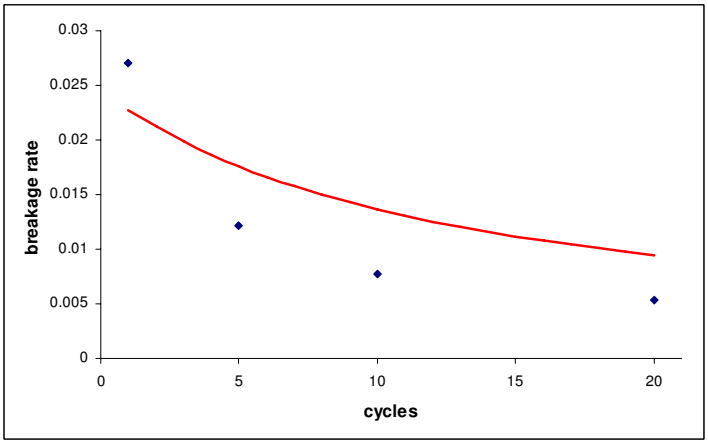

(a) At 2 bar air pressure

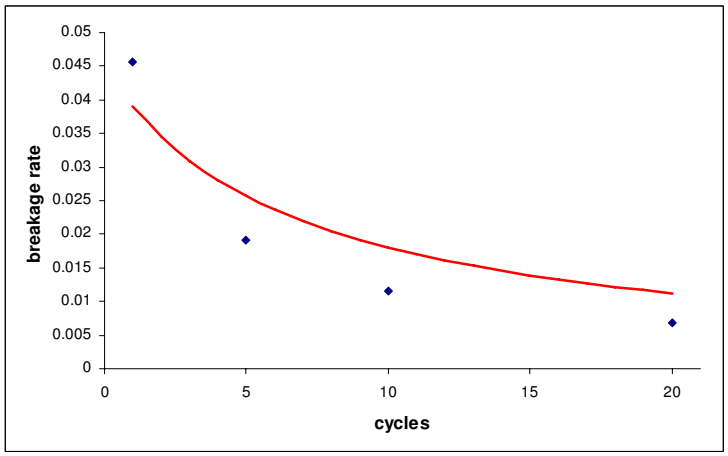

(b) At 3 bar air pressure

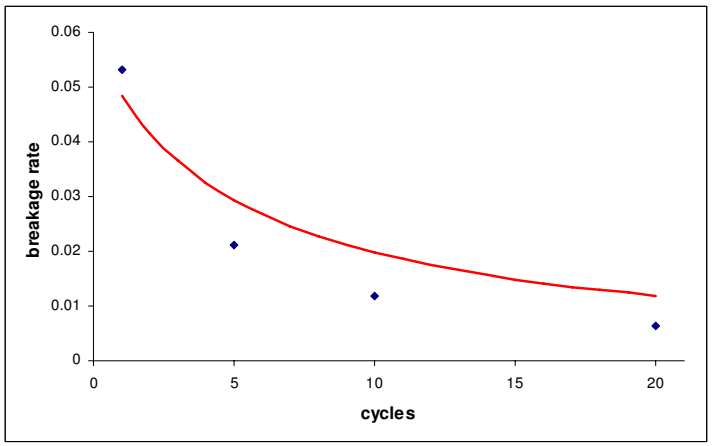

(c) At 4 bar air pressure

Figure 6.14: Particle breakage rate at various applied air pressures at 90^o pipeline for 300 rpm. (Continuous line displays model results, points are experimental data.)

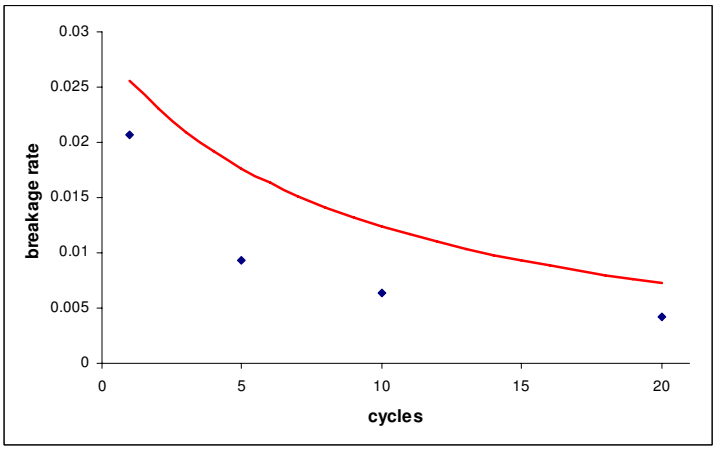

(a) At 2 bar air pressure

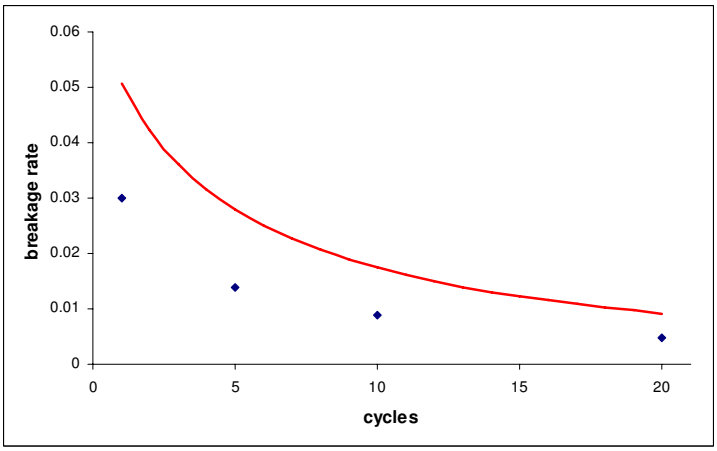

(b) At 3 bar air pressure

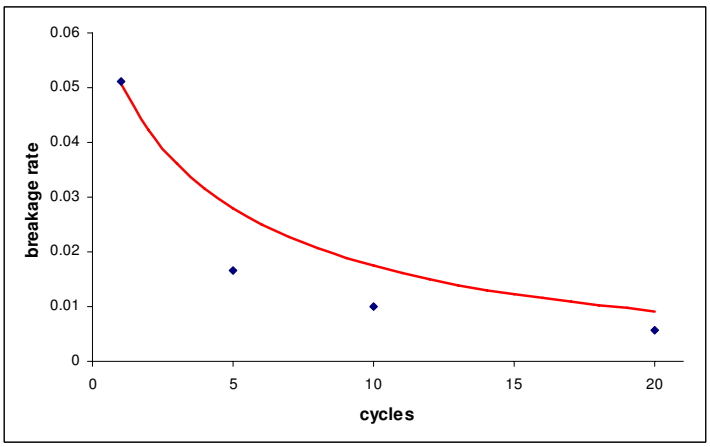

(c) At 4 bar air pressure

Figure 6.15: Particle breakage rate at various applied air pressures at two 45^o pipeline for 300 rpm. (Continuous line displays model results, points are experimental data.)

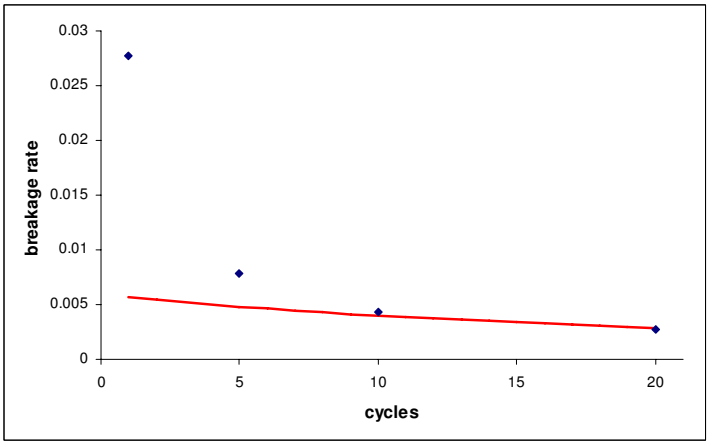

(a) At 2 bar air pressure

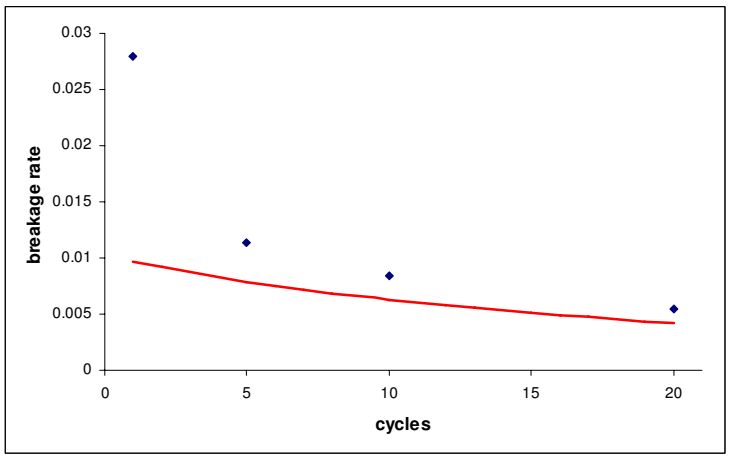

(b) At 3 bar air pressure

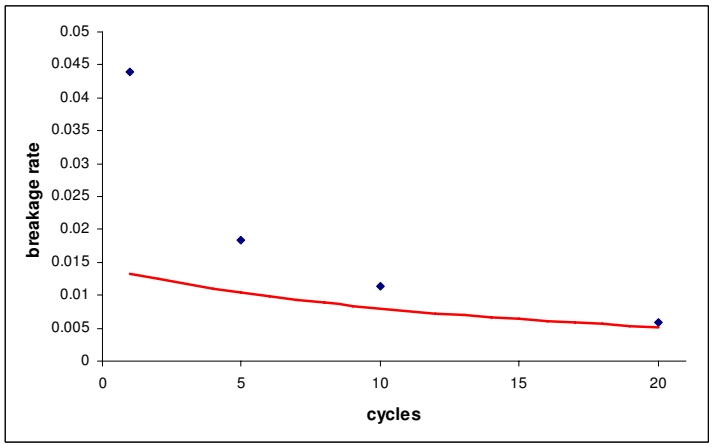

(c) At 4 bar air pressure

Figure 6.16: Particle breakage rate at various applied air pressures at straight (0^o bend) pipeline for 300 rpm. (Continuous line displays model results, points are experimental data.)

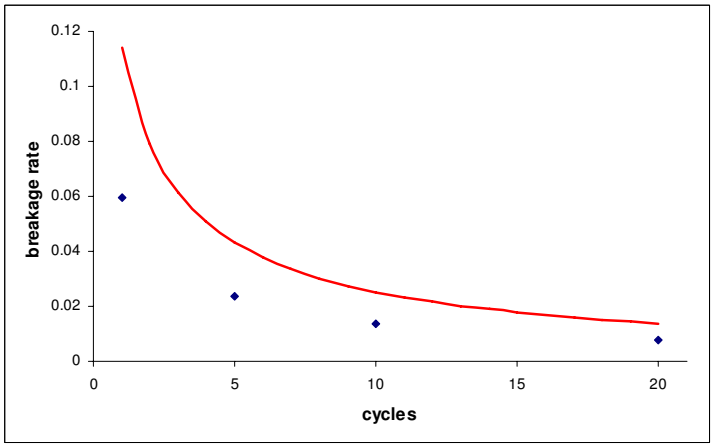

(a) At 150 rpm

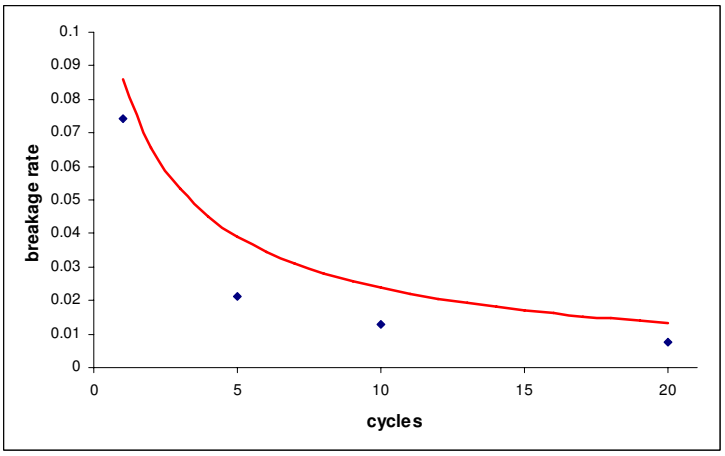

(b) At 200 rpm

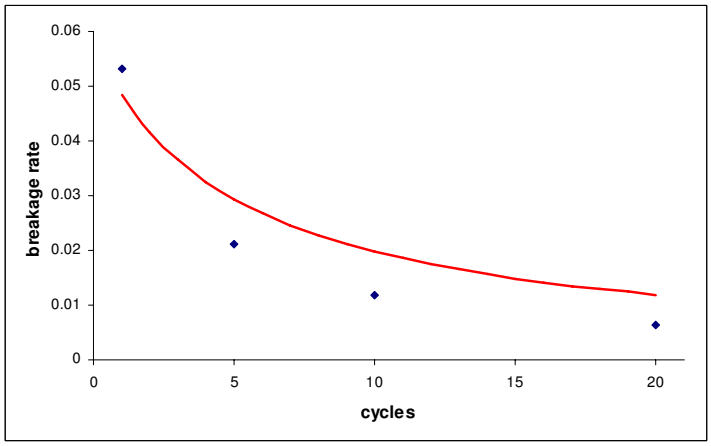

(c) At 300 rpm

Figure 6.17: Particle breakage rate at 42 ms^{-1} applied air pressures at 90^o pipeline for 150 rpm, 200 rpm and 300 rpm. (Continuous line displays model results, points are experimental data.)

Statistical analysis of the results has been undertaken. Fractional errors between model predictions and experimentally obtained data were also evaluated. Fractional errors were calculated by the ratio of the absolute difference between the expected D_{50} size and the experimentally measured D_{50} size to the experimentally measured D_{50} size at a number of cycles;

$$\text{Fractional error} = \frac{|\text{Expected } D_{50} \text{ size } - \text{ Experimental } D_{50} \text{ size}|}{\text{Experimental } D_{50} \text{ size}} \tag{6.32}$$

The resultant values are given in Table 6.3 and Table 6.4.

Table 6.3: Fractional errors between predicted and experimental D_{50} sizes for 300 rpm at 90^o bend pipeline at various air flow velocities.

	Fractional errors		
Cycle	2 bar	3 bar	4 bar
1	0.001	0.007	0.005
5	0.038	0.036	0.046
10	0.075	0.073	0.089
20	0.100	0.104	0.126

Table 6.4: Fractional errors between predicted and experimental D_{50} sizes at 42 ms^{-1} at 90^o bend pipeline at various agitation intensities.

	Fractional errors		
Cycle	150 rpm	200 rpm	300 rpm
1	0.058	0.013	0.005
5	0.112	0.099	0.046
10	0.134	0.123	0.089
20	0.140	0.138	0.126

6.5 Conclusion

In this chapter, the breakage of the granola during the pneumatic conveying has been examined. It was observed that the breakage rate of the particles depends on the flow geometry, air flow rate and the particle size. Moreover, it was also shown that the aggregate production history can significantly affect the breakage rate. Applied impeller shear rate (agitation intensity) during high shear granulation is seen as particularly important in this regard and there appears to be an agitation threshold above which hard strong granules are formed which exhibit little breakage during subsequent processing. The highest breakage rate observed at the 90^o bend pipeline geometry at 4 bar applied air pressure with the granola produced at the lowest impeller speed which is 150 rpm.

On the other hand, aggregates produced at low agitation intensities tend to exhibit a higher degree of friability and conveying conditions assume significantly greater importance.

A simple physical based model is derived to predict the particle breakage rates at various applied air velocities using a number of pipe configurations, taking into account shear histories. The proposed model allows the prediction of breakage rates for the D_{50} (median size) particle size as a representative size class of the whole particle size distribution. A more comprehensive model, which will be based on both physical phenomenon and the randomness that might be observed in this type of particulate process, will be developed in chapter 8.

Chapter 7

Breakage During Pneumatic Conveying; Products from Fluidised Bed Granulation

This chapter is dedicated to the particle breakage of granola during pneumatic conveying for granules produced in a fluidised bed granulator. Firstly, an introduction to fluidised bed granulation will be provided. Secondly, materials and methods will be outlined. Then, a breakage model describing the change in particle size incorporating physical phenomena based on the particle motion during conveying rig will be proposed. Finally, results and discussion will be presented and conclusions will be drawn.

7.1 Introduction

Fluidised bed processing has been used in the industry since the 1950s. It was originally designed as a process for drying pharmaceutical granules (Wurster, 1950). The first

research studies on fluidised beds trace back to the 1960s (Banks and Aulton, 1991). Over the years, fluid bed processing has become an important means of particle size enlargement particularly in industries concerned with pharmaceuticals, detergents, fertilisers, and food. It has also important applications such as granulation, drying, coating, and layering. Fluidised bed systems operate through agitation of the particles in a bed using upward gas flow at an appropriate rate. The fluidisation behaviour of the particles as a result of upward gas flow can be affected by combination of several forces including drag force, natural force of gravity, buoyancy, van der Waals, capillary and electrostatic forces. However, if the particle size is greater than $100\mu m$ and the particle density is three orders of magnitude bigger than gas density, gravity and drag forces are the principal factors in determining particle motion in the bed (Seville et al., 1997). Additionally, particle-particle and particle to (equipment) wall collisions may have important effects on the fluidisation (Li and Mason, 2002).

7.1.1 Granulation

Some common reasons for granulation include;

- To prevent segregation of well mixed powders
- To improve flowability
- To avoid cake formation during storage

In fluidised bed granulation, powder particles are fluidised by gas (typically air) flow in the bed. Particles move in the bed as a result of the forces by air flow and gravity. There are particle-particle and particle-wall collisions in the fluidised bed. A liquid binder is then injected into bed via a nozzle or nozzles. Depending on the position of the spraying nozzle there are three different types of fluidised bed granulation;

1. Top spray granulation
2. Bottom spray granulation
3. Tangential spray granulation

Because of the sprayed binder, particles in the bed become wet and sticky over time. After the required amount of binder has been added, the spray nozzle is turned off, though the fluidizing remains on to effect granule drying.

Top-spray method is more commonly employed in the food industry when compared to bottom-spray and tangential-spray due to its high versatility, relatively high batch size, and relative simplicity (Dewettinck, 1997).

The main advantage of fluidised bed granulation is that the granulation process steps of wetting, agglomeration, and drying occur in just one unit. This obviously decreases process costs and time for the process as well as providing for increased containment of potentially hazardous materials. Another advantage is that once the optimized parameters of the granulation process are achieved, good reproducibility can be obtained. On the other hand, a principal drawback of fluidised bed granulators is that finding optimized parameters can be quite difficult since there are many parameters which affect granule properties throughout the process.

7.2 Materials and Methods

7.2.1 Granola formation in the fluidised bed

Granola was produced in a fluidised bed granulator (Mini-Airpro, ProcepT, Belgium) as shown in Figure 7.1 and the corresponding schematic drawing displayed in Fig-

ure 7.2. The fluidized bed granulator has a glass container with the lower portion being conical in shape and a cylindrical upper portion. The whole container is $0.73\ m$ in height while the upper cylindrical portion has an inner diameter of $0.2\ m$ and is $0.28\ m$ in height. Spray from the nozzle is in a downward direction, counter current to the fluidising air flow. The granules are produced in the process column by spraying the binder solution from the top in counter current air flow and under pressure conditions. A pulsed back system is used for cleaning filters. The fluidising air was first preheated to $80^o\ C$ by an electrical heater and its flow rate (set at $0.95\ m^3/min$) was subsequently measured before entering the bed. The monitoring of the bed temperature was achieved by controlling the inlet fluidising air temperature and regular monitoring of outlet air temperature.

The composition of the granola includes oat flakes, corn flakes, puffed rice, malted buckwheat, malted barley, brown sugar, oat beta glucan and wheat germ. A honey-water mixture (85:15) was used as a binding agent. A more detailed description of the ingredients is displayed in Table 1.1 of Chapter 1. The ingredients were placed in the unit and were fluidised and mixed using air at a flow rate of $0.95\ m^3/min$ for $5\ min$. These conditions were maintained during subsequent binder addition and drying stages. Afterwards the binder solution was sprayed onto the fluidised bed using a peristaltic pump (adjustable for various desired spray flow rates). The binder is drawn up by peristaltic pump from a reservoir, positioned on a balance and through a spray nozzle. The binder flow rate is controlled by the pump speed and is monitored via the continuous recording of reservoir weight. Three peristaltic pump speeds of 5, 10 and $15\ \mathrm{rpm}$ were used resulting in binder flow rates of 0.4, 0.8 and $1.2\ g/s$ respectively. This corresponded with binder addition times of $46\ s$, $23\ s$ and $15\ s$ respectively. Nozzle air pressure of 2, 3 and $4\ \mathrm{bar}$ were used. Nozzle pressure affects binder droplet size emanating from the nozzle. Spraying was continued until all the binder solution was used. The granola was then dried on an oven at $160^o\ C$ for 10 minutes.

A Camsizer digital image analyzer (Retsch, Haan, Germany) was used for measuring particle size distributions and aggregate relative density.

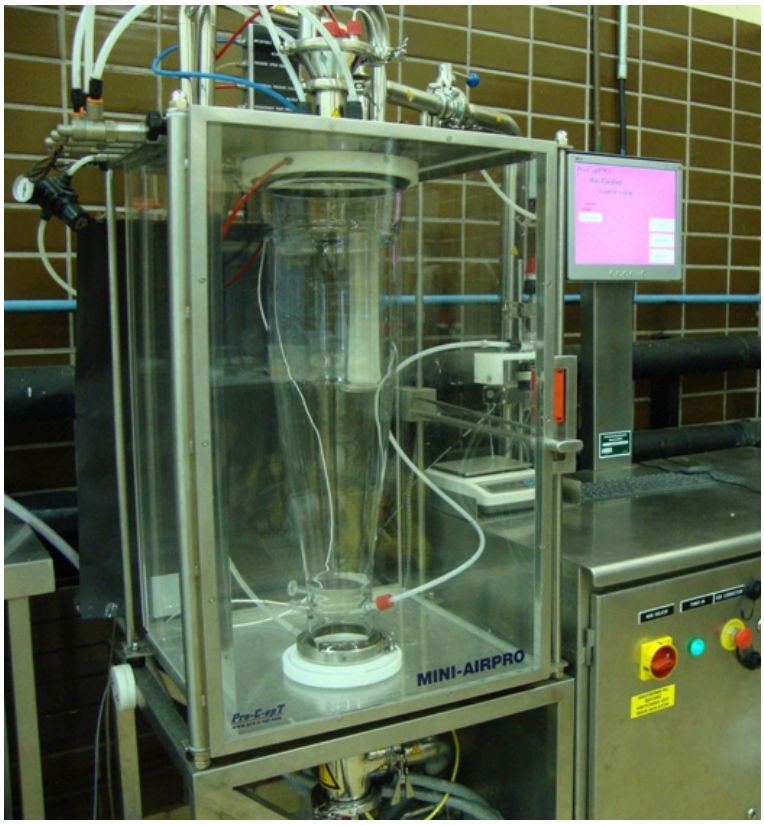

Figure 7.1: Laboratory scale of the fluidised bed granulator.

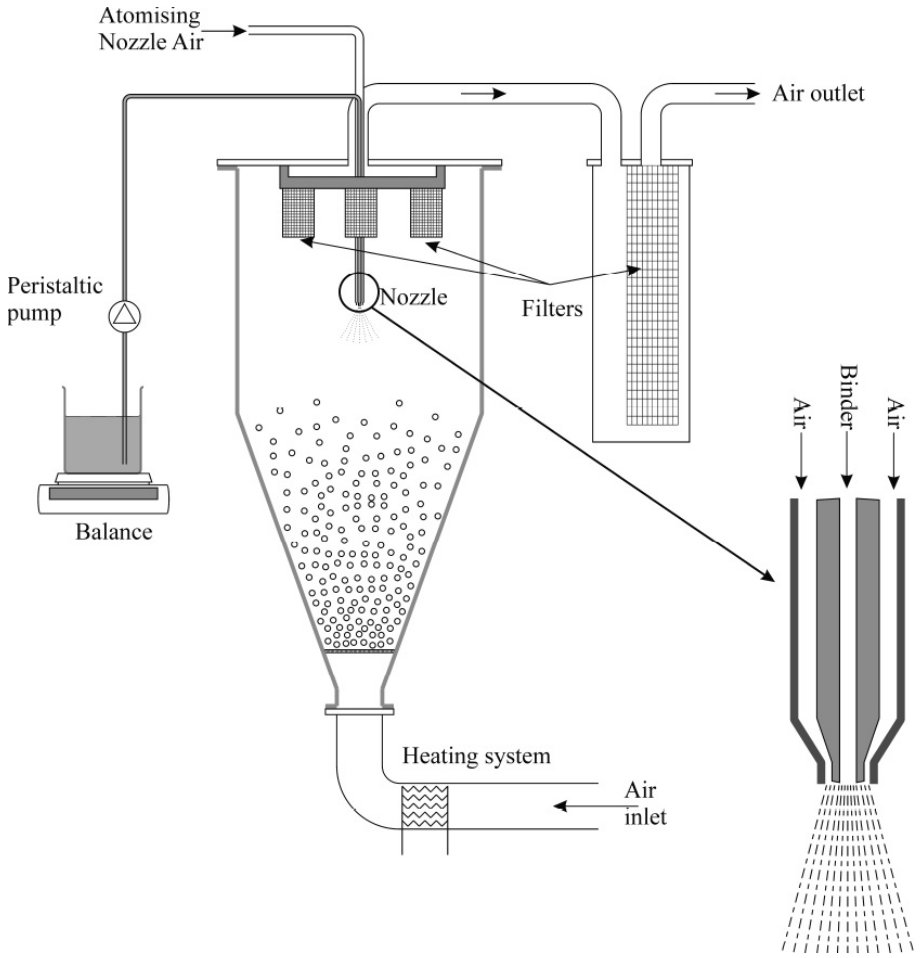

Figure 7.2: A schematic diagram of the fluidised bed granulator.

Table 7.1: Geometry of the high shear mixer.

Component	size
Impeller depth	$17\ cm$
Impeller blade width	$2.5\ cm$
Impeller blade inclination	45^o
Impeller blade length	$8\ cm$
Bowl diameter	$17\ cm$
Bowl depth	$18\ cm$
Chopper depth	$14.5\ cm$

Textural properties of samples were measured using a TA-XT2i texture analyzer (Stable Microsystems Ltd, Godalming, UK) equipped with an SMS P/75 compression platen ($d = 75\ mm$) and a $50\ kg$ load cell. A flat-ended cylindrical stainless steel plate having $75\ mm$ diameter was used for compression. The sample was placed

on the lower plate of the instrument and the flat-ended cylindrical plate that moved downwards until it reaches a distance of $15\ mm$ at a constant speed of $1.0\ mms^{-1}$. Each sample was measured in 5 replicates. During the test run, the resistance of the sample was recorded and plotted on a force (N) versus distance (mm). The hardness and crispness of granola were measured.

7.2.2 Conveying of granola products

The aggregation of the granola ingredients (Chapter 1, Table 1.2) took place in the fluidised bed granulator subject to three peristaltic pump speeds of 5, 10 and 15 rpm resulting in binder flow rates of 0.4, 0.8 and $1.2\ g/s$ respectively. Nozzle air pressure of 2, 3 and 4 bar were used. The aggregates were then baked in an oven for 10 minutes at 160^o.

The granola were then conveyed via a pneumatic conveying rig comprising a horizontal pipe of internal diameter $25\ mm$ with different bend configurations (straight pipe, two 45^o bends and a 90^o bend were employed)(Chapter 6, Figure 6.1). All sections of the pipeline are made of transparent PMMA (Perspex), so that granola breakage and flow behaviour can be observed. The outer diameter of the pipeline is $33.5\ mm$, giving a wall thickness of $4.25\ mm$. The particle size distribution of the granola was measured after passage through each rig configuration at each air pressure for repeative numbers of cycles.

The straight pipeline has $1.3\ m$ length horizontal axis and $25\ mm$ internal diameter (Chapter 6, Figure 6.2). A rig comprising two 45^o bends, comprised of an initial section $0.7\ m$ long and two short sections of $0.30\ m$ length with the same internal diameter of $25\ mm$ was also employed (Chapter 6, Figure 6.3). Finally, a 90^o bend conveying rig was used for propelling the granola. The initial section of the pipeline is

$1\ m$ long and a short $0.30\ m$ length of pipeline with the same diameter as the initial section was attached to the 90^o bend (Chapter 6, Figure 6.4).

Air is supplied by a compressor and regulated to deliver a pressure of $400\ kPa$. This resulted in a typical air velocity of about $42\ ms^{-1}$ for each of the configurations. The granola is fed into the apparatus by hand at the location indicated on the diagram. A soft, fine-mesh piece of cloth is used to capture the granola at the end of the rig for measurement of its particle size distribution.

The transparent PMMA (Perspex) pipeline enabled observation of the breakage behaviour of particles. Particle conveying through the pipeline was observed using a high speed camera (AOS, X-Motion, Switzerland) and visual inspection of particle flows appeared to suggest the type of breakage mechanism present.

A Camsizer (Retsch, Haan, Germany) digital image analyzer was used for measuring particle size distributions of the resultant granola before and after passage through a conveying rig where aggregates are transferred by compressed air for a number of passes (1, 5, 10 and 20 cycles).

7.3 Aggregation and Breakage in Fluidized Bed Granulation

7.3.1 Aggregation mechanism

The possible rate processes occurring in fluidised bed granulation defined by Snow et al. (1997b) are;

1. Wetting and nucleation

2. Consolidation and growth

3. Breakage

On the other hand, Tan et al. (2006a) have explained the rate processes occurring in fluidised bed melt granulation as being a combination of aggregation, binder solidification and breakage processes.

A series of papers have been published to study the influence of operating conditions on the kinetics of fluidised bed melt granulation (Tan et al., 2004b, 2005a,b, 2006a,b). In their first series they identified the rate processes responsible for the net growth in granule size in a top-sprayed fluidised bed granulator. They proposed a sequence of events based on these rate processes (Tan et al., 2006a). In the second series, incorporating the equipartition of kinetic energy (EKE) kernel into a population balance model, they extracted the effective aggregation rate constant that accounts for the net granule growth for fluidised bed melt granulation experiments (Tan et al., 2006b). In the third series they developed and verified tracer experiments (Tan et al., 2005a) while they developed and verified a suitable breakage model to describe the breakage kinetics in fluidised bed melt granulation by means of population balance modelling (Tan et al., 2004b). Finally in the last series they worked on simultaneous modelling of aggregation and breakage in fluidised bed melt granulation (Tan et al., 2005b).

Panda et al. (2001) studied the influence of process parameters, drying conditions, impact velocities and physical properties of sprayed solutions on the kinetics of granulation and on the morphology of the end product. They carried out the granulation process on a single spherical particle.

The dynamic contact angle of binder drop on the powder is one of the important factors affecting the wetting kinetics. Parfitt (1986) derived a the dynamic height of

rise of binder by ignoring gravity and considering the powder consisting of capillaries of radius R as;

$$h = \sqrt{\left[\frac{R\gamma^{lv}cos\theta}{2\mu}\right]t} \tag{7.1}$$

where $\gamma^{lv}cos\theta$ is the adhesion tension (γ^{lv}:liquid-vapor interfacial energy, θ:contact angle), t is time and μ is binder viscosity.

In another approach, Ennis et al. (1991) assumed that coalescence between granules occurs if the surfaces of granules are surrounded by a liquid to bind them. They found that successful coalescence occurs when the collisional kinetic energy was completely dissipated by viscous dissipation in the binder and elastic losses in the solid. On this basis, they derived a viscous Stokes number (St_{vis}) and a critical viscous Stokes number (St^*_{vis}).

Iveson and Litster (1998) defined two important types of growth behavior namely *steady growth* and *induction*. Where *steady growth* prevails the average granule size increases linearly with time. This occurs in systems where granules are weak and easily deform. Increasing the binder content increases the rate of growth, but produces weaker granules in nature. In general, *steady growth* occurs where particles are relatively coarse and narrowly sized and when the viscosity of binder is low. Where *induction growth* occurs, the period of growth is relatively long but stronger granules which are less easily deformable result. Increasing the binder content generally decreases the induction time. *Induction growth* occurs in systems where particles are fine with wide particle size distribution and the binder is generally viscous.

7.3.2 Breakage mechanism

In general, two breakage mechanisms can be defined; firstly erosion or attrition and secondly fracture or fragmentation (Iveson et al., 2001). Where erosion is the domi-

nant breakage mechanism, there results one large fragment of size close to the parent aggregate and a number of smaller fine particles. Where breakage is by fracture, this results in the production of a few smaller fragments. In addition, the fracture type of breakage is divided into two modes; cleavage in which parent particles break into a small number of fragments of similar size and shattering which results in many fragments of a wide range of sizes (Redner, 1990).

Yuregir et al. (1987) defined the fragmentation rate of organic and inorganic crystals as;

$$V \sim \frac{H}{K_c^2}\rho u^2 a \tag{7.2}$$

where a is the crystal length, ρ is the crystal density and u is impact velocity.

On the other hand, Iveson and Litster (1998) defined the granule impact deformation as a function of granule rheology and agitation intensity. The amount of impact deformation was characterized by the Stokes deformation number;

$$St_{def} = \frac{\rho_g U_c^2}{2Y_g} \tag{7.3}$$

where U_c is the collision velocity in the granulator and represents the process intensity, ρ_g is the granule density and Y_g is the dynamic yield stress. The deformation number is a measure of the ratio of impact kinetic energy to the plastic energy absorbed per unit strain. The proposed granule growth behavior as a function of pore saturation and deformation number on a regime map is shown in Figure 2.5, Chapter 2. Particles either remain as a dry free-flowing powder or form nuclei at very low s_{max}. A few larger granules which are too weak to form permanent granules will form a crumb material at medium s_{max}. A slurry or over-wet mass will form when very high liquid content is present.

Lui et al. (2000) extended the model of Ennis et al. (1991) to include granule defor-

mation behavior during collisions assuming the mechanical properties of granules to be strain-rate independent and not a function of stress–strain history. They defined the granule mechanical behavior by an elastic modulus, E, and dynamic yield stress, Y_d. Two types of coalescence model were considered, namely Type I and Type II. In Type I, granules coalescence by viscous dissipation in the surface of binder layer before their surfaces come into contact. In Type II coalescence, granules are slowed to a halt during rebound after initial contact of their surfaces.

Snow et al. (1997b) defined breakage rates by fragmentation and attrition for fluidized bed by drawing an analogy with the work of Yuregir et al. (1987). The fragmentation (B_f) and attrition (B_a) rates have the following forms;

$$B_a = \frac{d_0^{1/2}}{K_c^{3/4} H^{1/2}} h_b^{5/4} (U - U_{mf}) \tag{7.4}$$

$$B_f \sim \frac{H}{K_c^2} \rho (U - U_{mf})^2 a \tag{7.5}$$

where d is granule diameter, d_0 is primary particle diameter, $(U - U_{mf})$ is fluid-bed excess gas velocity, h_b is bed height, a is the radius and K_c is fracture toughness. A detailed discussion was previously provided in Chapter 2.

7.4 The Breakage Model

Particle size measurements of granola were carried out using a Camsizer (Retsch, Haan, Germany) digital image analyzer before and after passage through a conveying rig. D_{10}, D_{50} and D_{90} particle sizes were obtained as well as particle size distributions. In this study, the calculations were carried out using D_{50} values as a representative particle size of the granola since D_{10} and D_{90} values broadly track D_{50} values for the system under investigation and D_{50} is therefore here simply represented as D. Each

of the cycles were considered as a time step τ; particles were conveyed a number of times (cycles) through the rig. Henceforth in this discussion for the purpose of normalizing the particle size, the change in particle size after each cycle was divided by the initial particle size. Breakage rate of the particles was obtained by dividing the normalized particle size change by time step difference;

$$b = \frac{D_i - D_\tau}{D_i \Delta\tau} \tag{7.6}$$

In a similar approach to that taken in Chapter 6, the breakage model is considered to be a function of particle impact force and the force required to cause breakage of the particle (the threshold particle breakage force). The particle impact force, F_i is a function of impact velocity and particle mass. The threshold force required to break the particle is related to particle hardness (F_H) and this is function of the process parameters applied in the fluidised bed granulator (i.e., granola production history). That is,

$$F_i = Cmv_i \tag{7.7}$$

where C is a coefficient and v_i is impact velocity.

Since the operating parameters do not appear to have any obvious effect on granule strength, F_H is taken as a constant coefficient by taking an average value of measurements.

The impact velocity was calculated using equations 6.17 and 6.21 for air flow velocity of $42\ ms^{-1}$ relating to $4\ bar$.

As per work done in Chapter 6, a proposed breakage model which defines the breakage rate of granola during pneumatic conveying as a function of its shear history during formation (in the fluidised bed granulator) has the following form;

$$b = \frac{K_2 F_i \times \left[\frac{1}{\pi}\arctan\left(\frac{\theta-\theta_0}{\gamma}\right) + \frac{1}{2}\right] - F_H}{(F_H)^n} \tag{7.8}$$

where K_2 and n are proportionality coefficients.

7.5 Results and Discussions

Breakage of granola, which has been produced in a fluidised bed granulator, has been studied at three different geometries namely, a straight pipeline (0^o), a pipeline with two 45^o bends and a pipeline with one 90^o bend at applied air velocity of $42\ m/s$. The aggregated granola was produced subject to binder addition rates of $0.4\ g/s$, $0.8\ g/s$ and $1.2\ g/s$ at 2, 3 and $4\ bar$ nozzle pressures. The effects of flow geometry, binder addition rates and nozzle pressures on subsequent breakage rates will each be examined in turn. Equation (7.8) was employed for the modelling of granola breakage during pneumatic conveying.

7.5.1 Effect of flow geometry

The effect of flow geometry on breakage rate is displayed in Figure 7.3. The breakage rate of granules produced at 2 bar nozzle pressure at different binder addition rates are shown. Figure 7.3 suggests that more breakage occurred in the 90^o bend configuration then the breakage rate obtained in the two 45^o bend pipe and the straight pipe for all binder addition rates. As the number of cycles increases the overall breakage rates decrease and the effect of the pipe configuration becomes insignificant. However, this doesn't contradict a positive correlation between degree of breakage and impact angle.

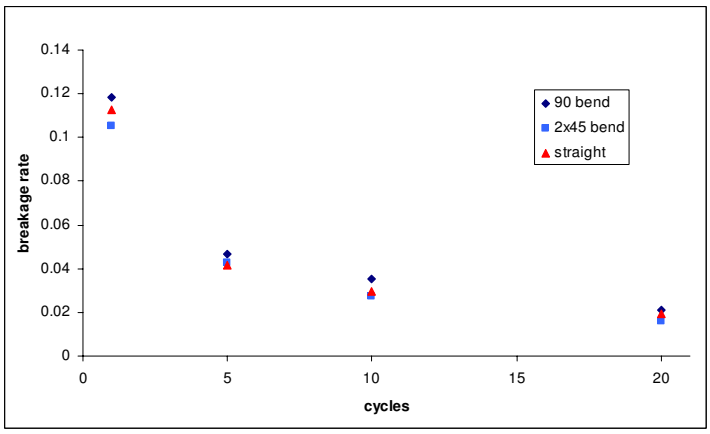

(a) Binder addition rate of 0.4 g/s

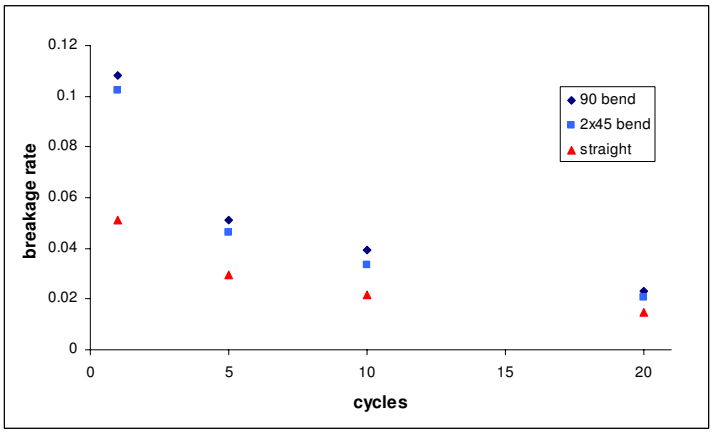

(b) Binder addition rate of 0.8 g/s

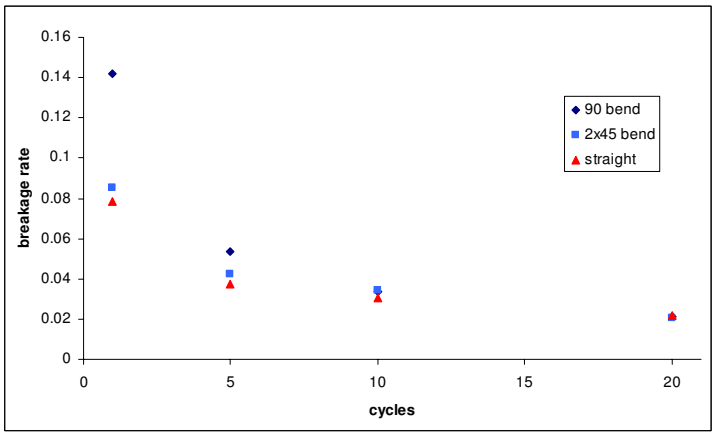

(c) Binder addition rate of 1.2 g/s

Figure 7.3: Breakage rates for different flow geometries. Granules produced at various binder addition rates at 2 bar nozzle pressure.

7.5.2 Effect of binder addition rate

The effect of binder addition rate on the particle breakage at different pipe configurations is displayed in Figure 7.4. Although, the results show that the $0.4\ g/s$ binder addition rate has the highest breakage rate after the first cycle for two of the configurations, the extent of the breakage rate after this is not significantly different as the number of cycles increases for all binder addition rates. This shows that the effect of the binder addition rate is not a significant factor with respect to the breakage rate. This is further strengthened by the results displayed comparing the effect of binder addition rate at different nozzle pressures in the 90^o bend pipeline, which has the highest breakage rate (Figure 7.5). According to results shown in Figure 7.5, it can be inferred that neither the binder addition rate nor the nozzle pressure applied during binder addition plays an important role in determining the breakage rate.

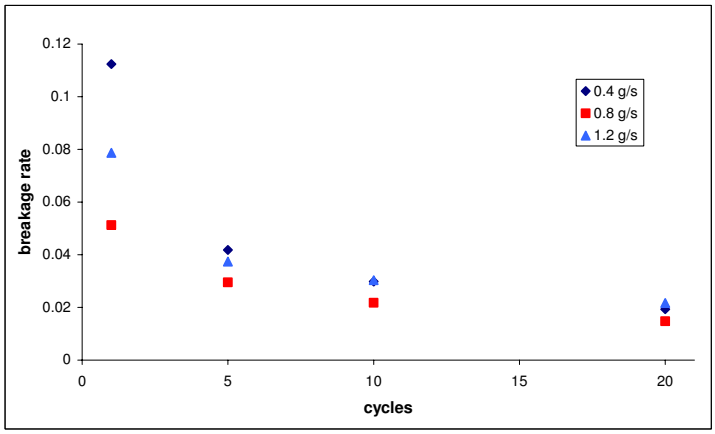

(a) A straight pipe

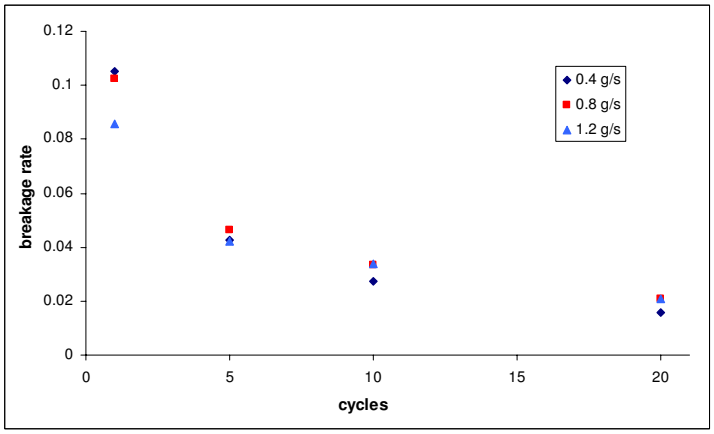

(b) A two 45^o bend pipe

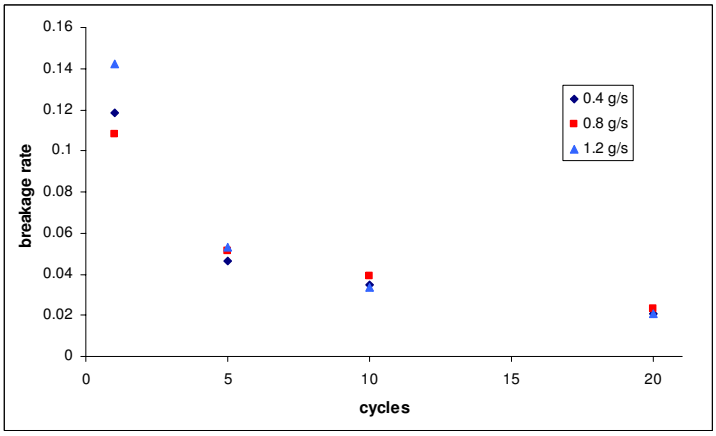

(c) A 90^o bend pipe

Figure 7.4: Breakage rates for granules produced at different binder addition rates at various flow geometries. Granules produced at 2 bar nozzle pressure.

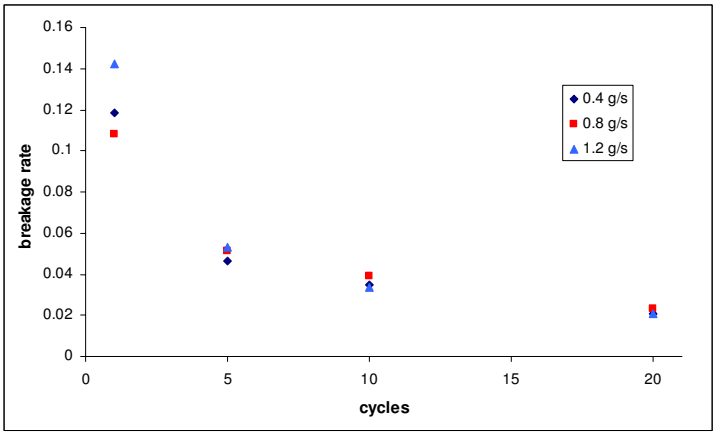

(a) At applied nozzle pressure of 2 bar

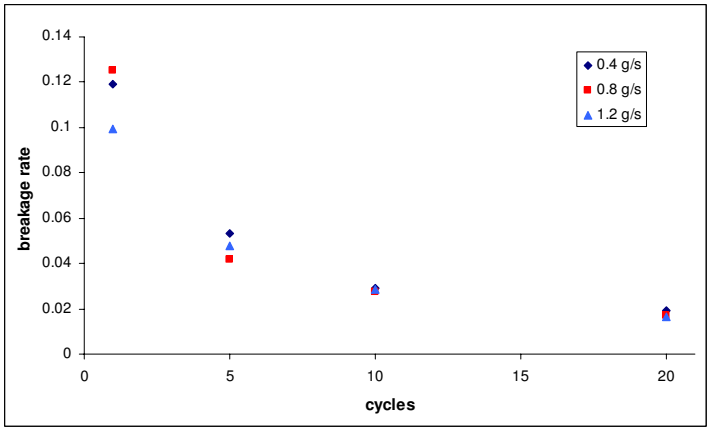

(b) At applied nozzle pressure of 3 bar

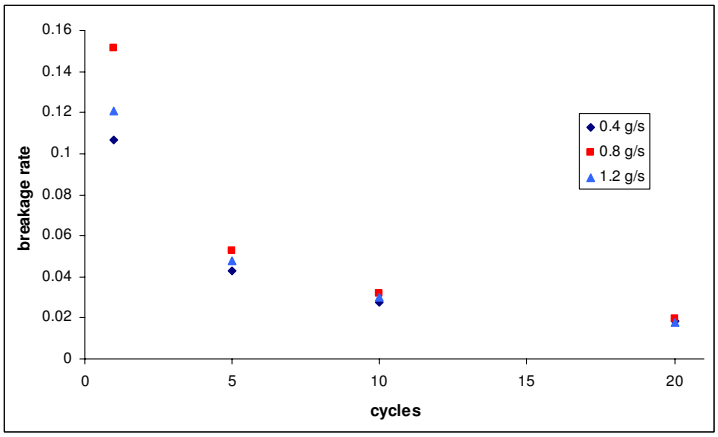

(c) At applied nozzle pressure of 4 bar

Figure 7.5: Breakage rates for different binder addition rates at various nozzle pressures in 90^0 pipeline.

7.5.3 Effect of nozzle pressure

The effect of nozzle pressure on the particle breakage at various binder addition rates in the 90^o bend pipeline configuration is illustrated in Figure 7.6. The breakage rate differs at the first cycle, but there is no consistency. For instance, while the granules produced at $4\ bar$ nozzle pressure had the highest breakage rate at $0.8\ g/s$ binder addition rate, the granules produced at $2\ bar$ nozzle pressure has the highest breakage rate at $1.2\ g/s$ binder addition rate. There are only slight differences among the breakage rates at higher numbers of cycles. Accordingly, as indicated in Figure 7.5, it seems to appear that the applied nozzle pressure history during granulation does not have an obvious effect on the rate of granola breakage.

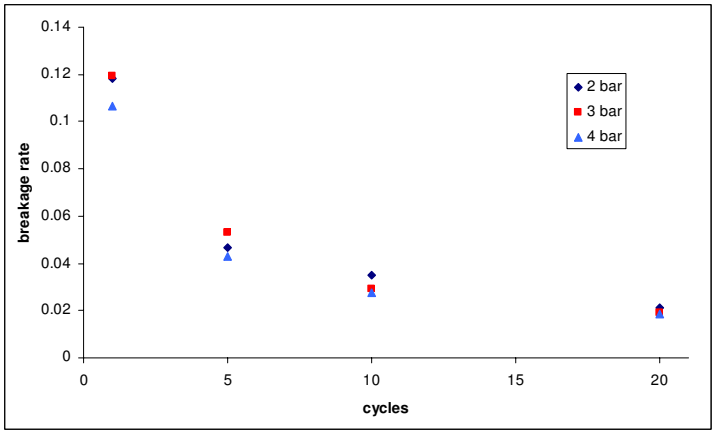

(a) Binder addition rate of 0.4 g/s

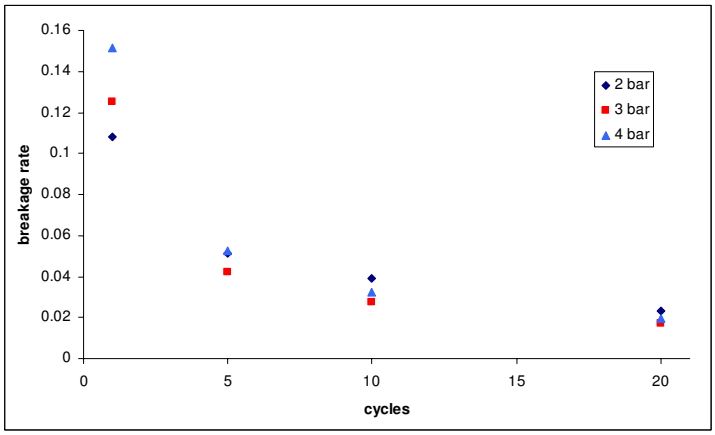

(b) Binder addition rate of 0.8 g/s

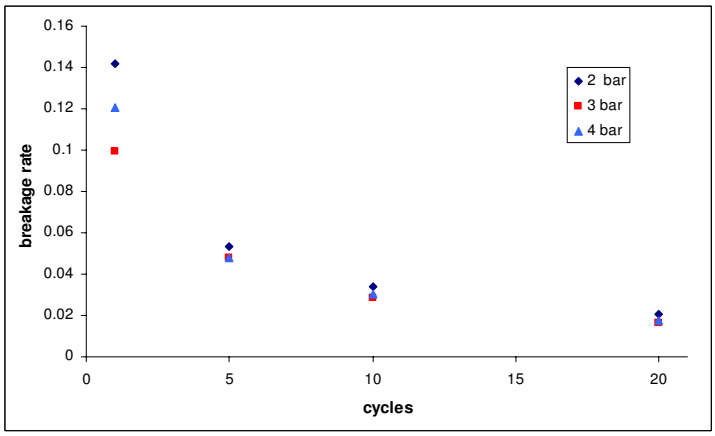

(c) Binder addition rate of 1.2 g/s

Figure 7.6: Breakage rates for granules produced at different nozzle pressures at various binder addition rates in 90^0 pipeline.

7.5.4 Model results

Modelling particle velocity

Equation (7.8) was used to model the breakage rate in the pneumatic conveying rig. The proportionality coefficients were estimated by minimizing the error between predicted and experimental breakage rate. The particle velocity was obtained using equations 6.17 and 6.21 in Chapter 6 for various rig configurations. Figure 7.7 displays particle velocity during various pipelines. The impact velocity at the 90^o bend is 15 ms^{-1} at 42 ms^{-1} air flow velocity. The particle leaves the pipeline with a velocity of 8 ms^{-1}. In the two 45^o bend pipeline configuration, particles reach a velocity of 12 ms^{-1} at the first bend, 6 ms^{-1} at the second bend, and leave from the pipe at a velocity of 5.7 ms^{-1} at 42 ms^{-1} air flow velocity. In this case of the straight pipeline , particles leave from the pipeline at a velocity of 15 ms^{-1} at 42 ms^{-1} air flow velocity.

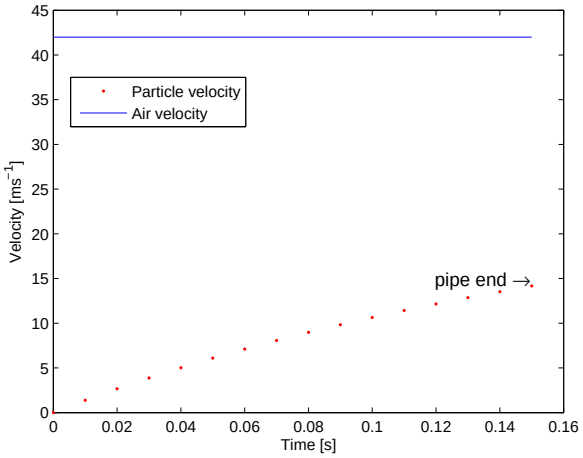

(a) In the straight pipeline

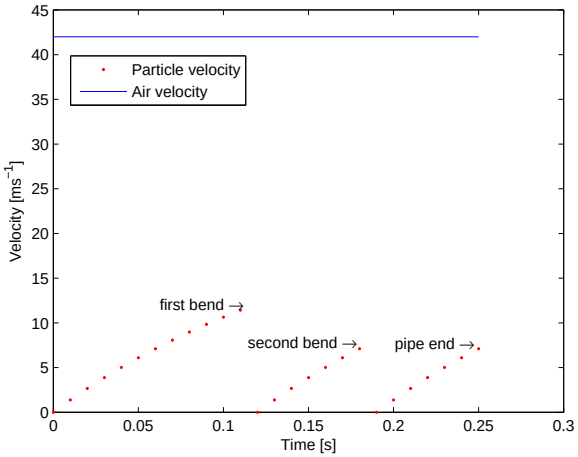

(b) In the two 45^0 bend pipeline

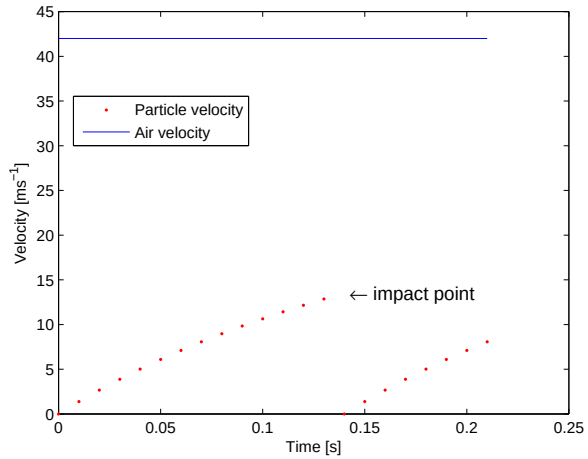

(c) In the 90^0 bend pipeline

Figure 7.7: Particle velocity at various pipe configurations.

Modelling breakage rates

The model results obtained from equation (7.8) were compared with experimental outputs. Figure 7.8 shows the comparison of the model with the experimental results for three different pipe configurations. Figures 7.8b and 7.8c exhibit good overall agreement between the model and the experimental results. Although the model marginally underpredicts the experimental results, it provides a reasonable estimate with respect to the experimental results. On the other hand, the model fails to predict the breakage rate during a straight pipeline (Figure 7.8a). This may be due to the fact that why particle-wall contacts were considered while particle-particle collisions, which may yield further breakage, were not considered (Reynolds et al., 2005; Pahk and Klinzing, 2008). Moreover, the model developed here assumed a constant shear history (during granule production) of particles.

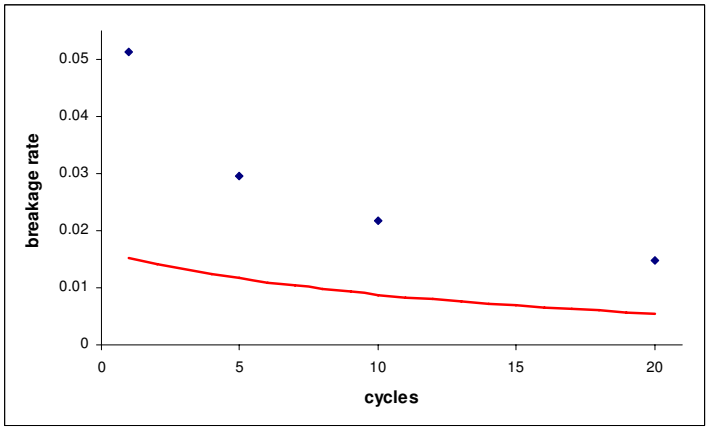

(a) A straight pipe

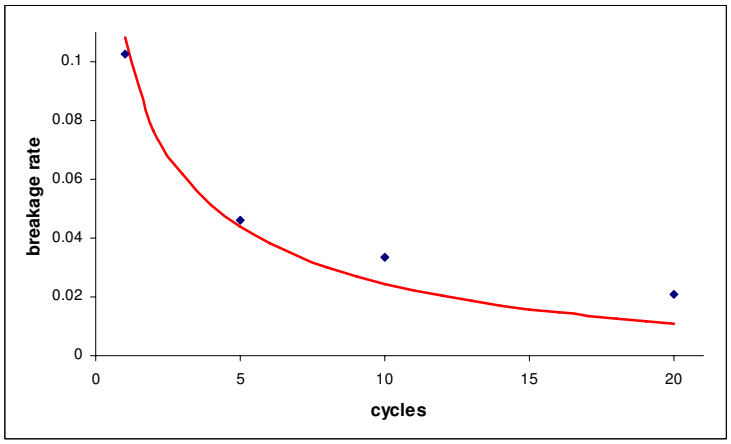

(b) A two 45^o bend pipe

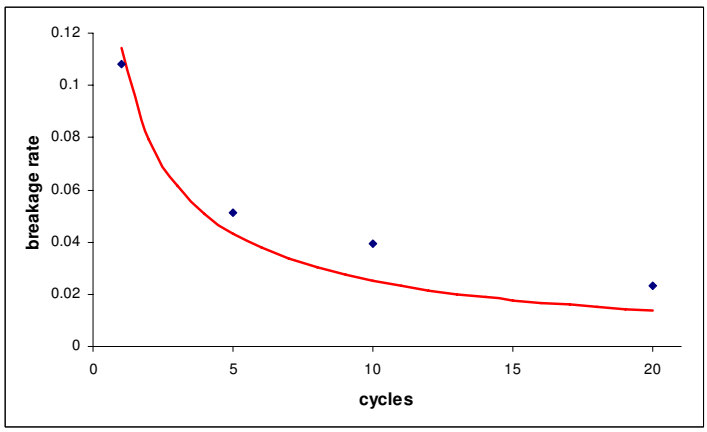

(c) A 90^o bend pipe

Figure 7.8: Particle breakage rates at various pipe geometries. (Continuous line displays model results, points are experimental data.)

7.6 Conclusion

In this chapter, the breakage of the granola during the pneumatic conveying has been examined. The particle breakage of granola produced in the fluidised bed granulator was taken into account. It was observed that the breakage rate of the particles depends on the flow geometry. Furthermore, it was also shown that the aggregate production history has no significant effect on the breakage rate. The highest breakage rate observed at 90^o bend pipeline geometry at 4 bar applied air pressure.

On the other hand, no apparent trend was observed for different nozzle pressures and various binder addition rates. Additionally, a simple physical based model is derived to predict the particle breakage rates using a number of pipe configurations, on the basis of a constant shear history. The proposed model allows the prediction of breakage rates for the D_{50} (median size) particle size as a representative size class of the whole particle size distribution.

Chapter 8

Population Balance Modelling of Granola Breakage during Pneumatic Conveying

This chapter describes particle breakage of granola during pneumatic conveying through the development of a population balance model. Firstly, an introduction will be provided. Thereafter, the breakage equation will be introduced and the application of Markov chains to the breakage equation will be presented. Then, results obtained from both model and experimentation will be discussed in the results and discussion section. Finally, conclusions of the work done in this chapter will be provided.

8.1 Introduction

The breakage of liquid-liquid, solid-liquid and solid-gas dispersions occurs in many industrial processes during the transport of particulate materials. The transportation of

particulate materials is usually achieved by moving through cylindrical pipes. Granola is a baked crispy food product where oats and other cereals are bound together with a binder, in this case honey, water and oil, to form a structured unit aggregate. The aggregates have dimensions ranging from the size of the primary ingredient particles up to about 10 mm and are roughly spherical in shape. They typically exhibit a high degree of friability. Particle breakage of the aggregated granola can occur during conveying as product is transferred as part of the production process on its way to packaging. Such breakage occurs as a result of particle-particle and particle-wall collisions.

In general terms two breakage mechanisms for dry granules have been proposed; firstly erosion or attrition and secondly fracture or fragmentation (Iveson et al., 2001). Where erosion is the dominant breakage mechanism, there results one large fragment of size close to the parent aggregate and a number of smaller fine particles. Where breakage is by fracture, this results in the production of a number of smaller fragments. In addition, the fracture type of breakage is divided into two modes; cleavage in which parent particles break into a small number of fragments of similar size and shattering which results in many fragments of a wide range of sizes (Redner, 1990). Particle breakage is usually considered an undesirable process since it can result in reduction in particle size, in changes to the particle size distribution, dust generation and handling and storage problems which may cause the particles to not satisfy the requirement specifications any longer (Salman et al., 2003).

In this chapter, population balance equations are used to model the breakage of granola that is conveyed through a pneumatic conveying pipeline rig (Figure 7.1, Chapter 7). Granola passing through a cylindrical pipe is examined and an experimentally derived breakage frequency is applied to construct a suitable population balance model to characterize the breakage process. The samples were conveyed through one particular rig and particle size distributions were measured before and after conveying

to quantify the amount of breakage which occurred. Parameters affecting the breakage rate can be divided into three categories: particle strength, conveying pipe line geometry and applied pressure during conveying.

Population balances are constructed to describe the breakage of granola for volume fraction density using a discretization method through the application of the Markov chains method. The Markov chains method is quite a powerful tool in stochastic theory. The main Markov property is that if an initial condition and a probability distribution of a state are known at a certain time, then the probability distribution of this state at any future time can be computed.

8.2 Breakage Equation

Modelling a breakage process can be achieved by constructing a population balance equation in the form of breakage functions. This can be either in continuous or in discrete form. Moreover, two types of breakage equations are defined;

- a number density based breakage equation
- a mass density based breakage equation

When particles display homogenous density then a mass density based breakage equation can be considered as a volume density based breakage equation. In this study, it is assumed that particles are spherical and of broadly homogenous density, thus a mass density based breakage equation will be used to model volume fraction.

8.2.1 Continuous population balances

The general continuous form of a homogenous breakage process describing the evolution of particle size distribution in time for a batch process can be described according to the following expression (Ramkrishna, 2000);

$$\frac{\partial f(x,t)}{\partial t} = \int_x^\infty q(x,y)b(y)f(y,t)dy - b(x)f(x,t) \tag{8.1}$$

In this equation $f = f(x,t)$ is the particle size distribution defined on the domain of particles of diameter x at time t. $q(x,y)$, which is known as breakage kernel or daughter size distribution (fragment size distribution), is the probability distribution of particles of diameter x resulting from the breakup of particles of diameter y. $b(x)$ is the breakage frequency (the breakage rate) at which particles of size x break per unit time.

Equation (8.1) states that the change in the number of particles of size x over an incremental time step at time t depends on the number of new particles of size x produced by break-up of a particle bigger than size x (the integral part in right hand side) and depends on the average number of particles lost by breakage of particles of size x.

Note that $q(x,y)$ should satisfy the mass conservation requirement such that the total mass of particles resulting from the break-up of a particle of size of y must be equal to mass of y (McGrady and Ziff, 1986).

$$\int_0^y m(x)q(x,y)dx = m(y) \tag{8.2}$$

where $m(x)$ and $m(y)$ are the mass of particle size of x and y respectively.

The average number of fragments resulting from the breakage of a single particle of diameter y can be defined as;

$$\nu(y) = \int_0^y q(x,y)dx \tag{8.3}$$

8.2.2 Discretized population balance

Classification of a continuous size range into discrete intervals is the first step in constructing a discretized population balance equation. Two main approaches can be used to select the classification of the states; uniform discretization and geometric discretization. These approaches were previously introduced in Chapter 4.

The discrete form of a breakage equation can be given as;

$$\frac{dN_i(t)}{dt} = \sum_{j=i+1}^{n} q_{ji} b_j N_j(t) - b_i N_i(t) \tag{8.4}$$

where $N_i(t)$ is the number of particles in the interval i at time t, b_i is the breakage frequency of particles in the interval i, and q_{ji} is the probability distribution of particles of interval i which are formed from a break-up of particles of interval j. Accordingly q_{ji} can be formulated as;

$$\begin{cases} q_{ji} = \int_{d_{i-1}}^{d_i} q(x, d_{j-1})dx, & \text{if } 2 \leq j \leq n \text{ and } 1 \leq i < j, \\ q_{ji} = 0 & \text{else.} \end{cases} \tag{8.5}$$

The common assumption in the literature is that if a particle of interval i breaks, its fragments cannot remain in the interval i, i.e., the size of any fragment particle must be sufficiently large to produce a transition within the discretization scheme. The

maximum interval of the fragment particle can be $i-1$. Additionally, particles in the lowest interval are assumed to be the smallest possible size and they cannot break. On this basis, the breakage frequency of the first interval b_1 equals 0.

8.2.3 The Markov Chain Method

A Markov process can be used to analyse stochastic processes in which some variable changes randomly in time. The main Markov property is that the future state of the variable only depends on its current state and is not dependent on the history of states that have been passed through. The construction of a Markov chain can be defined by a transition matrix $\mathbf{P}$, a state vector $\mathbf{a}(t)$ and a transition time step τ . The transition matrix has entries p_{ij} which is the conditional probability that the variable in state i, will move to state j, in a single time step. Accordingly, the transition matrix $\mathbf{P}$ is given by $n \times n$ square matrix as follows (L. Farina, 2000);

$$\mathbf{P} = \begin{pmatrix} p_{11} & p_{12} & \dots & p_{1n} \\ p_{21} & p_{22} & \dots & p_{2n} \\ \dots & \dots & \dots & \dots \\ p_{n1} & p_{n2} & \dots & p_{nn} \end{pmatrix}_{n \times n}$$

The vector $\mathbf{a}(t)$ which has components $a_1(t), a_2(t), ..., a_n(t)$ represents the state probability distribution vector of the system at time t.

Properties of the transition matrix are;

- The sum of all probabilities of state i equals 1,

  i.e., $p_{i1} + p_{i2} + ... + p_{in} = 1 \qquad \forall\, i = 1, ..., n$

- Each row of the transition matrix has at least one nonzero element.

- Entities of the transition matrix are nonnegative, since p_{ij} is a probabilistic ratio, i.e. p_{ij} values lie between 0 and 1.

If the probability for an entity currently in the state j at time t is denoted by $a_j(t)$, then the state probability distribution of state i for the next time step, $a_i(t+\tau)$, is given by the sum of product of all probabilities. This is formulated as follows;

$$a_i(t+\tau) = \sum_{j=1}^{n} p_{ji} a_j(t) \tag{8.6}$$

Accordingly, equation (8.6) can be represented in matrix notation as;

$$\begin{aligned} &\left[\ a_1(t+\tau), .., a_n(t+\tau)\ \right] \\ &\quad = \left[\ a_1(t), .., a_n(t)\ \right] \begin{pmatrix} p_{11} & p_{12} & \dots & p_{1n} \\ p_{21} & p_{22} & \dots & p_{2n} \\ \dots & \dots & \dots & \dots \\ p_{n1} & p_{n2} & \dots & p_{nn} \end{pmatrix} \end{aligned} \tag{8.7}$$

If the transition probabilities are independent on time, in other words the transition matrix $\mathbf{P}$ is a constant matrix, then the it is called a homogeneous Markov chain. Random walks is the most common example for the homogeneous chain (Kemeny and Snell, 1960). The game of snakes and ladders which has always been an eye catching example of Markov chains is another example of homogeneous chains (Cronin et al., 2007). In many chemical engineering applications, residence time distribution (RTD) can be modeled as a homogeneous Markov chain (Berthiaux and Mizonov, 2004). On the other hand, if the transition matrix $\mathbf{P}$ is not constant over time, it can be either linear non-homogeneous or non-linear non-homogeneous chain depending on the changing of $\mathbf{P}$ over time. If the chemical kinetics of the process is necessary to be

counted for the modelling, this kind of processes can be modeled by non-homogenous Markov chains. The general form of equation (8.6) for a time-homogeneous and non-homogeneous transition matrices $\mathbf{P}$ for different time steps can be given by the following equations respectively;

$$\mathbf{a}(t + m\tau) = \mathbf{a}(t)\mathbf{P}^m \tag{8.8a}$$

$$\mathbf{a}(t + \tau) = \mathbf{a}(t)\mathbf{P}(t) \tag{8.8b}$$

In addition, the selection of a time step is important for the Markov model. Some process systems have a natural periodicity such as rotating mixers (period of rotation), vibratory conveyors (period of excitation) for which the transition time step can be chosen from basic physics. For systems which have no period, the time step should be chosen taking process kinetics and total processing time into account. Also the state property under analysis (particle size in this work) must be divided into a sufficient number of intervals. Consequently, a good pair of (τ, n) should be selected to represent the time and particle property in discrete form efficiently.

Although, in the value of its development by Andrei Andreyevich Markov (1856-1922) (Markov, 1906) the Markov theory has been used in many fields such as astronomy, biology, computer science, communications, forecast, game theory and radio engineering, it has been under represented in chemical engineering to the point that it can be suggested it is still relatively unknown in this field. Indeed, there is only one book which was published in 1998 on applications of Markov chains in chemical engineering (Tamir, 1998) and relatively small number of papers on applications of Markov chains in chemical engineering have been published such as particle flow in fluidised bed (Fox and Fan, 1986; Dehling et al., 1999; Harris et al., 2002); particle mixing (Aoun-Habbache et al., 2002; Berthiaux et al., 2004; Ponomarev et al., 2009);

particle breakage (Berthiaux, 2000; Berthiaux et al., 2005).

8.3 Application of Markov Chains to Breakage Equation

Assuming that $b(x)$ and $q(x, y)$ are not affected by time, PBEs can be solved using a time-homogeneous Markov chain. It is also possible to apply different stationary (time-homogeneous) transition matrices for countable sub-time intervals. The Markov chain algorithm can be applied to equation (8.4) by taking the Markovian time step as $dt = \tau$ which yields following equation;

$$\triangle N_i(t) = \sum_{j=i+1}^{n} q_{ji}\tau b_j N_j(t) - \tau b_i N_i(t) \tag{8.9}$$

In this equation, $\triangle N_i(t)$ is the rate of change in the number distribution of state i. When $N_i(t)$ is added to both sides of the equality in equation (8.9), the following equation is obtained;

$$N_i(t) + \triangle N_i(t) = \sum_{j=i+1}^{n} q_{ji}\tau b_j N_j(t) + (1 - \tau b_i)N_i(t) \tag{8.10}$$

Equation (8.10) represents the summation of the number distribution and the rate of change in number distribution of interval i in a present state equals to its next future state. That is to say that the left hand side of the equality in equation (8.10) denotes the next future state of a given present state.

8.3.1 Transition matrix, $\mathbf{P}$

The transition matrix $\mathbf{P}$ is a key element of the Markov chain model and construction of this matrix $\mathbf{P}$ for a breakage process is based on the characterization of a diagonal matrix $\mathbf{D}$ and a lower triangular matrix $\mathbf{L}$. In this manner, equation (8.10) can be represented in matrix notation by dividing the whole system in two parts, such that;

i) define an $n \times n$ diagonal matrix $\mathbf{D}$ with entries;

$$D_{ii} = 1 - \tau b_i \tag{8.11}$$

$$\mathbf{D} = \begin{pmatrix} 1 & 0 & 0 & . & . & 0 \\ 0 & 1-\tau b_2 & 0 & . & . & 0 \\ . & . & . & . & . & . \\ . & . & . & . & . & . \\ 0 & 0 & 0 & . & 1-\tau b_{n-1} & 0 \\ 0 & 0 & 0 & . & . & 1-\tau b_n \end{pmatrix}_{n \times n}$$

ii) define an $n \times n$ lower triangular matrix $\mathbf{L}$ with entries;

$$L_i = \tau b_i Q_i \tag{8.12}$$

where L_i represents i^{th} row of $\mathbf{L}$ matrix, Q_i is i^{th} row of matrix Q which is built by q_{ij} (see equation (8.5)), and b_i is i^{th} element of row vector $\mathbf{b}$. In a breakage event when a particle breaks, each fragment of this particle can only go to lower states. Therefore the lower triangular matrix can be chosen since the upper entries are zero.

$$\mathbf{L} = \begin{pmatrix} 0 & 0 & . & . & 0 & 0 \\ \tau b_2 q_{21} & 0 & . & . & 0 & 0 \\ \tau b_3 q_{31} & \tau b_3 q_{32} & . & . & 0 & 0 \\ . & . & . & . & . & . \\ . & . & . & . & . & . \\ \tau b_n q_{n1} & \tau b_n q_{n2} & . & . & \tau b_n q_{n,n-1} & 0 \end{pmatrix}_{n \times n}$$

According to equation (8.11) while selecting τ it should be noted that τb_i cannot be greater than 1. Consequently the Markovian transition matrix $\mathbf{P}$ equals sum of matrices $\mathbf{L}$ and $\mathbf{D}$;

$$\mathbf{P} = \mathbf{L} + \mathbf{D} \tag{8.13}$$

Comments on transition matrix $\mathbf{P}$

If number distribution is being modelled rather than mass distribution and the total number of particles increases in a breakage process, then the usual sum to unity will not apply directly. Initially the number distribution function, $f(x,t)$, is normalized (i.e., area under $f(x,0)$ is 1). However, the total number in the system will increase with time as a result of the breakage events. This results in the area under the curve, $f(x,t)$, to be greater than 1 when $t > 0$. This is analogous to that for the transition matrix $\mathbf{P}$. Even if the sum of initial state probability distribution vector, $a(0)$, is 1, this sum will be greater than 1 at later stages. For the comparison, both $f(x,t)$ and $a(m)$ should be normalized to 1 for each time step. On the other hand, there is no need to renormalization procedure for the modelling of the mass distribution since the particle mass is an additive property. This is same for the transition matrix $\mathbf{P}$ which meets the condition of normalization under the case of mass distribution.

8.4 Breakage Functions

The breakage functions which include the breakage frequency, $b(x)$, and the fragment size distribution, $q(x, y)$, are the core elements of population balance equations (PBEs). In this work, the breakage frequency which is based on the granola aggregates flowing through the conveying pipe is derived from the experimental data. A power law breakage frequency was considered to be size dependent and to be a function of impact velocity, shearing history and impact angle. It has the following relationships;

$$b(x) \propto function(x; v_i, \theta) \tag{8.14a}$$

$$b(x) \propto \frac{1}{H} \tag{8.14b}$$

where $b(x)$ is directly proportional to the impact velocity v_i, particle diameter x and impact angle θ. $b(x)$ is inversely proportional to the particle hardness, i.e., the shearing forces. The breakage frequency was taken to be a function of the particle volume, i.e., its cubic diameter. The relationship between breakage frequency and the impact angle was defined in the form of a Cauchy distribution since an increase in impact angle will result in an increase in breakage force. It describes the distribution of random angle between the vertical axis and a tilted line segment. The cumulative distribution function of Cauchy distribution has the following form;

$$\frac{1}{\pi} \arctan\left(\frac{\theta - \theta_0}{\gamma}\right) + \frac{1}{2} \tag{8.15}$$

where θ is the bend angle, $\theta_0 > 0$ is the location parameter and $\gamma > 0$ is the scale parameter of the distribution. Furthermore, the hardness was found to be an inverse

exponential function of the impeller speed, w, as previously defined in Chapter 7.

Accordingly, $b(x)$ is as follows;

$$b(x) = k\frac{1}{\exp(-w)}v_i\left[\frac{1}{\pi}\arctan\left(\frac{\theta-\theta_0}{\gamma}\right)+\frac{1}{2}\right]x^3 \tag{8.16}$$

where k is a proportionality coefficient.

During the conveying part of the process, the transparent PMMA (Perspex) pipeline enabled observation of the breakage behaviour of particles. Particle conveying through the pipeline was recorded with a high speed camera (AOS, X-Motion, Switzerland) and visual inspection of the breakage mechanism appeared to suggest breakage was by attrition. Since attrition was observed, an erosion type breakage mechanism was chosen for fragment size distribution. In this work, two types of the fragment size distribution are considered; an erosion type and a modified erosion type. The erosion type fragment size distribution has the following form;

$$q_{ji} = \begin{cases} \frac{x_i^3}{x_i^3+x_{j-1}^3} & \text{if} \quad i=1 \\ \frac{x_i^3}{x_i^3+x_{j-1}^3} & \text{if} \quad i=j-1 \\ \\ 0 & \text{elsewhere} \end{cases} \tag{8.17}$$

where x_i and x_j are the representative diameter size of interval i and j respectively. Figure 8.1 displays size distribution probabilities of fragments resulting from the breakup of the parent particle of interval 10 which is arbitrarily selected for illustration. That is, if a particle in interval 10 breaks, the fragments can go to both interval 9 and 1.

Berthiaux et al. (2005) used the following formula for particle breakage in which the

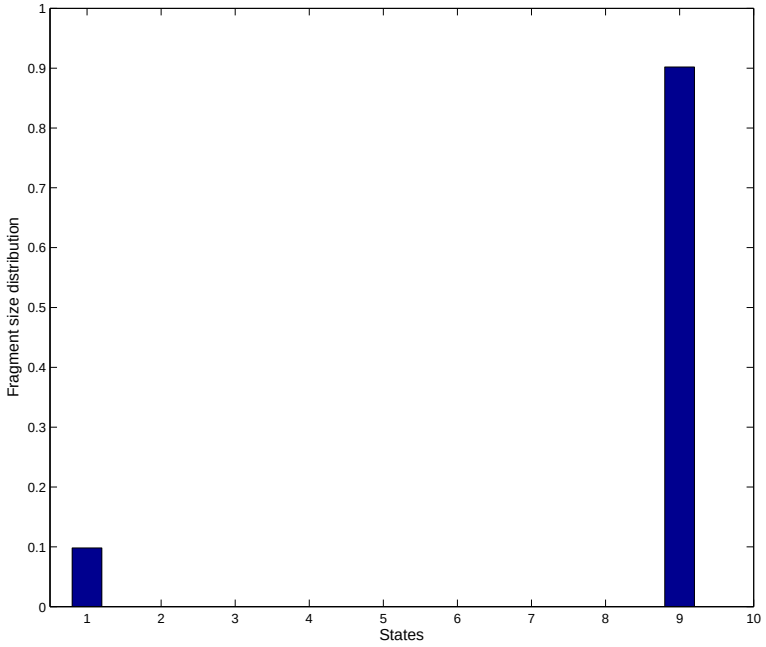

Figure 8.1: Erosion type fragment size distribution

particle can transit only into neighbouring intervals as;

$$q_{jm} = \frac{(x_m^3)^R}{(x_{j-1}^3)^R + (x_m^3)^R} \tag{8.18}$$

If the restriction on only permitting passage to adjacent states is removed, then the distribution function in equation (8.18) can be generalized as;

$$q_{ij} = \frac{(x_j^3)^R}{(x_1^3)^R + (x_2^3)^R + ... + (x_j^3)^R + ... + (x_{i-1}^3)^R} = \frac{(x_j^3)^R}{\sum_{k=1}^{i-1}(x_k^3)^R} \quad \text{for all } i \tag{8.19}$$

The value of R is selected as an adjustment parameter of the model. Berthiaux et al. (2005) reported that in applications to model a real process that R should lie in the range $1 < R < 2$. As the magnitude of the parameter R, is increased, the greater

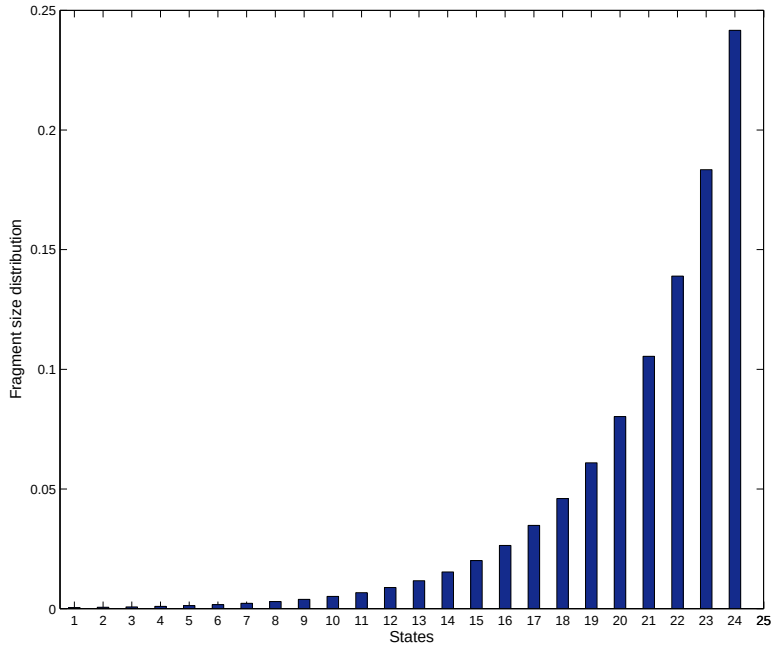

Figure 8.2: Modified erosion type fragment size distribution.

proportion of fragment particles will lie in size classes closer to the parent size class. Increasing R accentuates the fragment particle distribution and biases it towards the size classes closer to the parent class which is more indicative of attrition. For the system under study here, the R value will be taken as the default level of 1 which is indeed well known erosion type fragment size distribution.

The physical interpretation of equation (8.19) is that a granule can break and produce fragment particles in any size class lower than it and the closer the size class is to the parent size class, the greater the proportion of fragment particles that will be found in that class.

Figure 8.2 shows the fragment size distribution by volume fraction which is the proportion of fragment particles (for this example, from size 1 unit to size 24 unit) resulting from the breakup of the parent particle of interval 25.

As a result, the transition matrix $\mathbf{P}$ was constructed using the breakage functions b

and q_{ji} and has the following form;

$$\mathbf{P} = \begin{cases} p_{ji} = (1 - b_j) & \text{if} \quad i = j \\ p_{ji} = b_j q_{ji} & \text{if} \quad i < j \\ p_{ji} = 0 & \text{if} \quad i > j \end{cases} \tag{8.20}$$

Equation (8.20) states that the diagonal entries p_{ji} (when $i = j$) contain the probability that the particle can stay in the same interval after a transition time step. Lower entries (when $i < j$) of the diagonal comprise the breakage process and are the probability that the particle that goes to interval j from the interval i due to a breakage. Upper entries (when $i > j$) of the diagonal represent the aggregation process and are zero since the process involves purely breakage.

The representative particle diameter was found using a uniform ratio method. The whole size range from $0.05\ \mathrm{mm}$ to $11.62\ \mathrm{mm}$ was divided into 30 intervals with a consecutive diameter ratio of 0.4 and as a result, the representative size of each interval is calculated using the arithmetic mean of either ends of the intervals as;

$$x_i = \frac{x_i + x_{i-1}}{2} \tag{8.21}$$

where x_i and x_{i-1} are upper and lower size ends of i^{th} interval.

8.5 Results and Discussions

The aggregation of the granola ingredients took place in the high shear mixer granulator subject to impeller agitation at 150 rpm, 200 rpm and 300 rpm for 6, 9 and 12 minutes with binder addition flow rates of 0.22 g/sec, 0.33 g/sec and 0.65 g/sec.

The aggregates were then baked in an oven for 10 minutes at 160^o.

The pneumatic conveying rig comprised a horizontal pipe of internal diameter 25 mm with different bend configurations (straight pipe, two 45^o bend and 90^o bend). Trials were carried out by applying compressed air pressures of 200 kPa, 300 kPa and 400 kPa which resulted in air flow velocities of $23\ ms^{-1}$, $34\ ms^{-1}$ and $42\ ms^{-1}$ respectively. The particle size distribution of the granola was measured after passage through each rig configuration at respective air velocities for various numbers of cycles. Moreover, the transparent PMMA (Perspex) pipeline enabled observation of the breakage behaviour of particles. Particle conveying through the pipeline was recorded with a high speed camera (AOS, X-Motion, Switzerland) and visual inspection of particle flows appeared to suggest the type of breakage mechanism.

A Camsizer (Retsch, Germany) digital image analyzer was used for measuring particle size distributions of the resultant granola before and after passage through a conveying rig where aggregates are transferred by compressed air at a number of different flow rates.

Two different types of fragment size distribution were applied to the solution of the breakage equation. The results were compared for various sets of experimental results. The size dependent breakage frequency is estimated by minimizing the error between predicted and experimental mean size in time.

8.5.1 Erosion type fragment size distribution

To apply the Markov chains method, an initial state vector $\mathbf{a}(0)$ was set from the initial discrete volume density distribution of the granola aggregates. The transition matrix $\mathbf{P}_{40\times40}$ was calculated according to equation (8.20). Transition time step τ was selected to be 1 cycle since it is possible to examine the breakage process after

each cycle.

Firstly, an erosion type fragment size distribution (equation (8.17)) was applied to equation (8.20). Further calculations of the transition matrix $\mathbf{P}$ for different number of cycles at $23\ ms^{-1}$ air velocity in 90^o bend pipe yield the results shown in Figure 8.3. In this figure, the experimental and the model results show reasonable agreement, particularly for the first few cycles, though less so as the number of cycles increases. The model provides sufficient outputs for overall numbers of cycles.

The results of calculations for the same transition matrix **P** at $34\ ms^{-1}$ air velocity for different number of cycles in 90^o bend pipe are displayed in Figure 8.4. Again there is reasonable alignment between the model and the experimental data. However, the model deviates from the experimental results as the number of cycles increase. Finally, Figure 8.5 shows experimental and model results at $42\ ms^{-1}$ air velocity in 90^o bend pipe. Here again there is reasonable agreement between both experimental data and model at lower cycles, however at higher cycles there is significant deviation. With respect to smaller particles, the model underpredicts the number of small particles and fines. On the other hand, the model tends to slightly overpredict the volume density of larger particles after several runs.

Figures 8.6, 8.7 and 8.8 display the particle size distribution results using erosion type fragment size distribution of experimental results and model results for various numbers of cycles during two 45^o bend pipe at $23\ ms^{-1}$, $34\ ms^{-1}$ and $42\ ms^{-1}$ air velocity respectively. The similar results were found at all applied air pressures as in the case of 90^o bend pipe.

Finally, the particle size distributions of experimental results and model results for various numbers of cycles during 0^o bend pipe (straight pipe) at $23\ ms^{-1}$, $34\ ms^{-1}$ and $42\ ms^{-1}$ air pressures were shown in Figures 8.9, 8.10 and 8.11 respectively. Here again, agreement between the model predictions and experimental results with

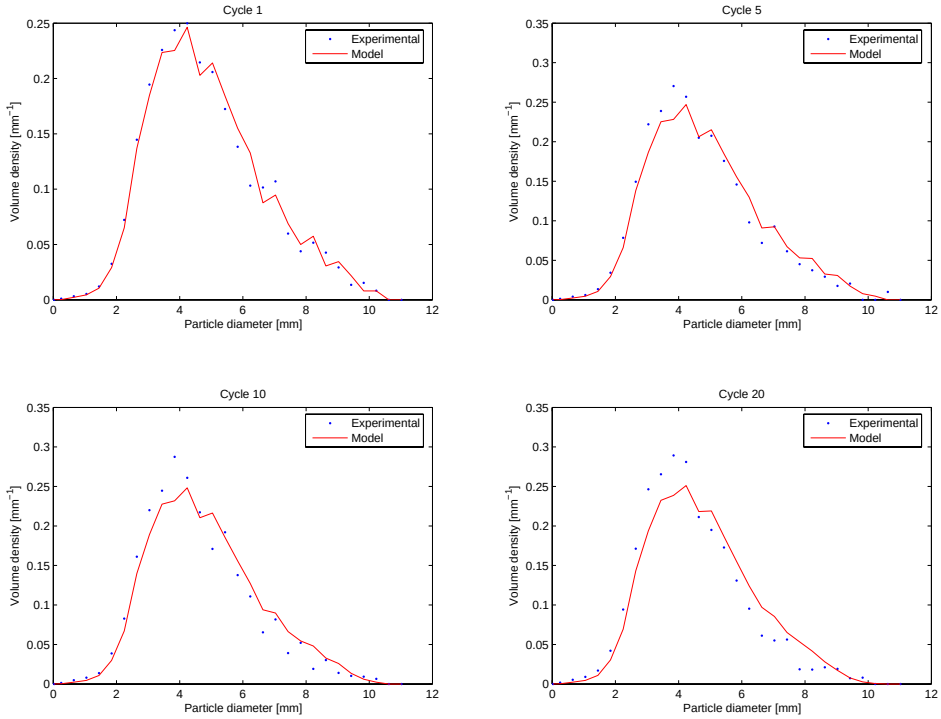

Figure 8.3: Comparisons between the particle size distribution of experimental results and model results for various numbers of cycles at 23 ms^{-1} air velocity during 90^o bend pipe using erosion type.

respect to small particles and fines deteriorates at higher number of cycles.

In this model when breakage occurs, one of the fragments goes to the smallest possible size while the other one goes to the next smaller interval of the parent particle. Thus, the model distribution becomes wider than the experimental distribution over time. This seems to suggest a breakage mechanism whereby aggregates experience a greater degree of breakage by fragmentation into a small number of smaller aggregates. And this seems to be the case to an ever greater extent as the number of cycles increases.

8.5.2 Modified Erosion type fragment size distribution

Using the outputs of erosion type fragment size distribution, a modified erosion type fragment size distribution (equation (8.19)) was employed to equation (8.20). The re-

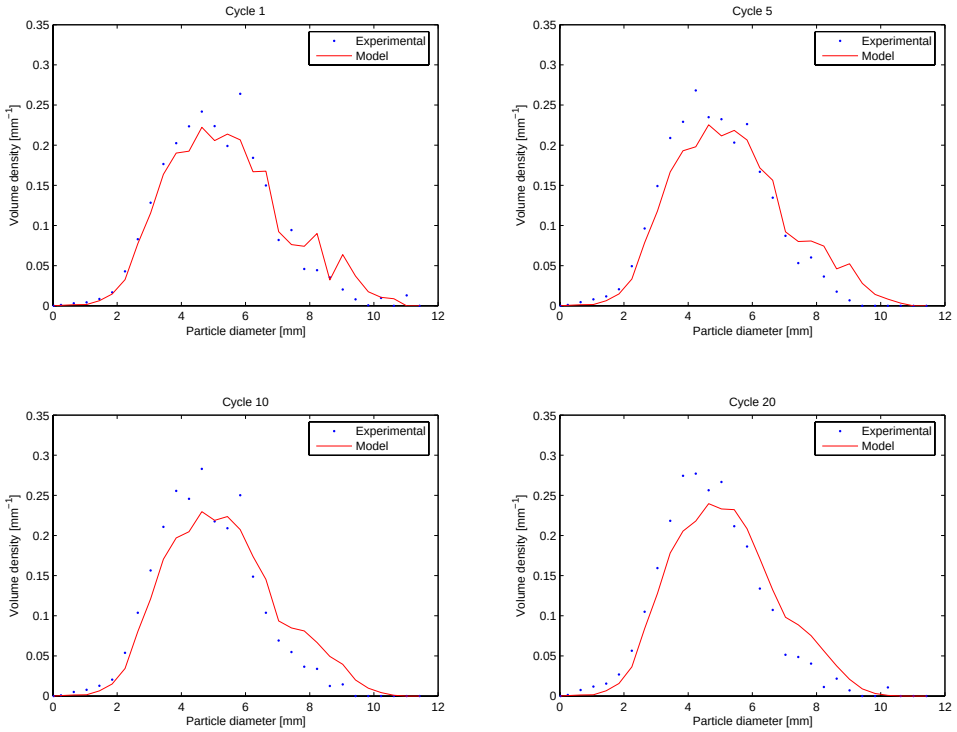

Figure 8.4: Comparisons between the particle size distribution of experimental results and model results for various numbers of cycles at $34\ ms^{-1}$ air velocity during 90^o bend pipe using erosion type.

sults were compared with the experimental data at various air pressures using different types of geometry for a number of cycles.

Figures 8.12, 8.13 and 8.14 shows results from 90^o bend pipe for different number of cycles at $23\ ms^{-1}$, $34\ ms^{-1}$ and $42\ ms^{-1}$ air pressures respectively. Although the agreement between the model predictions and experimental data is not terrific at $42\ ms^{-1}$ air pressure (Fig. 8.14), particularly for the 20^{th} cycle, there is a good agreement for all other cases.

Results from the model and experimental data were compared in Figures 8.15, 8.16 and 8.17 for the two 45^o bend pipe at different numbers of cycles at $23\ ms^{-1}$, $34\ ms^{-1}$ and $42\ ms^{-1}$ air velocities respectively. Similarly, the overall agrement between the model and experimental data is good though the model tends to overestimate the level of breakage compared with the experimental data for later cycles (10 and 20)

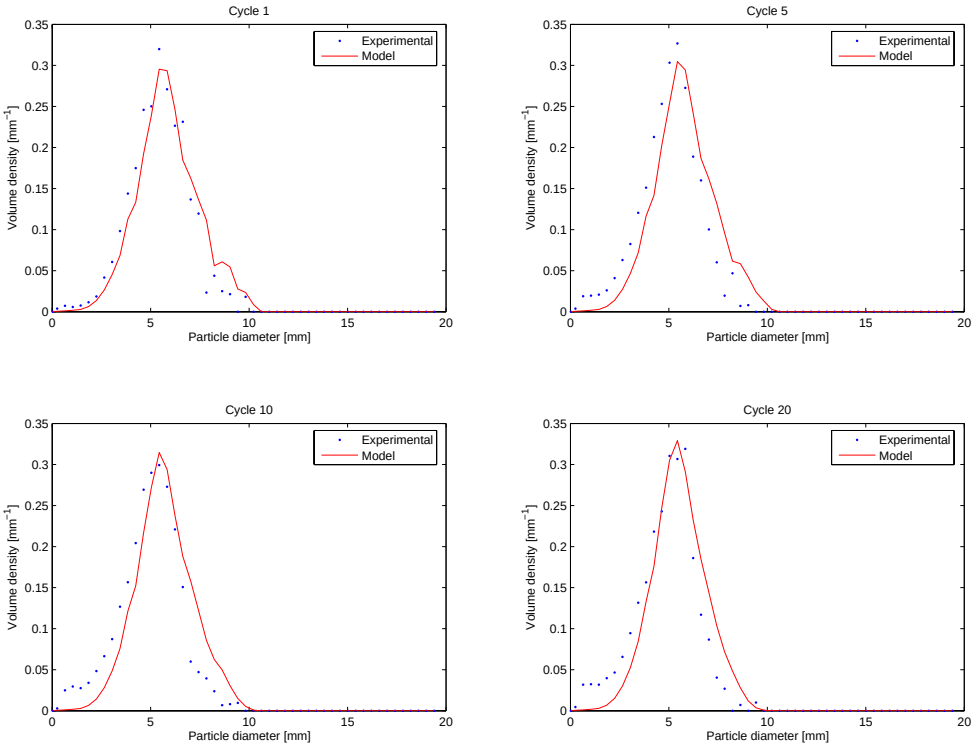

Figure 8.5: Comparisons between the particle size distribution of experimental results and model results for various numbers of cycles at $42\ ms^{-1}$ air velocity during 90^o bend pipe using erosion type.

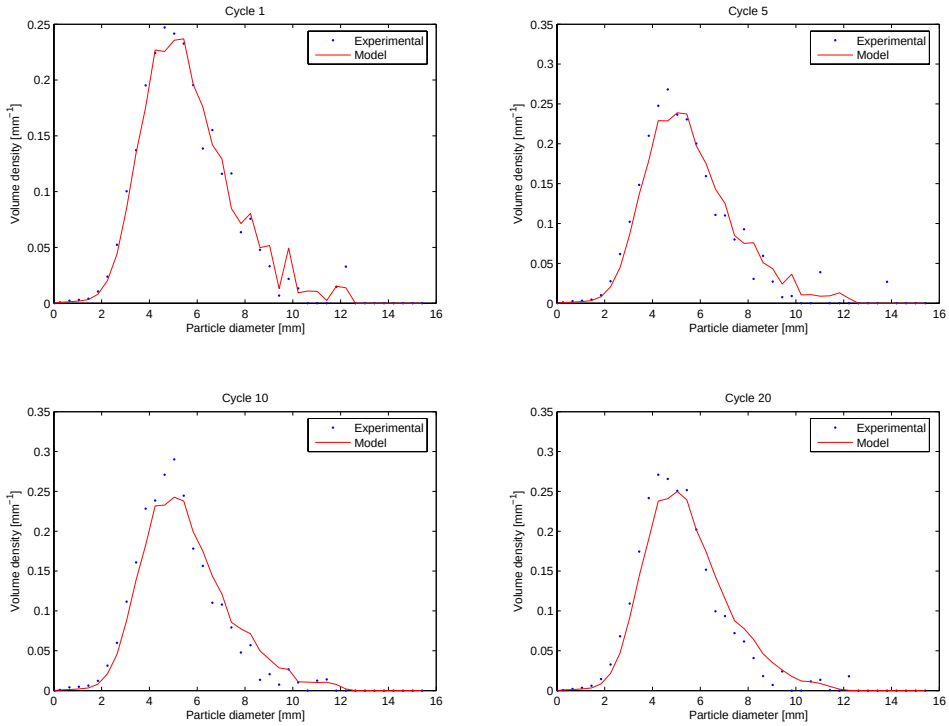

Figure 8.6: Comparisons between the particle size distribution of experimental results and model results for various numbers of cycles at 23 ms^{-1} air velocity during 45^o bend pipe using erosion type.

at the highest air velocity ($42\ ms^{-1}$) in rigs with bends. (Fig. 8.16, 8.17).

Lastly, the model was applied to the breakage occurring in a straight pipe for different number of cycles at $23\ ms^{-1}$, $34\ ms^{-1}$ and $42\ ms^{-1}$ air pressures and the results were compared in Figures 8.18, 8.19 and 8.20 respectively. There is good fit displayed between data over all cycles.

In this model, fragments do not go to the smallest possible size and to the next smaller interval of the parent particle only (as with the original erosion only model), but can go to all possible sizes. That is, when breakage occurs, the probability distribution of the fragments is proportional to size of fragment particles. A greater degree of breakage was achieved by using the modified erosion type fragment size distribution which is satisfactory in predicting the particle size distribution. In general, the model predictions using modified erosion type fragment size distribution depict more rea-

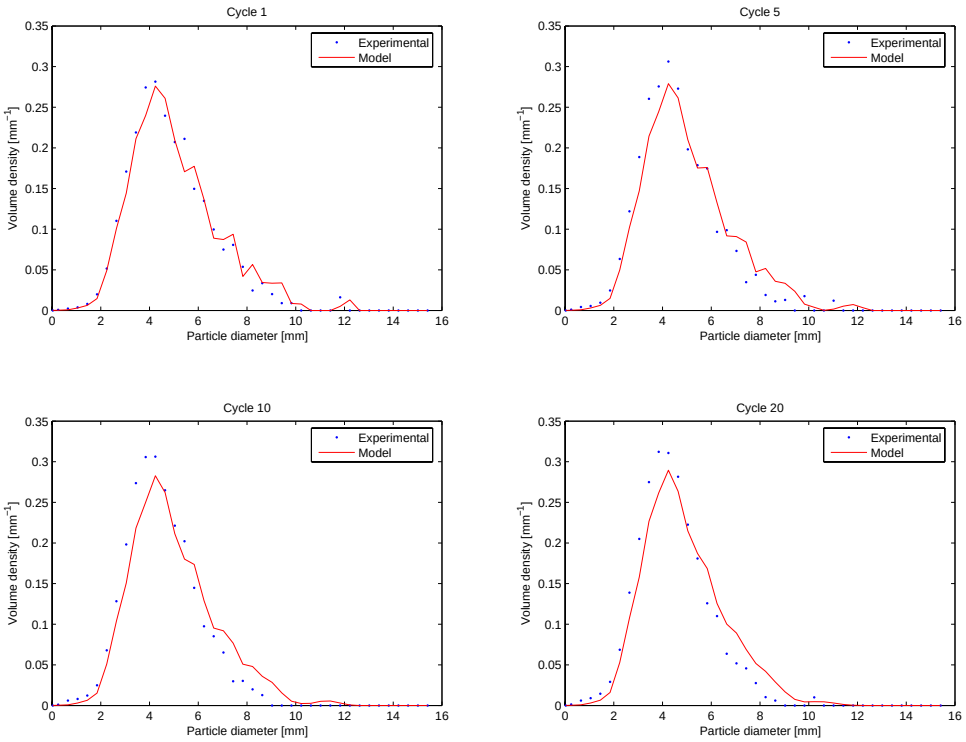

Figure 8.7: Comparisons between the particle size distribution of experimental results and model results for various numbers of cycles at $34\ ms^{-1}$ air velocity during 45^o bend pipe using erosion type.

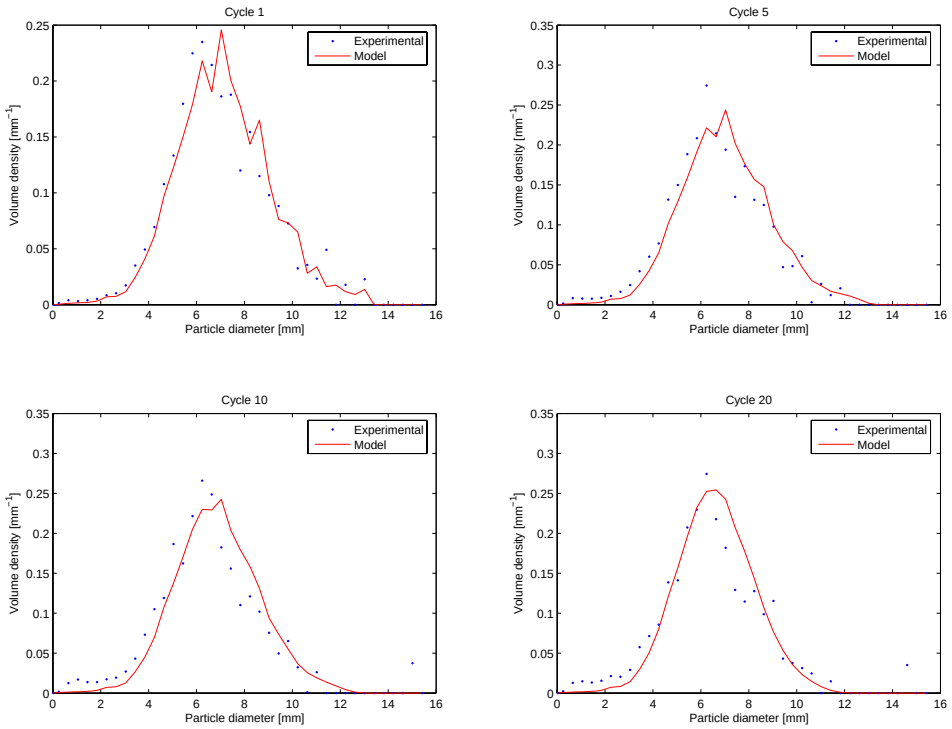

Figure 8.8: Comparisons between the particle size distribution of experimental results and model results for various numbers of cycles at $42\ ms^{-1}$ air velocity during 45^o bend pipe using erosion type.

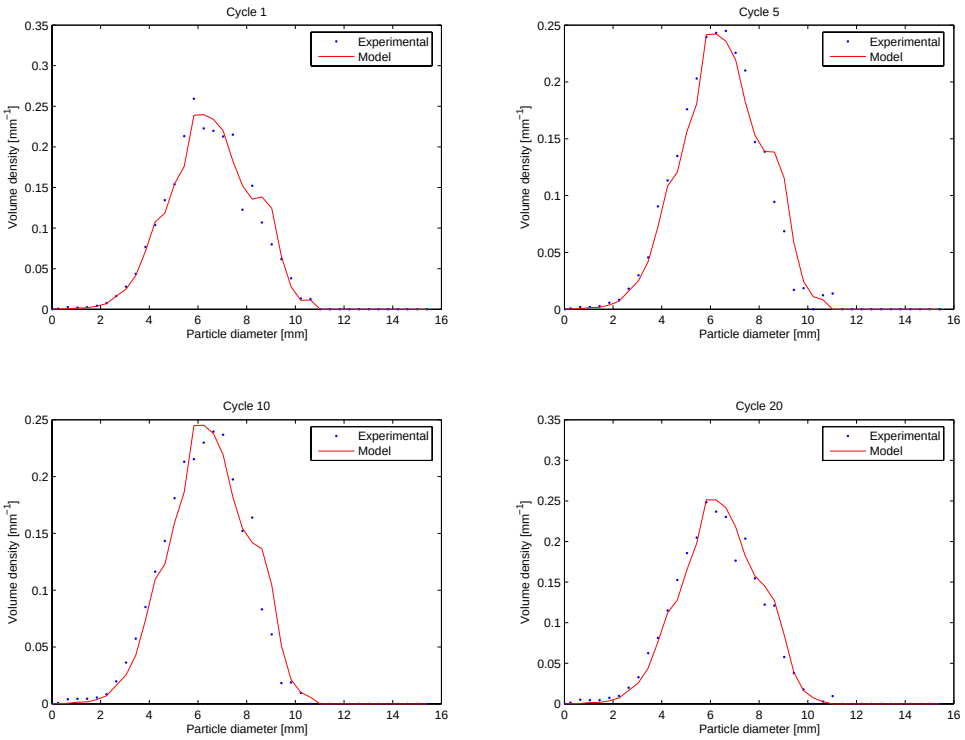

Figure 8.9: Comparisons between the particle size distribution of experimental results and model results for various numbers of cycles at 23 ms^{-1} air velocity using 0^o bend pipe using erosion type.

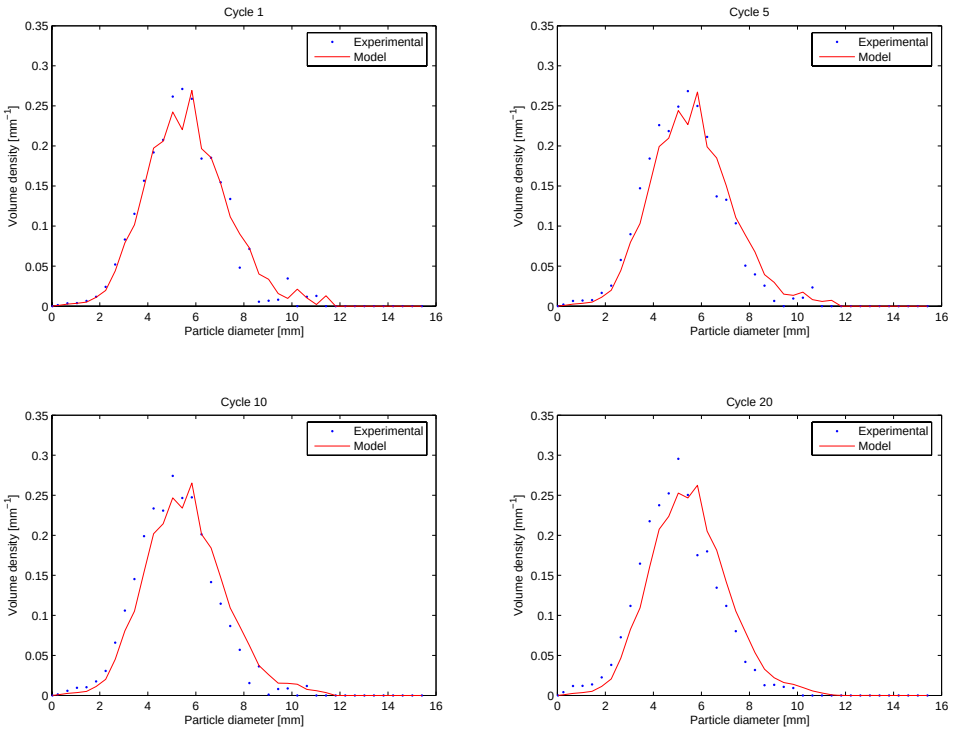

Figure 8.10: Comparisons between the particle size distribution of experimental results and model results for various numbers of cycles at $34\ ms^{-1}$ air velocity using 0^o bend pipe using erosion type.

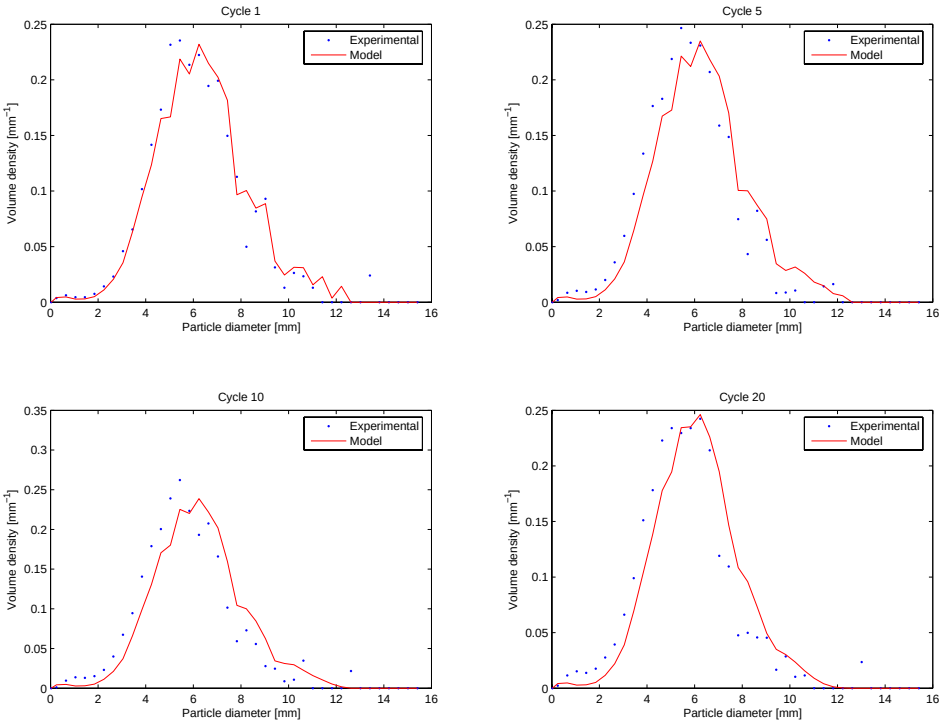

Figure 8.11: Comparisons between the particle size distribution of experimental results and model results for various numbers of cycles at $42\ ms^{-1}$ air velocity using 0^o bend pipe using erosion type.

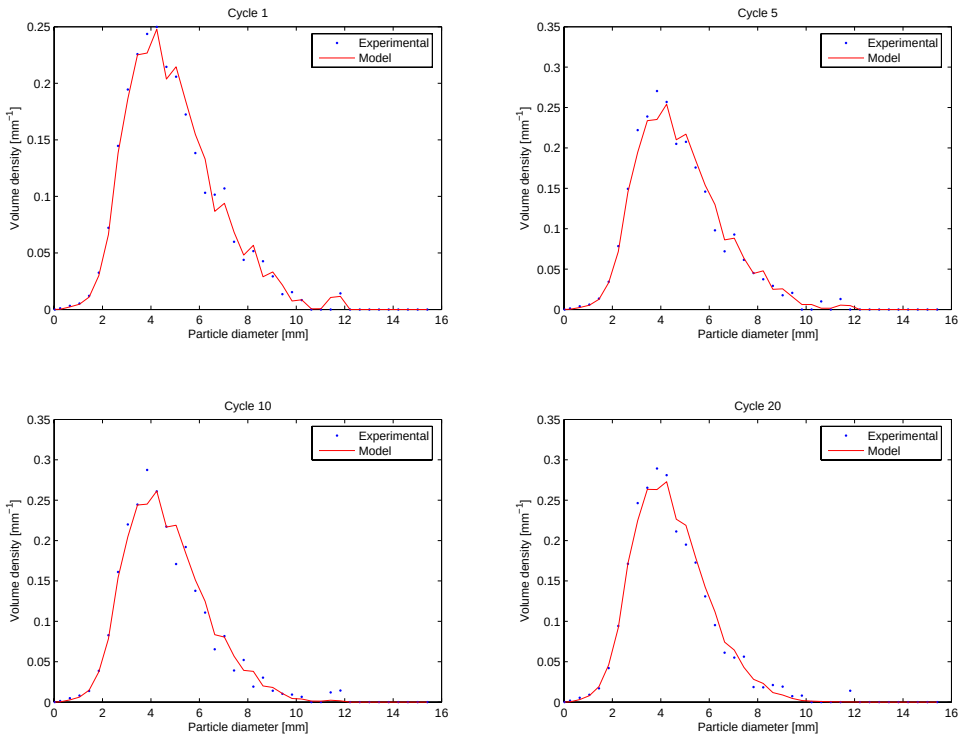

Figure 8.12: Comparisons between the particle size distribution of experimental results and model results for various numbers of cycles at 23 ms^{-1} air velocity during 90^o bend pipe using modified erosion type.

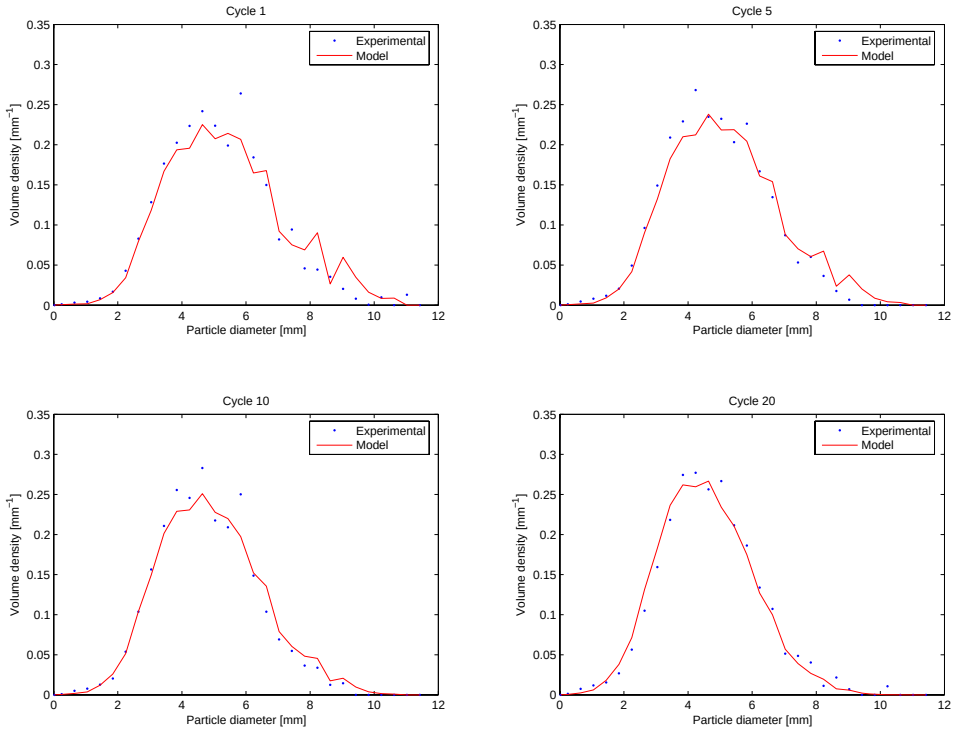

Figure 8.13: Comparisons between the particle size distribution of experimental results and model results for various numbers of cycles at $34\ ms^{-1}$ air velocity during 90^o bend pipe using modified erosion type.

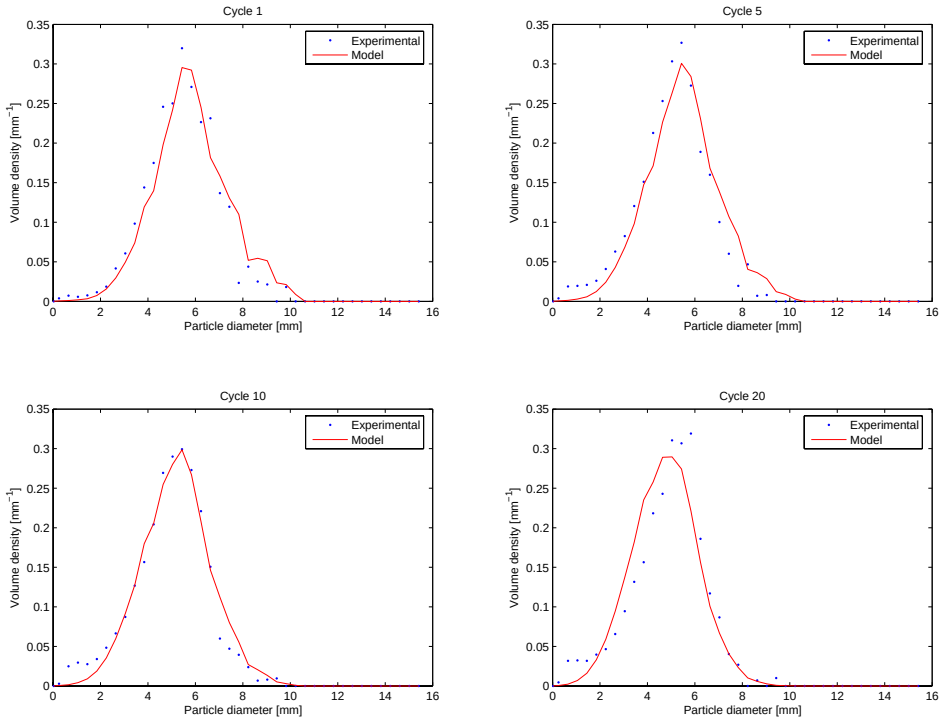

Figure 8.14: Comparisons between the particle size distribution of experimental results and model results for various numbers of cycles at $42\ ms^{-1}$ air velocity during 90^o bend pipe using modified erosion type.

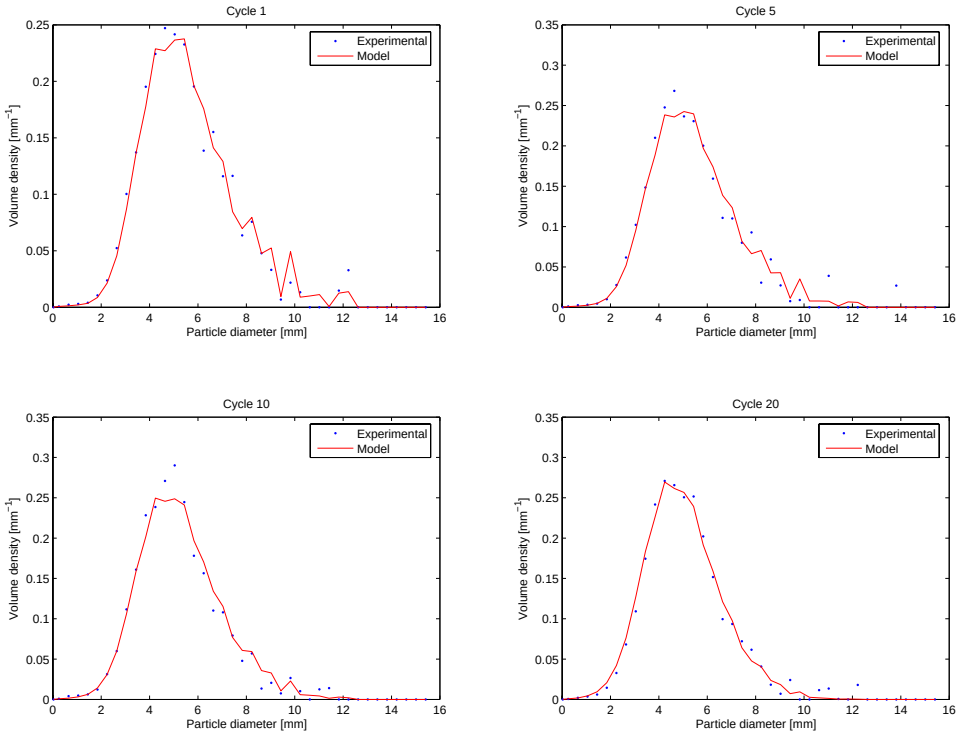

Figure 8.15: Comparisons between the particle size distribution of experimental results and model results for various numbers of cycles at $23\ ms^{-1}$ air velocity during 45^o bend pipe using modified erosion type.

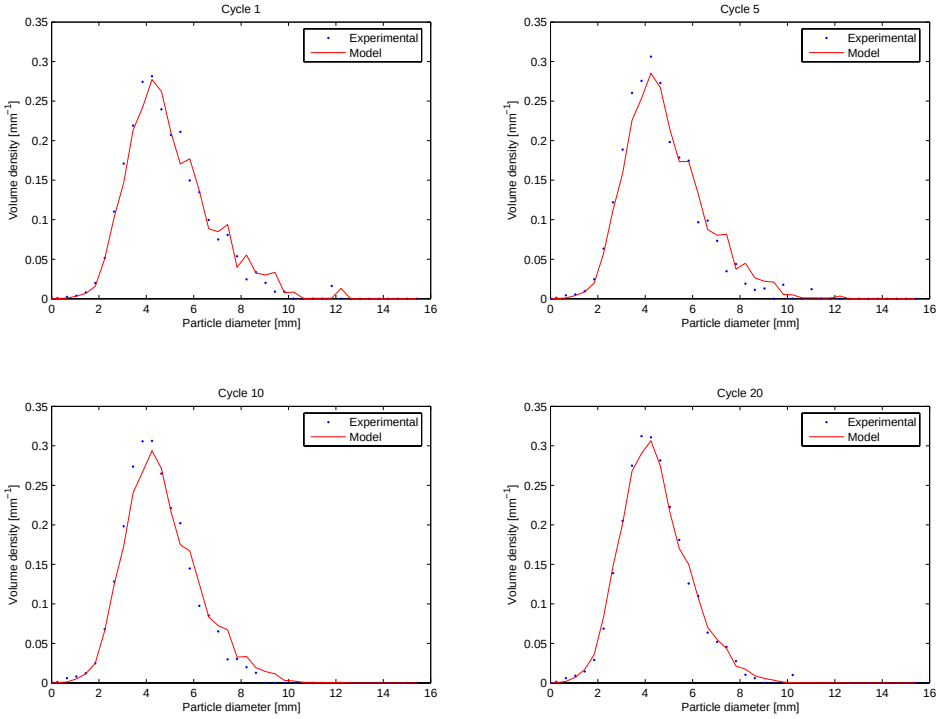

Figure 8.16: Comparisons between the particle size distribution of experimental results and model results for various numbers of cycles at $34\ ms^{-1}$ air velocity during 45^o bend pipe using modified erosion type.

sonable results than erosion only type, though it overpredicts the size distribution of experimental data at increased numbers of cycles at higher air velocity for 90^o and two 45^o bends configurations. This may imply that at these latter conditions erosion type breakage is dominant.

8.6 Conclusion

The population balance equations that govern this breakage process are solved using discretization. The Markov chain method was used for the solution of PBEs for this process. Two types of fragment size distribution were applied for model calculations based on visual observations; an erosion type and a modified erosion type. The breakage frequency was considered to be size dependent and a function of impact

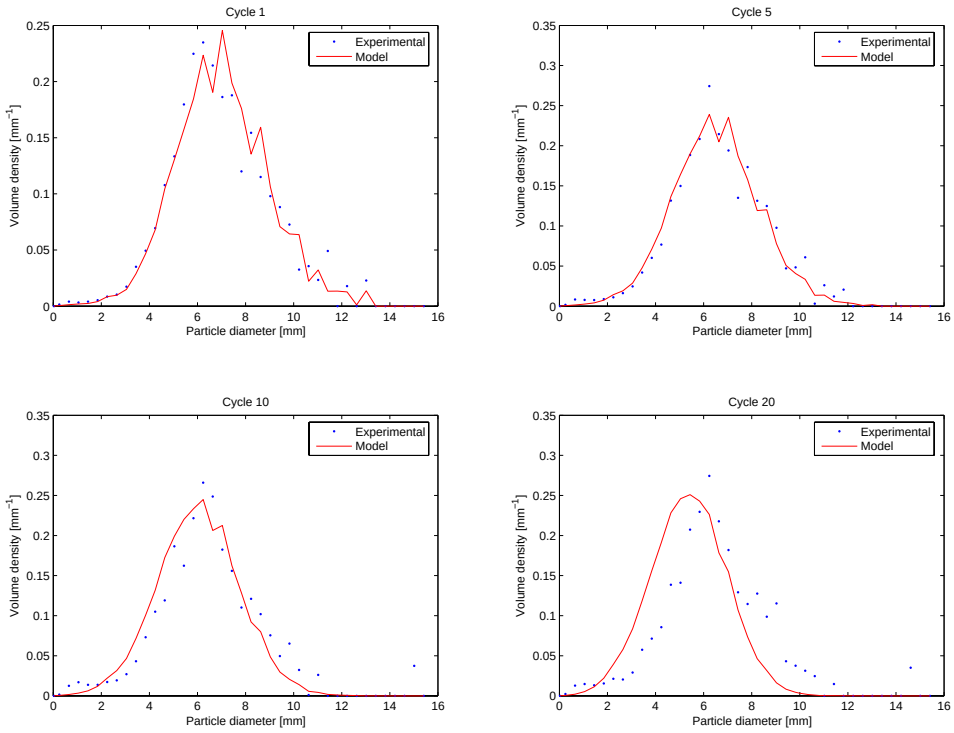

Figure 8.17: Comparisons between the particle size distribution of experimental results and model results for various numbers of cycles at $42\ ms^{-1}$ air velocity during 45^o bend pipe using modified erosion type.

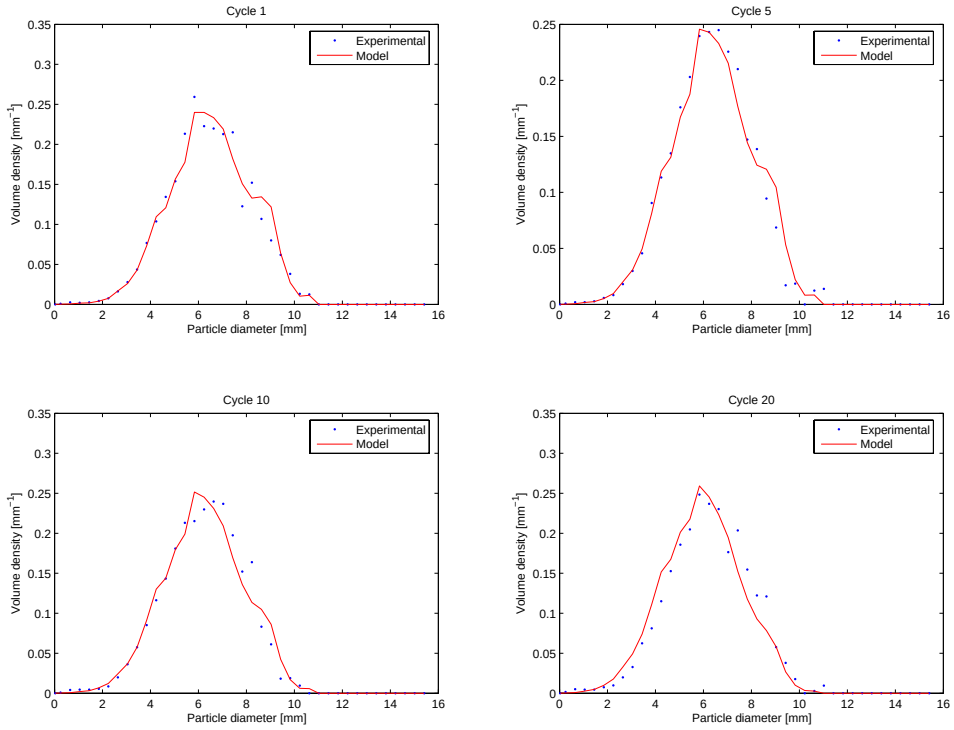

Figure 8.18: Comparisons between the particle size distribution of experimental results and model results for various numbers of cycles at $23\ ms^{-1}$ air velocity during 0^o bend pipe using modified erosion type.

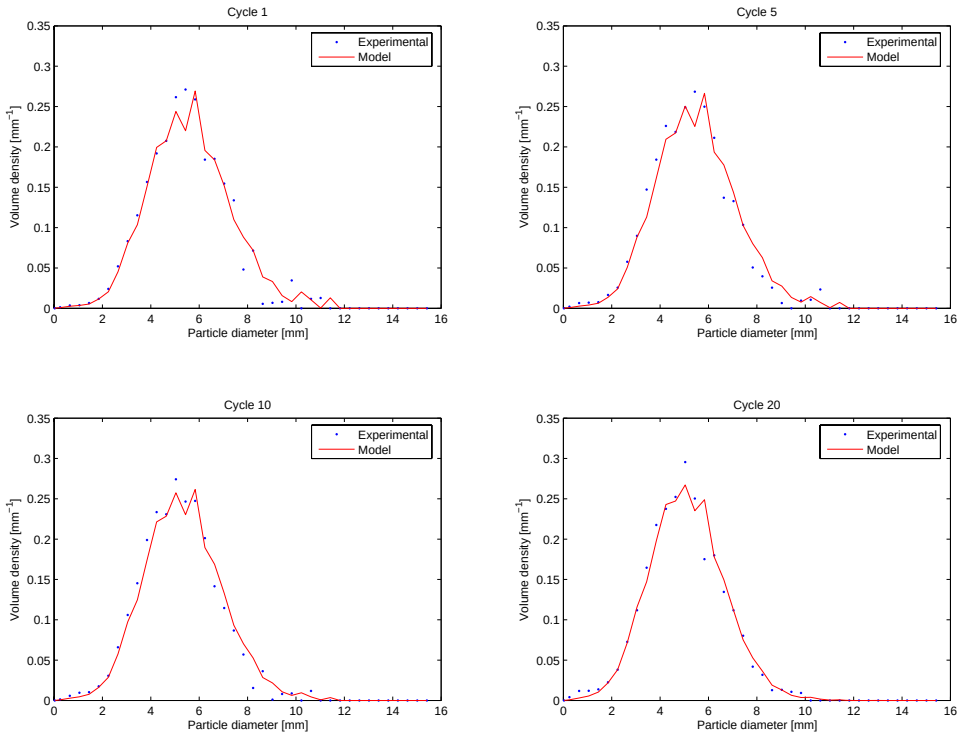

Figure 8.19: Comparisons between the particle size distribution of experimental results and model results for various numbers of cycles at $34\ ms^{-1}$ air velocity during 0^o bend pipe using modified erosion type.

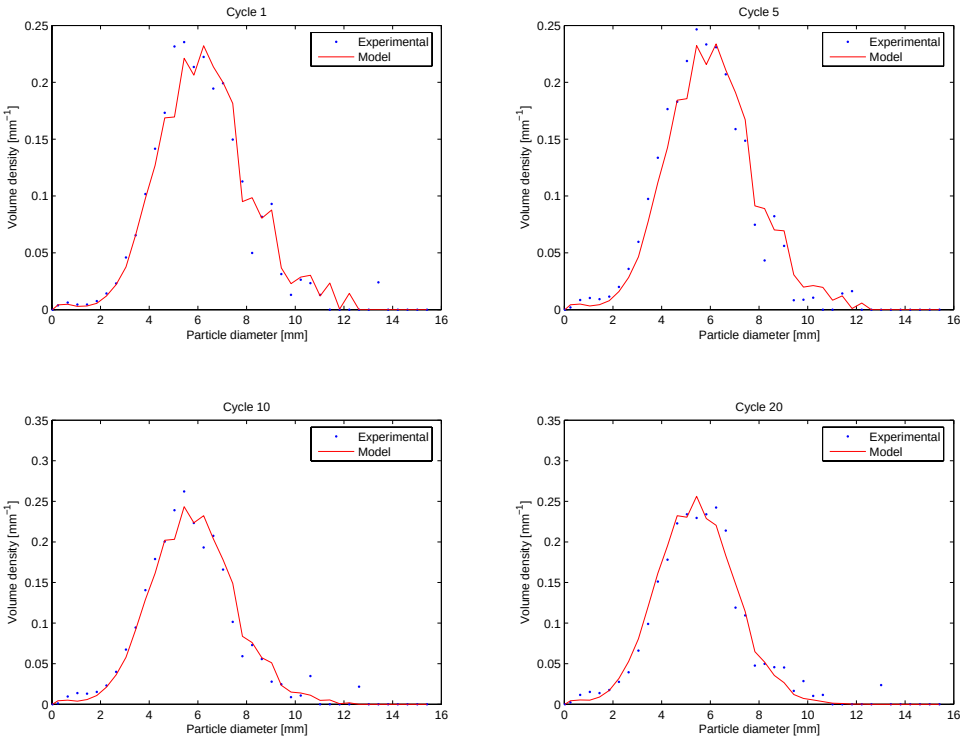

Figure 8.20: Comparisons between the particle size distribution of experimental results and model results for various numbers of cycles at $42\ ms^{-1}$ air velocity during 0^o bend pipe using modified erosion type.

velocity (as a result of applied air velocity), bend angle and shear history. Even though the results show that erosion type fragment size distribution appears to provide a satisfactory basis for an appropriate model, the modified erosion type fragment size distribution displays comparatively better agreement. However, at increased number of cycles the predicted attrition rate does not match the experimental results. This pattern was observed over the higher of flow rates during 90^o bend and two 45^o bend pipes. It maybe that after exposure for longer periods over a number of cycles at high impact velocities the cores of the aggregates may become weaker and are more likely to exhibit fracture into a large number of small sub aggregates and fines. This study found that increasing the air velocity (by increasing the air pressure to the rig), results in increased breakage among granola aggregates. Furthermore, the analysis carried out in this work provides that a greater degree of breakage of granola aggregates occur in line with an increase in bend angle.

Chapter 9

General Discussion and Conclusions

This chapter involves a general discussion and conclusions on the work done.

In this PhD study, mathematical modelling and optimisation of granola production has been carried out. Granola is an aggregated food product used in breakfast cereals and cereal bars. It is a baked crispy food product typically incorporating oats, other cereals and nuts bound together with a binder, such as honey, water and oil, to form a structured unit aggregate.

Aggregate food products can be produced via a number of ways. In this work, the design and operation of two parallel processes to produce aggregate granola products were incorporated:

i) a high shear mixing granulation stage (in a designated granulator) followed by drying/toasting in an oven.

ii) a continuous fluidised bed followed by drying/toasting in an oven.

High shear granulation is a more straightforward process compared with fluidised bed granulation. It is easy to handle fine particles and highly viscous liquid binder in a high shear granulator (HSG). In addition, there are less dusty particles associated with the final product produced in the HSG than that produced in fluidised bed granulator (FBG). However, high shear granulation is more amenable to producing granules which one denser and more spherical than FBG, particularly over extended processing times. This isn't preferred for commercial food products such as breakfast cereals. Therefore, it is suggested that the total granulation time should be carefully selected to avoid producing overly dense granules. Moreover, it was observed that the dry mixing period, which takes place prior to the wet massing period, has a positive effect on the homogeneity of the final granola products. Therefore, it is essential to include a prior dry mixing period as part of the total granulation process despite the fact that this will increase the total energy consumption during the granulation.

In a FBG, aggregation and drying processes occur in the same place; therefore it is economically efficient and advantageous from a containment perspective. On the other hand, for the granola system studied, it is very difficult to find optimum operating parameters via this mode due to the range of ingredients, both fine and coarse, and the inherent of natural variability that they posses. Additionally, a mixture of honey and water was used as a binding agent which has high viscosity. This restricts spraying of binder liquid onto the particles effectively as it sticks to the wall of the fluidised bed chamber. Another limitation of using FBG is that very hygroscopic ingredients such as inulin cannot be used as they become very hard due to the high air velocity through the bed. Moreover it is difficult to achieve fluidisation when aggregates are too wet and heavy. For this reason the total amount of liquid binder is lower in the fluidised bed granulator (honey plus water plus oil) than in the high shear granulator.

A growth model based on physical properties for granola production in a high shear mixer was developed. Impeller speeds and binder addition rates were selected as variable parameters. The median particle size was chosen as the indicative output parameter for the model. It was observed that the granule growth was directly proportional to the impeller speed and the binder addition rate.

In this study, the particle breakage of granola during pneumatic conveying produced by both a HSG and a FBG process was examined. Products were pneumatically conveyed in a purpose built conveying rig designed to mimic product conveying and packaging. Three different conveying rig configurations were employed; a straight pipe, a rig consisting two 45^o bends and one with 90^o bend. It was observed that the least amount of breakage occurred in the straight pipe while most breakage occurred through a 90^o bend pipe. Moreover, lower levels of breakage were observed in a two 45^o bend pipe than the 90^o bend pipe configuration. In general, increasing the impact angle increases both the levels and rate of breakage. This is a result which tallies with previously published research (Salman et al., 2003; Samimi et al., 2004). Additionally for the granules produced in the HSG, those produced at 300 rpm have the lowest breakage rates while the granules produced at 150 rpm have the highest breakage rates. This effect clearly shows the importance of shear history (during granule production) on breakage rates during subsequent processing. This is because of the fact that granules become denser and stronger with increased applied shear force. In terms of the FBG there was no single operating parameter that was deemed to have a significant effect on breakage during subsequent conveying.

Population balance modelling is very powerful tool in analysing overall evolution of particle size distribution. Nonetheless, an adequate solution method must accompany the population balance model as it includes partial integro-differential equations. There are several solution techniques such as Monte Carlo simulation, method of moments, and discrete formulations. In this study, the Markov chain method, which is

developed and validated by our project team, has been used to solve the population balance equations in discrete form. Employing a Markov chain method in this regard is extremely useful due to its efficiency and simplicity compared with other approaches; it is to be recommended for other such studies.

A breakage model describing the change in particle size incorporating physical phenomena based on particle motion within a conveying rig is developed in this work. Physical based models are very useful tools in understanding and analysing processes rigorously. However, it is a challenge to involve all sub-processes in building a unique model. In addition, it is difficult to examine the evolution of the particle size distribution using all physical phenomena in the process. Accordingly, a single representative variable such as median size (D_{50}) was employed.

Stokes number which is based on some deterministic assumptions, is a popular tool used to model aggregation and breakage processes in the literature. Although Stokes criteria includes fairly basic assumptions, it nevertheless provides a good basis to understand the mechanisms being studied. This reflects not alone granulation as a whole but also the subprocesses of aggregation and breakage which themselves involve complex mechanisms. Particles show extremely unpredictable behavior during some granulation phenomena such as particle-particle collisions, binder dispersion and particle-wall (equipment) collisions. To model the these systems in an appropriate manner, unpredictable behaviors may be treated as random variables. For instance, in Stokes criteria only head-on particle collisions were considered. In practise, particles may collide with different angles. Nevertheless, it was possible to model the rate of breakage through the D_{50} (as an indicative parameter) with some degree of success for the complex natural systems that pertain in both the HSG and the FBG. For future work, integration of the Stokes criteria approach and stochastic approach could be applied to such granulation process to better model these and other real systems.

Nomenclature

δ	granule deformation, [-]
ϵ	the fragment particle size, [-]
ϵ_v	pore volume, [m^3]
η	the attrition propensity parameter, [-]
γ	the scale parameter of Cauchy distribution, [-]
$\mathbf{a}(t)$	the state vector, [-]
$\mathbf{D}$	the diagonal triangular matrix, [-]
$\mathbf{L}$	the lower triangular matrix, [-]
$\mathbf{P}$	the transition matrix, [-]
μ	the binder viscosity, [$Pa.s$]
μ_a	dynamic viscosity of the air, [$Pa.s$]
ν_i	the impact velocity, [ms^{-1}]
$\overline{St}_{vis}$	the spatial average of the viscous Stokes number, [-]
ρ	the the granule density, [kgm^{-3}]
ρ_1	the density of liquid, [kgm^{-3}]

ρ_a air density, $[kgm^{-3}]$

ρ_p the particle density, $[kgm^{-3}]$

σ_{cr} the critical strain, [-]

τ time step for cycles, $[s]$

θ angle between blades, $[rad]$

θ the impact angle, $[Degree]$

θ_0 the location parameter of Cauchy distribution, [-]

$\tilde{D}$ the harmonic granule diameter, $[m]$

$\tilde{m}$ the harmonic granule mass , $[kg]$

ε granule porosity, [-]

ε_{min} the minimum porosity, [-]

$a(x, \epsilon)$ the aggregation kernel, [-]

$a(x_{i,j})$ the discrete aggregation kernel, [-]

$a^*(x, \epsilon)$ the size dependent part of aggregation kernel, [-]

a_0 the size independent part of aggregation kernel, [-]

A_p cross sectional area of particle, $[m^2]$

$b(x)$ the breakage frequency, $[s^{-1}]$

b_i the discrete breakage rate, $[s^{-1}]$

c the curve fitting parameter, [-]

C_d drag coefficient, [-]

c_T turbulent drag coefficient, [kgm^{-1}]

D granule diameter, [m]

d particle diameter, [m]

e coefficient of restitution, [-]

$f(x,t)$ the particle size distribution function, [m^{-1}]

F_d air drag force, [N]

F_g gravity force, [N]

F_H the threshold force required to break the particle, [N]

F_i the impact force, [N]

h binder layer thickness, [m]

h_a surface roughness, [m]

k the breakage constant, [-]

K_c the fracture toughness, [-]

l the characteristic particle size, [m]

l_i the representative particle size, [m]

m particle mass, [kg]

m the curve fitting parameter, [-]

$m(x)$ the mass of particle size of x, [kg]

N_0 the number of unbroken particles, [-]

N_i the discretized particle size distribution function, [-]

$P(x, y)$ the cumulative fragment size distribution, [-]

p_{ij} the entries of transition matrix, [-]

$q(x, y)$ the fragment size distribution, [-]

q_{ij} the discrete fragment size distribution, [-]

r radius, $[m]$

r_{cr}^{coal} the critical granule size for coalescence, $[m]$

r_{cr}^{def} the critical granule size for deformation, $[m]$

Re_p Reynolds number, [-]

S angular displacement, $[rad.m]$

s^* granule saturation, [-]

s_{max} the maximum pore saturation, [-]

St_{vis}^* the critical viscous Stokes number, [-]

St_{def} the Stokes deformation number, [-]

St_{def}^* the critical Stokes deformation number, [-]

St_{vis} the viscous Stokes number, [-]

t the time, $[s]$

u_a air velocity, $[ms^{-1}]$

u_b blade velocity, $[ms^{-1}]$

u_h horizontal component of the blade velocity, $[ms^{-1}]$

u_p particle velocity, $[ms^{-1}]$

u_T the terminal velocity of the particle, $[ms^{-1}]$

u_v vertical component of the blade velocity, $[ms^{-1}]$

v_i the impact velocity, $[ms^{-1}]$

V_{br} volumetric binder addition rate, $[m^3s^{-1}]$

w the impeller agitation, $[s^{-1}]$

Y_g the dynamic yield strength, $[Nm^{-2}]$

Bibliography

Adetayo, A. and Ennis, B. (1997). A unifying approach to modelling granule coalescence mechanisms. *AIChE Journal*, 43:927–934.

Adetayo, A. and Ennis, B. (2000). A new approach to modelling granulation processes for simulation and control purposes. *Powder Technology*, 108:202–209.

Aoun-Habbache, M., Aoun, M., Berthiaux, H., and Mizonov, V. (2002). An experimental method and a markov chian model to describe axial and radial mixing in a hoop mixer. *Powder Technology*, 128:159–167.

Austin, L. G. (1972). Introduction to mathematical description of grinding as a rate process. *Powder Technology*, 5:1–17.

Ayazi Shamlou, P., Stravrinides, S., Titchener-Hooker, N., and Hoare, M. (1994). Growth-independent breakage frequency of protein precipitates in turbulently agitated bioreactors. *Chemical Engineering Science*, 49:2647–2656.

Banks, M. and Aulton, M. (1991). Fluidized bed granulation: a chronology. *Drug Development and Industry Pharmacy*, 17:1437–1463.

Bapat, P., Tavlarides, L., and Smith, G. (1983). Monte carlo simulation of mass transfer in liquid-liquid dispersions. *Chemical Engineering Science*, 38:2003–2013.

Batterham, R., Hall, J., and Barton, G. (1981). Pelletizing kinetics and simulation of

full scale balling. circuits. *Proceedings, 3rd International Symposium on Agglomeration, Nurnberg.*, page A136.

Berthiaux, H. (2000). Analysis of grinding processes by markov chains. *Chemical Engineering Science*, 55:4117–4127.

Berthiaux, H., Marikh, K., Mizonov, V., Ponomarev, D., and Barantzeva, E. (2004). Modelling continues powder mixing by means of the theory of markov chains. *Particulate Science and Technology*, 22:379–389.

Berthiaux, H. and Mizonov, V. (2004). Applications of markov chains in particulate process engineering: A review. *The Canadian Journal of Chemical Engineering*, 82:1143–1168.

Berthiaux, H., Mizonov, V., and Zhukov, V. (2005). Application of the theory of markov chains to model different processes in particle technology. *Powder Technology*, 157:128–137.

Bilgili, E., Yepes, J., and Scarlett, B. (2006). Formulation of a non-linear framework for population balance modeling of batch grinding: Beyond first-order kinetics. *Chemical Engineering Science*, 61:33–44.

Boadway, J. (1978). Dynamics of growth and breakage of alum floc in presence of fluid shear. *Journal of the Environmental Engineering Division: Proceedings ASCE*, 104:901–915.

Boltzmann, L. (1872). Weitere studien ber das wrmegleichgewicht unter gasmoleculen. *Wien Ber.*, 66:275. *Translation in English can be found in: Brush, S.G. (Ed.), Selected Readings in Physics, Kinetic Theory, vol. 2. Irreversible Processes.*

Capes, C. (1980). *Handbook of Powder Technology Particle Size Enlargement*. Elsevier, Amsterdam.

Capes, C. and Danckwerts, P. (1965). Granule formation by the agglomeration of damp powders: Part 1. The mechanism of granule growth. *Transactions of the Institute of Chemical Engineers*, 43:116–124.

Coulaloglou, C. A. and Tavlarides, L. L. (1977). Description of interaction processes in agitated liquidliquid dispersions. *Chemical Engineering Science*, 32:1289–1297.

Cronin, K., Bas, N., and Byrne, E. (2007). Development of a computer-based teaching tool in probabilistic modelling. Dublin City University, Ireland. First International Symposium for Engineering Education. Url: `http://www.ndlr.ie/mecheng/symp/papers/RL0/Bas-Cronin-Byrne_ISEE07.pdf`.

Darelius, A., Rasmuson, A., Björn, I. N., and Folestad, S. (2005). High shear wet granulation modellinga mechanistic approach using population balances. *Powder Technology*, 160:209–218.

Dehling, H., Hoffmann, A., and Stuut, H. (1999). Stochastic models for transport in a fluidized bed. *SIAM J. Appl. Math.*, 60:337–358.

Dewettinck, K. (1997). *Fluidised bed coating in food technology: process and product quality*. PhD thesis, University of Ghent.

Diemer, R. and Olson, J. (2002a). A moment methodology for coagulation and breakage problems: Part 1– analytical solution of the steady-state population balance. *Chemical Engineering Science*, 57:2193–2209.

Diemer, R. and Olson, J. (2002b). A moment methodology for coagulation and breakage problems: Part 2–moment models and distribution reconstruction. *Chemical Engineering Science*, 57:2211–2228.

Diemer, R. and Olson, J. (2002c). A moment methodology for coagulation and breakage problems: Part 3–generalized daughter distribution functions. *Chemical Engineering Science*, 57:4187–4198.

Ennis, B., Tardos, G., and Pfeffer, R. (1991). A microlevel-based characterization of granulation phenomena. *Powder Technology*, 65:257–272.

Fox, R. and Fan, L. (1986). Stochastic analysis of axial solids mixing in a fluidised bed. 1st world congress on particle technology.

Friedlander, S. K. (2000). *Smoke, Dust and Haze: Fundamentals of Aerosol Dynamics*. Oxford University Press, New York.

Gantt, J. and Gatzke, E. (2005). High−shear granulation modeling using a discrete element simulation approach. *Powder Technology*, 156:195–212.

Gelbard, F. and Seinfeld, J. (1980). Simulation of Multicomponent Aerosol Dynamics. *Journal of Colloid and Interface Science*, 78:485.

Gelbard, F. M. and Seinfeld, J. H. (1978). Dynamics of source−reinforced, coagulating, and condensing aerosols. *Journal of Colloid and Interface Science*, 63:426–445.

Ghadiri, M. and Zhang, Z. (2002). Impact attrition of particulate solids. part 1: A theoretical model of chipping. *chemical Engineering Science*, 57:3659–3669.

Harris, A., Thorpe, R., and Davidson, J. (2002). Stochastic modelling of the particle residence time distribution in circulating fluidised bed risers. *Chemical Engineering Science*, 57:4779–4796.

Hidy, G. M. and Lilly, D. (1965). Solutions to the Equations for the Kinetics of Coagulation. *J. Coil. Sci.*, 20:867.

Hilbert, J. (1984). The best of bulk solids handling, pneumatic conveying of bulk powders. *Trans Tech Publications*, 86:107–110.

Hill, P. J. and Ng, M. K. (1995). New Discretization Procedure for the Breakage Equation. *AIChE Journal*, 41:1204–1216.

Hill, P. J. and Ng, M. K. (1996). New Discretization Procedure for the Agglomeration Equation. *AIChE Journal*, 42:727–741.

Hounslow, M. (1998). The population balance as a tool for understanding particle rate processes. *Kona*, 16:179–193.

Hounslow, M., Pearson, J. M. K., and Instone, T. (2001). Tracer studies of high-shear granulation: Ii. population balance modeling. *AIChE Journal*, 47:1984–1999.

Hounslow, M., Ryall, R., and Marshall, V. (1988). A discretized population balance for nucleation, growth, and aggregation. *AIChE Journal*, 34:1821–1832.

Huber, N. and Sommerfeld, M. (1998). Modelling and numerical calculation of dilute-phase pneumatic conveying a pipe systems. *Chemical Engineering Science*, 99:90–101.

Hulburt, H. and Katz, S. (1964). Some problems in particle technology. A statistical mechanical formulation. *Chemical Engineering Science*, 19:555–574.

Immanuel, C. and Doyle-III, F. (2005). Solution technique for a multi−dimensional population balance model describing granulation processes. *Powder Technology*, 156:213–225.

Iveson, S. and Litster, J. (1998). Growth regime map for liquid-bound granules. *AIChE J.*, 44:1510–1518.

Iveson, S., Litster, J., Hapgood, K., and Ennis, B. (2001). Nucleation, growth and breakage phenomena in agitated wet granulation processes: a review. *Powder Technology*, 117:3–39.

Kalman, H. (1999). Attrition control by pneumatic conveying. *Powder Technology*, 104:214–220.

Kapur, P. (1972). Self-preserving size spectra of comminuted particles. *Chemical Engineering Science*, 27:425–431.

Kapur, P. and Fuerstenau, D. (1964). Kinetics of green pelletization. *Transactions of AIME.*, 229:348–355.

Kapur, P. and Fuerstenau, D. (1969). A coalescence model for granulation. *Industrial and Engineering Chemistry Process Design and Development*, 8:56–62.

Kemeny, J. G. and Snell, J. L. (1960). *Finite Markov Chains*. D. Van Nostrand, New York.

Kostoglou, M. (2006). On the evolution of particle size distribution in pipe flow of dispersions undergoing breakage. *Industrial & Engineering Chemistry Research*, 45:2143–2145.

Kostoglou, M. and Karabelas, A. (2002). An assessment of low−order methods for solving the breakage equation. *Powder Technology*, 127:116–127.

Kostoglou, M. and Karabelas, A. (2004). Analytical treatment of fragmentation−diffusion population balance. *AIChE Journal*, 50:1746–1759.

Kostoglou, M. and Karabelas, A. (2007). On the breakage of liquid−liquid dispersions in turbulent pipe flow: Spatial patterns of breakage intensity. *Industrial & Engineering Chemistry Research*, 46:8220–8228.

Kramer, T. A. and Clark, M. M. (1999). Incorporation of aggregate breakup in the simulation of orthokinetic coagulation. *Journal of Colloid and Interface Science*, 216:116–126.

Kristensen, H., Holm, P., and Schfer, T. (1985). Mechanical properties of moist agglomerates in relation to granulation mechanisms: Part 1. Deformability of moist, densified agglomerates. *Powder Technology*, 44:227–238.

Kumar, S. and Ramkrishna, D. (1996a). On the solution of population balance equations by discretization−I: A Fixed Pivot Technique. *Chemical Engineering Science*, 51:1311–1332.

Kumar, S. and Ramkrishna, D. (1996b). On the solution of population balance equations by discretization−I: A Moving Pivot Technique. *Chemical Engineering Science*, 51:1333–1342.

L. Farina, S. R. (2000). *Positive Linear Systems: Theory and Application*. Wiley.

Li, J. and Mason, D. (2002). Application of the discrete element modeling in air drying of particulate solids. *Drying Technology*, 20:255–282.

Litster, J., Ennis, B., and Liu, L. (2004). *The Science and Engineering of Granulation Processes*. Kluwer Academic Publishers, Netherlands.

Lui, L. and Litster, J. (2002). Population balance modelling of granulation with a physically based coalescence kernel. *Chemical Engineering Science*, 57:2183–2191.

Lui, L., Litster, J., Iveson, S. M., and Ennis, B. J. (2000). Coalescence of deformable granules in wet granulation processes. *AIChE Journal*, 46:529–539.

Luo, H. and Svendsen, H. F. (1996). Theoretical model for drop and bubble breakup in turbulent dispersions. *AIChE Journal*, 42:1225–1233.

Marchisio, D. L., Pikturna, J. T., Fox, R. O., Vigil, D. R., and Barresi, A. A. (2003). Quadrature Method of Moments for Population-Balance Equations. *AIChE Journal*, 49:1266–1276.

Marchisio, Daniele L. Vigil, D. R. and Fox, R. O. (2003). Quadrature method of moments for aggregation-breakage processes. *Journal of Colloid and Interface Science*, 258:322–334.

Markov, A. (1906). Extension of the law of large numbers to dependent events. *Bulletin of the Society of the Physics Mathematics, Kazan, Russia*, 15:155–156.

Maxim, R., Salman, A., and Hounslow, M. (2002). Impact of granules: failure distribution. In *Proceedings of World Congress on Particle Technology*, Sydney, Australia.

McGrady, E. and Ziff, R. M. (1986). "Shattering" Transition in Fragmentation. *Phys. Rev. Lett.*, 58:892–895.

Nere, N. K. and Ramkrishna, D. (2005). Evolution of drop size distributions in fully developed turbulent pipe flow of a liquid−liquid dispersion by breakage. *Industrial & Engineering Chemistry Research*, 44:1187–1193.

Newitt, D. and Conway-Jones, A. (1958). A contribution to the theory and practice of granulation. *Transactions of the Institute of Chemical Engineers*, 36:422–442.

Nicmanis, M. and Hounslow, M. J. (1998). Finite−element methods for steady−state population balance equations. *AIChE Journal*, 44:2258–2272.

Ouchiyama, N. and Tanaka, T. (1975). The probability of coalescence in granulation kinetics. *Industrial and Engineering Chemistry Process Design and Development*, 14:286–289.

Pahk, J. B. and Klinzing, G. E. (2008). Comparison of flow characteristics for dilute phase pneumatic conveying for two different plastic pellets. *Journal of the Chinese Institute of Chemical Engineers*, 39(2):143 – 150.

Panda, R., Zank, J., and Martin, H. (2001). Modeling the droplet deposition behavior on a single particle in fluidized bed spray granulation process. *Powder Technology*, 115:51–57.

Pandya, J. and Spielman, L. (1982). Floc breakage in agitated suspensions: theory and data processing strategy. *Journal of Colloid and Interface Science*, 90:517.

Papadopoulos, D. and Ghadiri, M. (1996). Impact breakage of pmma extrudates: I. chipping mechanism. *Advanced Powder Technology*, 7:183–197.

Parfitt, R., editor (1986). *Dispersion of Powders in Liquids Volume 10*. Elsevier Applied Science Publishers Ltd., The Netherlands.

Parikh, D. M. (2000). *Handbook of Pharmaceutical Granulation Technology*. Marcel Dekker, INC. New York.

Ponomarev, D., Mizonov, V., Gatumel, C., Berthiaux, H., and Barantzeva, E. (2009). Markov-chain modelling and experimental investigation of powder-mixing kinetics in static revolving mixers. *Chemical Engineering and Processing*, 48:828–836.

Poon, J. M.-H., Immanuel, C. D., F.J. Doyle, I., and Litster, J. D. (2008). A three–dimensional population balance model of granulation with a mechanistic representation of the nucleation and aggregation phenomena. *Chemical Engineering Science*, 63:1315–1329.

Prasher, C. L. (1987). *Crushing and Grinding Process Handbook.* John Wiley & Sons Ltd., New York.

Rajniak, P., Dhanasekharan, K., Sinka, C., MacPail, N., and Chern, R. (2008). Modelling and measurement of granule attrition during pneumatic conveying in a laboratory scale system. *Powder Technology*, 185:202–210.

Ramkrishna, D. (2000). *Population Balances Theory and applications to Particulate Systems in Engineering*. Academic Press, USA.

Randolph, A. and Larson, M. (1964). A population balance for countable entities. *Canadian Journal of Chemical Engineering*, 42:280–281.

Redner, S. (1990). *Fragmentation Statistical Models for the Fracture of Disordered Media.* Elsevier, Amsterdam.

Reynolds, G., Fu, J., Cheong, Y., Hounslow, M., and Salman, A. (2005). Breakage in granulation: A review. *Chemical Engineering Science*, 60(14):3969 – 3992.

Rhodes, M. (2008). *Introduction to Particle Technology.* John Wiley and Sons Ltd., England.

Salman, A., Ghadiri, M., and Hounslow, M., editors (2007a). *Handbook of Powder Technology: Particle Breakage*. Elsevier, Amsterdam ; London.

Salman, A. and Gorham, D. (2000). The fracture of glass spheres under impact loading. *Powder Technology*, 102:179–185.

Salman, A., Gorham, D., Szabó, M., and Hounslow, M. (2005). Spherical particle movement in dilute pneumatic conveying. *KONA*, 153:43–50.

Salman, A., Gorham, D., and Verba, A. (1995). A study of solid particle failure under normal and oblique impact. *Wear*, 186–187:92–98.

Salman, A., Hounslow, M., and Seville, J., editors (2007b). *Hand Book of Powder Technology Volume 11 Granulation*. Elsevier, The Netherlands.

Salman, A., Hounslow, M., and Verba, A. (2002). Particle fragmentation in dilute phase pneumatic conveying. *Powder Technology*, 126:109–115.

Salman, A., Reynolds, G., and Hounslow, M. (2003). Particle impact breakage in particulate processing. *KONA*, 21:88–99.

Samimi, A., Moreno, R., and Ghadiri, M. (2004). Analysis of impact damage of agglomerates: effect of impact angle. *Powder Technology*, 143–144:97–109.

Sastry, K. and Fuerstenau, D. (1973). Mechanisms of agglomerate growth in green pelletization. *Powder Technology*, 7:97–105.

Sastry, K. and Fuerstenau, D. (1975). Similarity size distribution of agglomerates during their growth by coalescence in granulation or green pelletization. *International Journal of Mineral Processing*, 2:187–203.

Schafer, T. (2001). Growth mechanisms in melt agglomeration in high shear mixers. *Powder Technology*, 117:68–82.

Seville, J., Tüzün, U., and Clift, R. (1997). *Processing of particulate solids*. Kluwer, Great Britain.

Sherrington, P. J. and Oliver, R. (1981). *Granulation*. Heyden and Son Limited, London.

Shipway, P. and Hutchings, I. (1993). Fracture of brittle spheres under compression and impact loading: Ii. results for lead-glass and sapphire spheres. *Philosophical Magazine A*, 67:1405–1421.

Snow, R., Allen, T., Ennis, B., and Litser, J. D. (1997a). *Perry's Chemical Engineering Handbook: Size Reduction and Size Enlargement*. McGraw-Hill, USA.

Snow, R., Allen, T., Ennis, B., and Litser, J. D. (1997b). *Perry's Chemical Engineering Handbook: Size Reduction and Size Enlargement*. McGraw-Hill, USA, seventh edition.

Tamir, A. (1998). *Applications of Markov Chains in Chemical Engineering*. Elsevier, Amsterdam, The Netherlands.

Tan, H., Goldschmidt, M., Boerefijn, R., Hounslow, M., Salman, A., and Kuipers, J. (2004a). Building population balance model for fluidized bed melt granulation: lessons from kinetic theory of granular flow. *Powder Technology*, 142:103–109.

Tan, H., Salman, A., and Hounslow, M. (2004b). Kinetics of fluidised bed melt granulation IV: Selecting the breakage model. *Powder Technology*, 143–144:65–83.

Tan, H., Salman, A., and Hounslow, M. (2005a). Kinetics of fluidised bed melt granulation III: tracer studies. *Chemical Engineering Science*, 60:3835–3845.

Tan, H., Salman, A., and Hounslow, M. (2005b). Kinetics of fluidised bed melt granulation V: simultaneous modelling of aggregation and breakage.. *Chemical Engineering Science*, 60:38473866.

Tan, H., Salman, A., and Hounslow, M. (2006a). Kinetics of fluidised bed melt granulation I: Effect of process variables. *Chemical Engineering Science*, 61:1585–1601.

Tan, H., Salman, A., and Hounslow, M. (2006b). Kinetics of fluidised bed melt granulation II: Modelling the net rate of growth. *Chemical Engineering Science*, 61:3930–3941.

Tardos, G., Irfan-Khan, M., and Mort, P. (1997). Critical parameters and limiting conditions in binder granulation of fine powders. *Powder Technology*, 94:245–258.

Tavares (2007). *Breakage of Single Particles: Quasi-Static*, pages 3–68. Elsevier, Amsterdam ; London, handbook of powder technology: Particle Breakage edition.

Turton, R. and Levenspiel, O. (1986). A short note on the drag coefficient for spheres. *Powder Technology*, 47:83–86.

Vanni, M. (1999). Discretization procedure for the breakage equation. *AIChE Journal*, 45:916–919.

Vanni, M. (2000). Approximate Population Balance Equations for Aggregation-Breakage Processes. *Journal of Colloid and Interface Science*, 221:143–160.

Vonk, P., Guillaume, C., Ramaker, J., Vromans, H., and Kossen, N. (1997). Growth mechanism of high-shear pelletisation. *Int. J. Pharm.*, 157:93–102.

Wojcik, J. A. and Jones, A. G. (1998). Particle disruption of precipitated $caco_3$ crystal agglomerates in turbulently agitated suspensions. *Chemical Engineering Science*, 53:1097–1101.

Wurster, D. (1950). Means for applying coating to tablets or like. *Journal of the American Pharmaceutical Association*, 48:451.

Xiang, J. and McGlinchey, D. (2004). Numerical simulation of particle motion in dense phase pneumatic conveying. *Granular Matter*, 6:167–172.

York, P. and Rowe, R. (1994). Monitoring granulation size enlargement processes using mixer torque rheometry. In *First International Particle Technology Forum*, Denver,USA.

Yuregir, K., Ghadiri, M., and Clift, M. (1987). Impact attrition of sodium chloride crystals. *Chemical Engineering Science*, 42:843.